PLANAR ELECTROMAGNETIC SENSORS: CHARACTERIZATION AND EXPERIMENTAL RESULTS

A Project Report
submitted in partial fulfilment of the
requirements for the Degree of

Master of Engineering

in

INFORMATION AND TELECOMMUNICATIONS ENGINEERING

By

CHINTHAKA P. GOONERATNE

INSTITUTE OF INFORMATION SCIENCES AND TECHNOLOGY
MASSEY UNIVERSITY
PALMERSTON NORTH
NEW ZEALAND

AUGUST 2005

To my parents:

Mahendra Gooneratne

and

Vajira Gooneratne

ABSTRACT

Planar type electromagnetic sensors have simple structures and are very useful for the inspection of material properties, in a non-destructive and non-invasive way. The operating principle of the sensing technique is based on the interaction of electromagnetic fields with the materials under test. Three types of planar sensors: meander, mesh and interdigital configuration have been analyzed to determine their characteristics. Finite element software has been used for the analysis of flux distribution for all three types of sensors. The nature of the impedance characteristics has also been obtained through experiments. It has been reported that meander and mesh type sensors respond well at moderately high frequencies. To avoid relatively costly instrumentation systems at high frequencies, interdigital sensors having good response at low frequencies have been considered. The response of all the sensors, especially the interdigital types to milk of varying fat content, quality estimation of saxophone reeds and non-invasive estimation of fat content of pork belly cuts have been determined. The different types of sensors can be made as a sensor array, to estimate the properties of mixtures of electric, magnetic and dielectric materials. A microcontroller based low cost sensing system is under development.

ACKNOWLEDGEMENTS

I'm infinitely grateful to my supervisor, Dr. Subhas Mukhopadhyay for giving me the opportunity to do my masters study, continuously supervising my research work, providing valuable advice and expert guidance, and above all for his technical, financial and emotional support.

I would like to thank the Institute of Information Sciences and Technology (IIST) and Massey University Technical Assistance Award (UTA), for providing me financial support to pursue my studies. My special thanks go to Mr. G. Sen Gupta for his help and guidance related to microcontroller programming.

Part of the work presented in this thesis was done in close consultation with Associate Professor Roger Purchas. I would like to thank him for his valuable advice and insightful input into the research. I would also like to acknowledge the Institute of Food Nutrition and Human Health (IFNHH) for providing samples for experimentation.

I would like to acknowledge the efforts of Mr. Ken Mercer and Mr. Colin Plaw for their help on technical matters. I would like to thank Mr. Humphrey O'Hagan for his help on mechanical fabrication.

On a personal level I would like to thank Associate Professor Ravi Gooneratne and Dr. Anoma Gooneratne, my Uncle and Aunty, for all the help and support they have given me. I would like to thank Ms. Margaret J. Humphreys and Mrs. Alexandra G. Cook (Nana), for providing me a place to stay, constant encouragement and for all the interesting and informal talks, which were always a welcome and refreshing break from study. I would like to acknowledge Mr. Joe Manning for being kind enough to proof read my thesis. Many thanks go to all my friends and my twin brothers, Dinuk and Dinal, for helping me in various ways.

Finally and most importantly I would like to thank my parents for their unconditional love and support. Thank you for all the sacrifices you have made to give me a better chance in life.

CONTENTS

LIST OF FIGURES

LIST OF TABLES

CHAPTER 1

INTRODUCTION

1.1 Introduction

Sensors are widely used in scientific research and as an integral part of commercial products and automated systems. A sensor is a device which is used to record the presence of something or changes in something. Sensors gather information from the environment and act as transducers, converting the energy form associated with the information that is sought into a form in which it can be easily processed [1]. The energy forms typically involved in sensing processes include chemical, electrical, magnetic, acoustic, mechanical, optical and thermal.

Table 1.1: Signal domains with examples [1]

Energy Form	Examples
(Bio)Chemical	Composition, Concentration, pH, Reaction rate
Electrical	Current, Voltage, Electric field, Conductivity, Permittivity
Magnetic	Magnetic field, Magnetic Flux, Permeability
Acoustic	Wave velocity, Spectrum, Wave(amplitude, phase)
Mechanical	Acceleration, Force, Stress, Pressure, Torque, Mass, Density
Optical	Wave velocity, Refractive Index, Refractivity, Absorption
Thermal	Temperature, Flux, Specific Heat, Thermal conductivity

Sensors are classified into passive or active sensors [2]. Passive sensors can only be used when naturally occurring energy is available. Hence for all reflected energy, this can take place only when the sun is illuminating the earth. Given that the amount of energy is large enough to be recorded, naturally emitted energy such as thermal infrared can be detected anytime of the day.

Active sensors emit their own energy that travels from the instrument to the target to be investigated. The reflected radiation from the target is detected and measured by the sensor. Active sensors can obtain measurements anytime, as well as examining wavelengths which are not sufficiently provided by the sun (e.g. microwaves). They also have better control of the way a target is illuminated. The disadvantage of active sensors is the large amount of energy that has to be generated by the system, to adequately illuminate targets.

Sensors are calibrated for certain conditions and are capable of reporting changes at certain speeds. Many sensors need to be amplified to be useful [1]. Sensors are either direct indicating (e.g. mercury thermometer) or are paired with an indicator (usually indirectly through an analog to digital converter, a computer and a display) to make it easier to read values. In general, most sensors fall into one of two categories: digital and analog sensors. Digital sensors involve representation of quantities in discrete units. The output signal is a digital representation of the input signal, and has discrete values of magnitude measured at discrete times. The logic level output of the digital sensor must be compatible with the digital receiver. Some standard logic levels include transistor-transistor logic (TTL) and emitter-coupled logic (ECL). Examples of digital sensors include switches and position encoders. Some digital sensors are more complicated. These sensors produce pulse trains of transitions between the 0 volt state and the 5 volt state. With these types of sensors, the sensor's measurement is conveyed through the frequency characteristics or shape of this pulse train.

Analog sensors produce an output signal that is directly proportional to the input signal, and is continuous in both magnitude and in time. The sensors employed by the author for experimentation measures impedance (magnitude) and phase (time). Physical variables that are continuous in nature such as air flow, temperature and speed can be measured by analog sensors. Examples of analog sensors include resistance temperature devices (RTD), microphones and strain gauges. Disadvantages of analog type sensors are crosstalk or electrical system noise as well as performance reductions over transmitting the analog signal over long distances.

The general properties of a good sensor are:

- optimum measurement accuracy (not as good as possible, but as good and as accurate as necessary)
- durability
- ease of calibration and reconditioning
- sensitivity and good resolution
- selectivity
- provision of reproducible measurements
- long term stability

- fast response (important for control)
- continuous operation
- insensitivity to electrical and other environmental interference
- low operation and maintenance cost
- acceptance by users
- meet safety requirements

Sensors play an important part in real-world systems, straddling a variety of applications such as industrial, medical, robotic, military, consumer and automotive applications. Sensors are critical to today's society since they provide the connection between the "real" world and the world of process control and computers. The overall accuracy and the reliability of the control system is determined by the sensors accuracy. Environmental concerns along with health and safety issues have necessitated in an increased use of sensors in the areas discussed above. Sensor technology has been successful in improving energy efficiency and service and product quality and reducing emissions [2]. Selecting a sensor depends on many factors such as availability, cost, power consumption, environmental conditions etc. Sensors are integral when it comes to controllability, reliability and profitability of a process [1, 2].

Sensor technology follows a pattern of continuous development and many prototypes will be introduced destined for success on the long run. The feasibility of a sensor technology is determined by various factors. The main factors that sensor manufactures will keep in mind when designing sensors are: cost reduction, reliability, system compatibility, safety in hazardous/hostile environments and non-invasive/non-intrusive design.

Sensing devices have been traditionally developed by employing trial-and-error techniques rather than following a solid scientific approach. Many of the sensor technologies that are in use today apply complex mixtures of several different materials, where the principles of functionality of each component is not known or well understood [3]. Furthermore, the degeneration methods that lead to aging behavior are not fully understood in most cases. For the successful implementation of novel sensor technologies it is therefore essential to have a good grasp of sensing mechanisms and their degradation behavior. This will aid in the development of advanced, affordable, reliable and novel technologies that will have a major impact on today's society. Fundamental understanding of the material characteristics is also

important in selecting the appropriate combination of sensing elements to achieve selectivity in complex array structures [3]. Hence, important sensor performance parameters such as stability, sensitivity and selectivity must be improved, even in the case of commercially available products [1]. These parameters depend mainly on the physical and chemical characteristics of the materials that were used to build the sensing device.

There is a high demand for novel sensors that are able to cope in extreme hostile/hazardous environments [4]. Novel technologies which are reliable in extreme environments are continuously being researched and developed. However, the specifications and the boundaries for sensing systems are becoming more demanding (e.g. example operation of sensors to detect landmines in harsh environments). It is therefore important to understand the sensing mechanisms and how they operate in each case. The miniaturization of such devices seems to be the next step in sensor technology, and the importance of designing materials with controlled microstructures was clearly shown in the semiconductor industry's paradigm.

1.2 Sensors and Non-Destructive Sensing

Non-destructive testing (NDT) or Non-destructive evaluation (NDE) has evolved over the years to become one of the critical measurement techniques in industry today. It is a very broad and an interdisciplinary field that can be used to detect defects and measure physical or mechanic characteristics of a material or component, independent of orientation. It is a reliable and a cost effective way to detect and evaluate structural components and systems and seeing if they are performing to their potential. The popularity and acceptance of NDT as a measurement technique is due to the fact that the system or material under test is not harmed or damaged during testing, and thus the integrity of the object under test is retained [25]. In an age where health and safety standards in industry have reached high limits, the importance of NDT is even more. NDT has the potential to stop many disasters that are waiting to happen. Typical engineering failures such as airplane crashes, pipeline explosions, reactor failures, machine failure, bridge failure and trains derailing can be successfully avoided with NDT. NDT is used many areas including automotive, nuclear, aviation, aerospace, construction, petro-chemical, electronics, food industry, medical science, power, transportation and the metal industry [24, 25]. There are NDT applications at almost any stage in the production or the lifecycle of a component.

The demand for highly reliable and high performance inspection techniques during manufacturing, production and use of a system or structure is increasing daily. Hence the number of suitable inspection techniques is also on the rise. Shown below are a few of the most commonly used methods in NDT.

- Visual and Optical Testing [5,6]

  This is the most basic NDT inspection method. The methods range from visual examiners checking the object of interest for visible imperfections, to computer controlled camera systems which automatically recognize and measure features of the system under test.

- Radiography Testing [7]

  In radiography testing, penetrating gamma or x-rays are employed to analyze the defects and internal features of the object under consideration. A source of radiation is required when an object is being tested with radiography techniques. Normally an X-ray machine or a radioactive isotope is used for this purpose.

- Magnetic Particle Testing [8]

  In magnetic particle testing a magnetic field is induced in a ferromagnetic material. The surface is then dusted with iron particles, which are either dry or suspended in liquid. Testing is done so that defects in the material under test can be observed. When a surface or a near surface flaw is detected, magnetic poles are produced or the magnetic field is distorted so that the iron particles are attracted and concentrated. This paves the way for visible detection of defects on the surface of the material.

- Ultrasonic Testing [9]

  Ultrasound detection involves the transmissions of sound waves with a frequency higher than 20 kHz into a medium. These sound waves are then reflected on boundaries between materials with different acoustical properties.

The detection of imperfections or the location of changes in material properties are achieved this way.

- Penetrant Testing [11]

  A solution that contains a visible or fluorescent dye is used to coat the object that is being tested. After excess solution is removed from the surface of the object it is left in surface breaking defects. The penetrant is then removed from the defects using a developer. The next step involves detecting the imperfections. In the case of fluorescent dyes, imperfections are visible when ultraviolet light is used to make the bleed out fluoresce brightly. Visible dyes on the other hand have vivid color contrasts between the penetrant and the developer, which makes it easier to see "bleedout".

- Leak Testing [10]

  A leak can be flow of a gas or liquid through the wall of a vessel, due to holes or cracks in the system. There are various techniques that are used to detect and locate leaks in pressure vessels, pressure containments and structures. Methods such as gauge measurements, liquid and gas penetrant techniques, soap-bubble tests and electronic listening devices can be used for detection.

- Acoustic Emission Testing [12]

  The structural or the material integrity of the object under test is based on the short energy of acoustic energy called "emissions" that are emitted, when the object is stressed. Special receivers are used to detect these acoustic emissions. The intensity of the emissions as well as the arrival time to collect information about the source of the energy, such as their location can be used to evaluate the status of the object under test.

- Electromagnetic Testing [13]

  There are several methods such as eddy current inspection, remote field testing, flux leakage and Barkhausen noise that use the electromagnetism as the principle of operation. Eddy current testing (ECT) is the most commonly used method of inspection. The principles of ECT is used for the mesh and meander type sensors that have been used by the author.

Electromagnetic induction is the root of ECT. The English scientist Michael Faraday discovered electromagnetic induction in 1831. The brilliance of Faraday was instrumental in discoveries such as electromagnetic induction, electromagnetic rotations, the magneto-optical effect, diamagnetism and many others. In 1879, metals of different conductivity and permeability were tested with a coil, and the changes in the coil were recorded by Welsh Professor David Edward Hughes. However it was not until World War 2 that these effects were put into practical use for the inspection of materials. The now widely used and well understood ECT was pioneered by Friedrich Forster in the 1940s. He was an important figure in the introduction of ECT as a non-destructive method of inspection.

ECT has developed rapidly since its practical introduction in the 1940s. ECT can be performed on any material that is electrically conducting. A brief overview of the industries and the areas that use ECT is shown below [24].

- Metal Industry – for the inspection of cracks, defects and any other flaws and their characterization, wall thickness, quality assurance, fatigue estimation, determination of hardness and coating thickness testing etc in steel production and steam and pressure vessel construction.
- Power stations – Conventional and nuclear power plants
- Civil engineering – inspection of bridges, concrete structures, infrastructure due to aging
- Aviation – fatigue estimation in aircraft surface and other parts
- Pipe inspection – inspection of pipes and piping systems in industrial plants

Unlike volumetric techniques such as radiography and ultrasonic, ECT, like liquid penetrant and magnetic particle techniques is a surface technique, and can only be used to detect surface and near surface defects.

In the case of testing materials with poor electrical conductivity Dielectric Analysis (DEA) techniques have been used [27-32]. DEA is based on the principles of electrostatics. Electrostatics is one of the oldest branches of physics, and it continues to this day to be an ever emerging field, and an important part of our daily lives. DEA techniques are non-destructive and can be used to relate molecular motions observed in an electrical field, to a variety of polymeric properties. Capacitive sensing dielectrometry is used to provide information for materials with poor conductivity in electroquasistatic applications [29]. Through measurements of the material electrical properties such as dielectric constant, conductivity, loss tangent or complex permittivity, information on things such as layer thickness, thermal conductivity, presence of defects, porosity and cure state can be obtained.

Dielectric analysis as a measurement tool in industry started more than 20 years ago, and is developing rapidly in industry today. Some of the industries and areas that dielectric analysis is used are shown below.

- Metal Industry – material characterization, presence of defects
- Pharmaceutical Industry – coating thickness of tablets, size of tablets
- Paper Industry – estimation of moisture and fiber concentrations in paper pulp
- Landmine detection – detection and imaging of plastic landmines
- Food Industry – estimating dielectric properties of various types of meat

1.3 Sensing based on Planar Electromagnetic Sensors

The sensors designed and fabricated for the non-contact measurement of material properties are of planar type and can be used in curved, bent surfaces. The operation principle is based on the electromagnetic field. A high frequency electric or magnetic field is created by the exciting coil of the sensor in the system under test. The system usually interacts with the high frequency electric [27-32] or magnetic field [15-21, 24-26] and modifies either or both. The modified field is usually detected by a separate coil known as the sensing coil or by the exciting

coil itself [24]. The modified field is usually manifested by a change of impedance or transfer impedance of the sensor [26]. The impedance or the change of impedances is related to the system properties in a very complex way. The impedance is used for the indirect determination of system properties. The detailed description and operating principle of the sensors are discussed in chapter 2.

1.4 Organization of the Thesis

This thesis is organized into nine chapters. After the general introduction in chapter 1, chapter 2 describes the configuration and operating principle of planar electromagnetic sensors. The finite element model formulation for the characterization of all three types of sensors, meander, mesh and interdigital configuration is described in chapter 3. Chapter 4 describes the experimental characterization of the sensors. The application of the sensors for the non-invasive determination of fat content in milk has been investigated and the details are given in chapter 5. The application of the sensors for the quality inspection of saxophone reeds is described in chapter 6. The main contribution of the work done for this thesis is the experiments conducted to observe the interaction of planar sensors to pork belly cuts, and the non-invasive estimation of fat content of pork meat, which is described in chapter 7. Chapter 8 describes the development of a low cost sensing instrumentation system based on the Cygnal 8051CF020 mixed signal microcontroller. Finally the work is concluded in chapter 9.

CHAPTER 2

DESCRIPTION OF THE SENSORS

2.1 Introduction

Three types of sensors, meander, mesh and interdigital, have been designed and fabricated to study the interaction of these sensors on conducting, magnetic and dielectric materials. The sensors are of planar type and have a very simple structure. They have been fabricated using simple printed circuit board (PCB) fabrication technology. The operating principle of these sensors is based on the interaction of the electromagnetic field generated by the sensors with the neighboring materials under investigation [25]. Meander, mesh, interdigital or a combination of the three can be used depending on the application.

2.2 Planar Meander and Mesh type Sensors

The representation of the sensors is shown in figure 2.1. The sensor consists of two coils: one coil is known as the exciting coil and the other coil is known as the sensing coil. The exciting coil carries high frequency current and generates a high frequency electromagnetic field on the system under test. The induced electromagnetic field in the testing system will generate eddy currents on the system under test, given that the material under test is of conducting or magnetic type. Due to the flow of eddy current the induced field in the testing system will modify the generated field, and the resultant field will be detected by the pick-up coil or sensing coil, which is placed above the exciting coil [24-26].

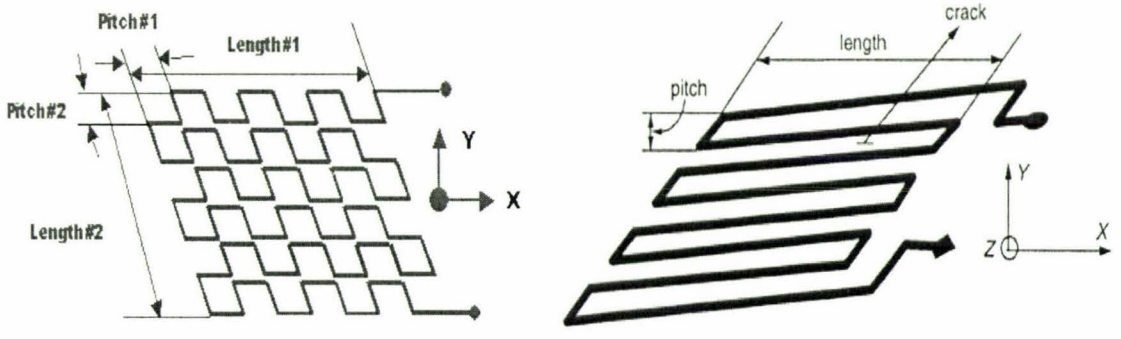

(a) Mesh type (b) Meander type

Figure 2.1: Configuration of planar electromagnetic sensors

The sensor can be either of a meander type or of a mesh type, the type of sensors to be chosen depending on the applications. Meander type sensing coils used for testing the integrity of materials has been reported in [17-19, 24-26]. If the meander type sensor is used to detect cracks in a metal, the disadvantage is that the performance of the sensor is not independent of the alignment of the cracks or non-homogeneity of the material structure (in the process of evaluating material integrity), with respect to the sensor configuration (figure 2.1b) [26]. To overcome this problem the mesh type sensor (figure 2.1a) has been developed [22-26]. In the mesh type sensor the eddy currents take a more circular pattern thus dismissing the geometry/alignment effects encountered in meander type sensors, with the material under test.

The structural configuration of the planar type sensor is shown in Fig. 2.2. The exciting coil and the sensing coil are separated by a polyimide film of 50μm thickness. In order to improve the directivity of flux flow a magnetic plate of NiZn is placed on top of the sensing coil [24]. The size of the sensor depends on the number of pitches used in that. The optimum pitch size depends on the application [14].

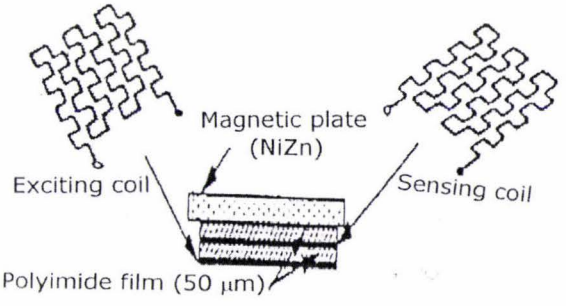

Figure 2.2: Structure of the sensor

2.3 Design and Fabrication of Sensors

Three meander type and four mesh type sensors of varying lengths and pitches (table 2.1 and 2.2) were designed on Protel DXP 2004. The sensor schematics are shown in figure 2.3 and 2.4.

Table 2.1: Meander sensor parameters

Sensor	Pitch (mm)	Length (mm)
1	2	20
2	5	25
3	6	30
4	8	40

Table 2.2: Mesh sensor parameters

Sensor	Pitch 1 (mm)	Pitch 2 (mm)	Length 1 (mm)	Length 2 (mm)
1	2	2.5	10	10
2	3	3.5	14	14
3	3	3.5	20	14
4	4	5	27	18

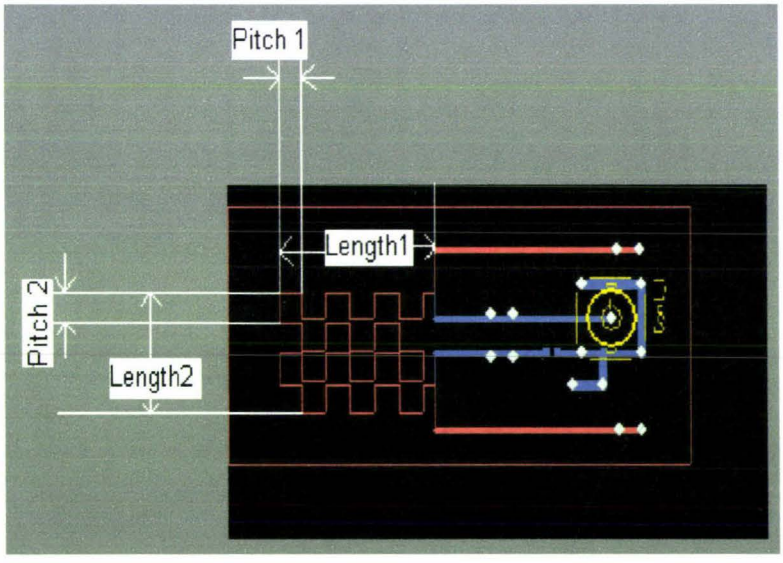

Figure 2.3: Schematic diagram of mesh type sensor

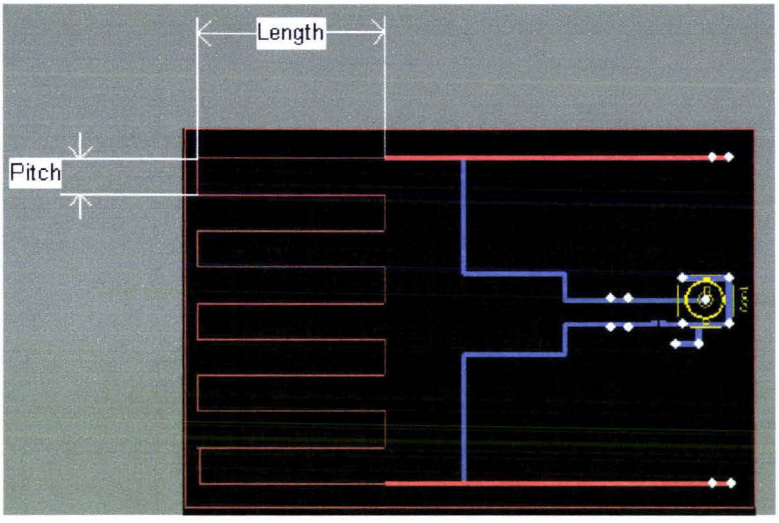

Figure 2.4: Schematic diagram of meander type sensor

It is seen from the diagrams that the coils are connected to a Bayonet Neill Concelman (BNC) connector. The BNC connector is normally connected to a AC voltage source through a coaxial cable. The AC voltage source drives the exciting coil. Since the resistance of the coil is very low the sensing voltage is measured across a resistor of an appropriate value. The two coils (exciting and sensing) are designed on top of each other but on opposite sides. On the schematics above the colour blue represents the exciting coil while red represents the sensing coil. The exciting coil cannot be seen as the sensing coil overlaps it. The fabricated sensors are shown in figures 2.5 and 2.6.

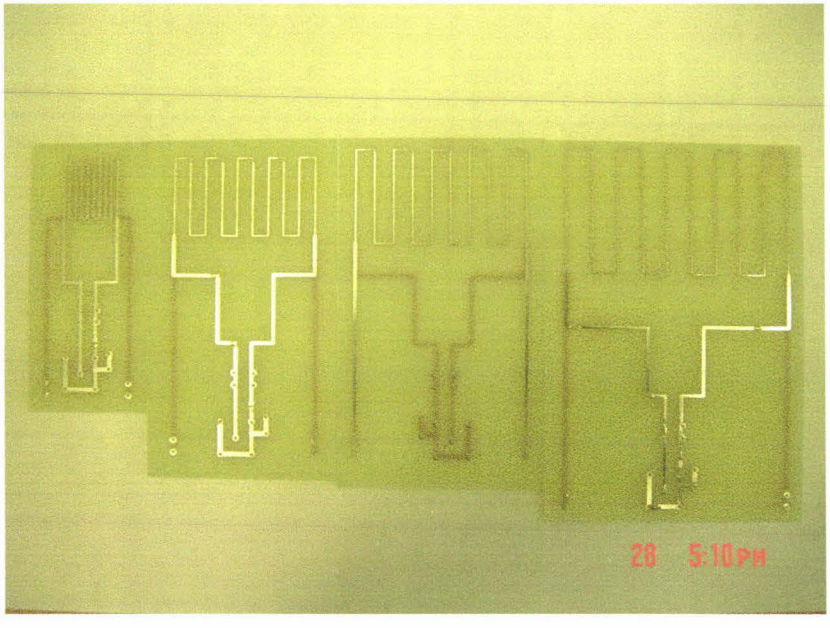

Figure 2.5: Fabricated meander type sensors

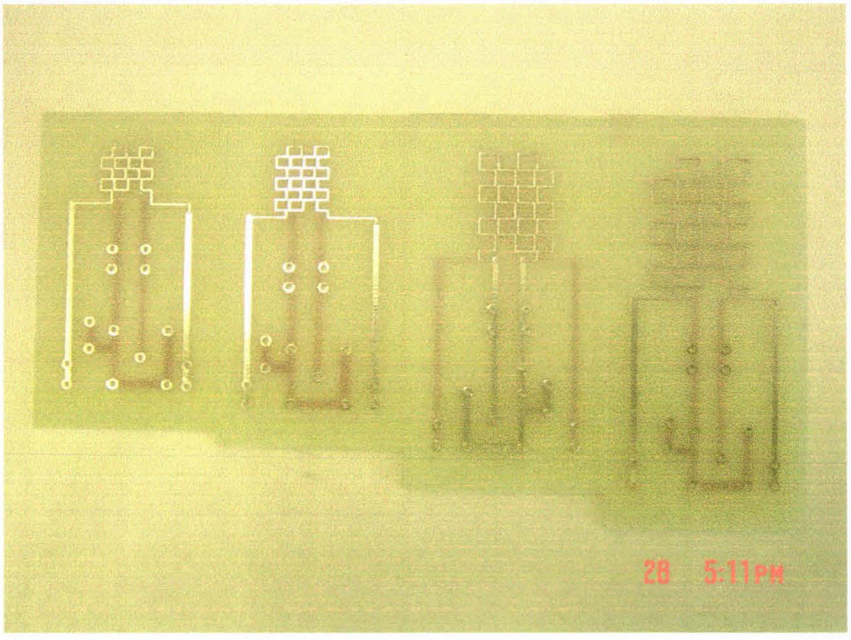

Figure 2.6: Fabricated mesh type sensors

2.4 Planar Interdigital Sensors

The operating principle behind the interdigital sensor is very similar to the one observed in a parallel plate capacitor [29]. Figure 2.7 shows the relationship between a parallel plate capacitor and an interdigital sensor, and how the transition occurs from the capacitor to a sensor. There is an electric field between the positive and negative electrodes and figure 2.7a, b and c shows how these fields pass through the material under test (MUT). Thus material dielectric properties as well as the electrode and material geometry affect the capacitance and the conductance between the two electrodes.

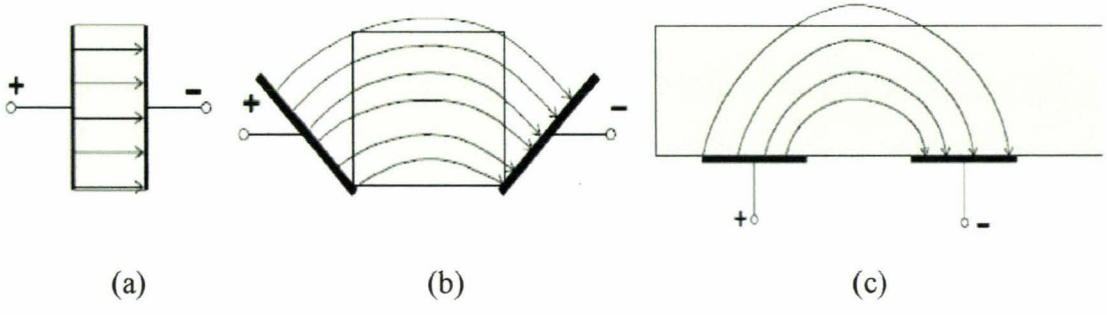

(a) (b) (c)

Figure 2.7: An interdigital sensor can be visualized as a parallel plate capacitor whose electrodes open up to provide a one sided access to the MUT

The electrodes of an interdigital sensor are coplanar [29]. Hence, the measured capacitance will have a very low signal-to-noise ratio. In order to get a strong signal the electrode pattern can be repeated many times. This leads to a structure known as an interdigital structure. The term "interdigital" refers to a digit-like or finger-like periodic pattern of parallel in-plane electrodes, used to build up the capacitance associated with the electric fields that penetrate into a material sample [29]. This is shown in figure 2.8 and the side view shown in figure 2.9. In figure 2.8 one set of electrodes are connected or driven by an AC voltage source while the other set are connected to ground. An electric field is formed between the driven and the ground electrodes. This can be seen more clearly in figure 2.9. It can be seen that the depth of penetration of the electric field lines vary for different wavelengths. The wavelength (λ) of interdigital sensors is the distance between two adjacent electrodes of the same type. In figure 2.9 there are three lengths (l_1, l_2 and l_3) showing the different penetration depths with respect to the wavelength of the sensor.

Planar interdigitated array electrodes have many applications such as gas detection [28], determining components in aqueous solutions [30], estimation of fiber, moisture and titanium dioxide in paper pulp [31, 32] and complex permittivity characterization of materials [27].

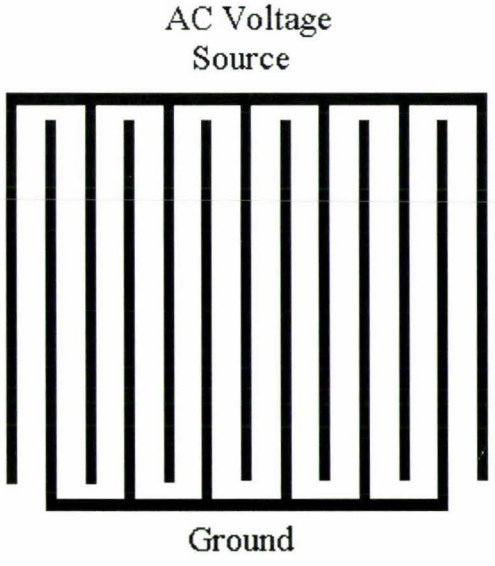

Figure 2.8: Interdigital sensor structure, where the electrodes follow a finger-like or digit-like pattern

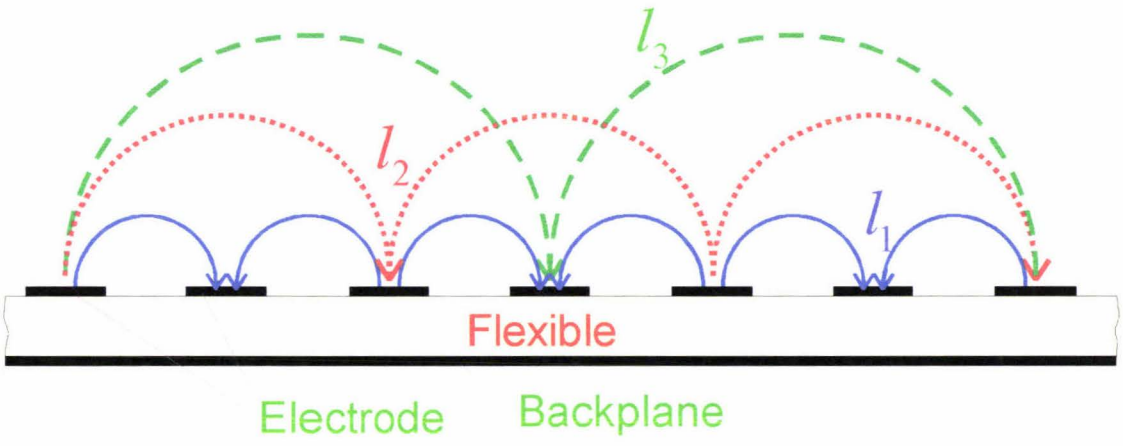

Figure 2.9: Electric field formed between driven and ground electrodes for different wavelengths

2.5 Design and Fabrication of Interdigital Sensors

Four interdigital sensors of different wavelengths and lengths were designed on Protel DXP 2004. The sensor parameters are shown in table 2.3 below. The sensor schematic is shown in figure 2.10.

Table 2.3: Interdigital sensor parameters

Sensor	Wavelength, λ (mm)	Length (mm)
1	5	20
2	6	30
3	8	40
4	10	50

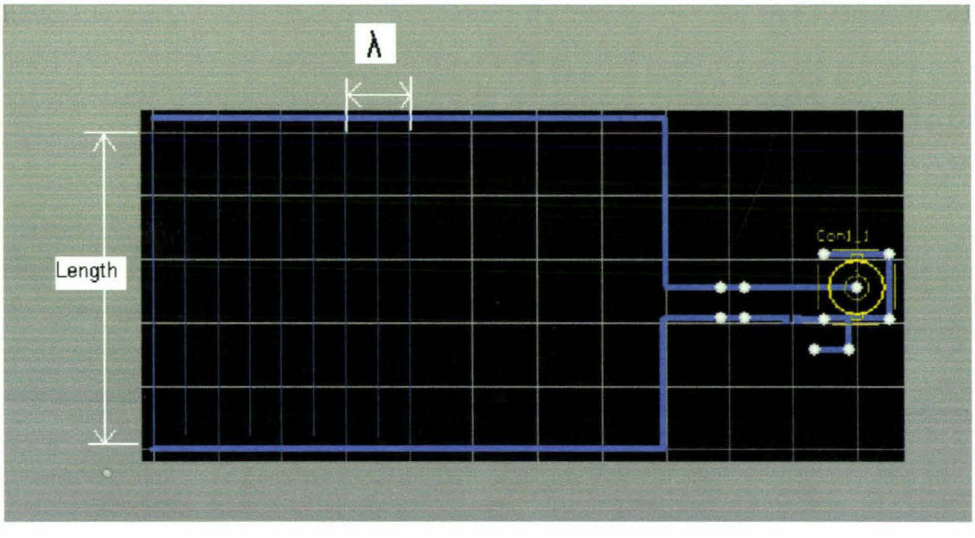

Figure 2.10: Schematic diagram of interdigital type sensor

The schematic diagram in figure 2.10 shows an interdigital sensor with 9 electrodes. The BNC connector is connected to an AC voltage source, which in turn is connected to 4 electrodes as shown above. These four electrodes act as the excitation/driving electrodes. The other five electrodes are connected to ground. When there is a material between the electrodes the electric fields from the driving electrodes penetrates through most of the material that is under test, and then terminates on the sensing electrodes. The electric field lines are affected by the dielectric properties of the material under test [27, 29, 31, 32]. Thus the potential or the current at the sensing electrodes is also a function of the material's dielectric properties. The advantage of using interdigital sensors is that it has only one sided access to the material under test [29]. Fabricated sensors are shown in figure 2.11.

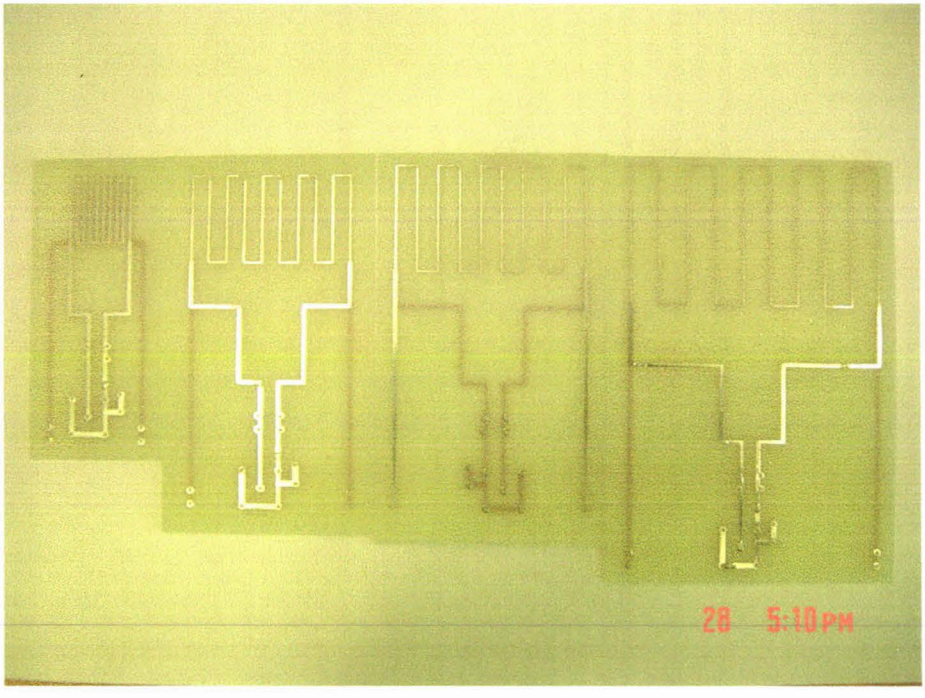

Figure 2.11: Fabricated interdigital type sensors

2.6 Conclusion

Three different types of planar electromagnetic sensors are described in this chapter: meander, mesh and interdigital configuration. The sensors are used for the estimation of material properties in a non-invasive way, non-destructive way. The sensors generate a high frequency electromagnetic field by carrying an alternating current. The generated electromagnetic field interacts with the material under test and is modified. The modified field is measured and is used for the estimation of system properties in an indirect way.

CHAPTER 3

FINITE ELEMENT MODELING OF SENSORS

3.1 Introduction

In this chapter the characterization of all types of sensors, meander, mesh and interdigital types have been carried out using finite element modeling. Before experimentation all three sensors are modeled to analyze the distribution of electric field and magnetic flux. The finite element software FEMLAB by COMSOL is used to model and analyze the field distribution of all three types of sensors. FEMLAB solves all kinds of scientific and engineering problems based on partial differential equations (PDEs).

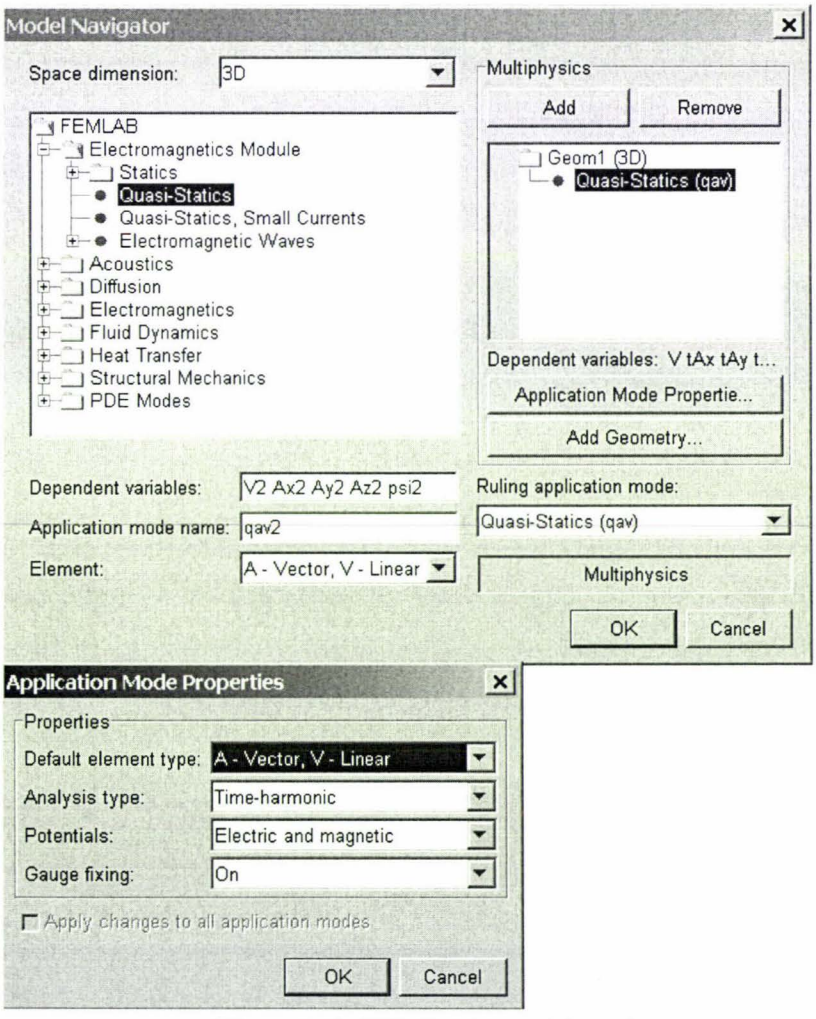

Figure 3.1: FEMLAB model navigator

In the model navigator "Multiphysics" is chosen since electric and/or magnetic fields are used to model the three types of sensors. Electromagnetics Module in 3-D mode is selected and then Quasi-statics (qav) mode is chosen as shown in figure 3.1.

One of the effects of Maxwell's equation is that there is no synchronization between the changes of the electromagnetic field and changes in time of currents and charges. Due to the finite speed of propagation of electromagnetic waves the changes of the fields are always not in line with respect to the changes of the sources. Quasi-static approximation involves ignoring this effect, and obtaining electromagnetic fields by considering stationary currents at every instant. The approximation can be considered valid given that the variations in time are small, and that the models are considerably smaller than the wavelength.

Quasi-static analysis is used for the modeling of the three types of sensors. In quasi-static analysis it is assumed that $\frac{\partial D}{\partial t} = 0$ [3.1]

Hence Maxwell's equations can be written as:

$$\nabla \times H = J = \sigma(E + v \times B) + J^e \quad [3.2]$$

$$\nabla \times E = -\frac{\partial B}{\partial t} \quad [3.3]$$

$$\nabla \bullet B = 0 \quad [3.4]$$

$$\nabla \bullet D = \rho \quad [3.5]$$

$$\nabla \bullet J = 0 \quad [3.6]$$

Table 3.1: Symbols used in the derivation

Symbol	
H	Magnetic field Strength
J^e	Externally applied current density
σ	Electrical conductivity
E	Electric field intensity
v	Velocity of the conductor
B	Magnetic flux density
ρ	Volume charge density
D	Electric flux density

It is important that the currents and the electromagnetic field vary slowly in a quasi-static approximation.

Using the definitions of the potentials,

$$B = \nabla \times A \qquad [3.7]$$

$$E = -\nabla V - \frac{\partial A}{\partial t} \qquad [3.8]$$

And the relationship between magnetic field, magnetic field strength and Magnetization (M)

$$B = \mu_0 (H + M) \qquad [3.9]$$

Ampere's law can be rewritten as

$$\sigma \frac{\partial A}{\partial t} + \nabla \times (\mu_0^{-1} \nabla \times A - M) - \sigma v \times (\nabla \times A) + \sigma \nabla V = J^e \qquad [3.10]$$

Where A = magnetic vector potential and μ_0 is the magnetic permeability of free space

Taking the divergence of the equation above gives the equation of continuity

$$-\nabla.(\sigma \frac{\partial A}{\partial t} - \sigma v \times (\nabla \times A) + \sigma \nabla V - J^e) = 0 \qquad [3.11]$$

In the "Application Mode Properties" dialog box the default element type is given as A-Vector and V-Linear. Equations 3.10 and 3.11 give a system of equations for A and V.

A time harmonic analysis is chosen as the "Analysis Type" and both electric and magnetic fields are chosen as the potentials. "Gauge Fixing" is turned on. Gauge transformation involves a variable transformation of the potentials. The electric and magnetic fields are not uniquely defined through the electric and magnetic potentials (equations 3.7 and 3.8).

Introducing two new potentials

$$\tilde{A} = A + \nabla \Psi$$

$$\tilde{V} = V - \frac{\partial \Psi}{\partial t} \qquad [3.12]$$

When substituted into equations 3.7 and 3.8 they give the same electric and magnetic fields,

$$E = -\frac{\partial A}{\partial t} - \nabla V = -\frac{\partial(\tilde{A} - \nabla\Psi)}{\partial t} - \nabla(\tilde{V} + \frac{\partial\Psi}{\partial t}) = -\frac{\partial\tilde{A}}{\partial t} - \nabla\tilde{V} \qquad [3.13]$$

$$B = \nabla \times A = \nabla \times (\tilde{A} - \nabla\Psi) = \nabla \times \tilde{A} \qquad [3.14]$$

A particular gauge is chosen to obtain a unique solution. This means that constraints are put on Ψ . A constraint can also be put on $\nabla.A$. If both $\nabla.A$ and $\nabla \times A$ are given a vector field can be uniquely defined up to a constant (Helmholtz's theorem). Coulomb gauge ($\nabla.A$ =0) is used.

The inductance (mesh and meander) and capacitance (interdigital) are calculated for a range of frequencies. Hence Time-Harmonic Quasi-Statics is used. In 3-D time-harmonic quasi-statics, both the electric and magnetic fields are used as the potentials. There is full coupling between both the fields.

The equations are

$$-\nabla.((j\omega\sigma - \omega^2\varepsilon_0)A - \sigma v \times (\nabla \times A) + (\sigma + j\omega\varepsilon_0)\nabla V - (J^e + j\omega P)) = 0 \qquad [3.15]$$

$$(j\omega\sigma - \omega^2\varepsilon_0)A + \nabla \times (\mu_0^{-1}\nabla \times A - M) - \sigma v \times (\nabla \times A) + (\sigma + j\omega\varepsilon_0)\nabla V = J^e + j\omega P \qquad [3.16]$$

where $\omega = 2 \times \pi \times f$ (frequency)

ω is the angular frequency and f is the frequency

$D = \varepsilon_0 E + P$ is used for the electric field, where P is electric polarization

3.2 Analysis of Planar Meander Sensor

The meander sensor has winding tracks [15, 17-19, 24] on the sensor substrate as shown in figure 3.2. The aim of the modeling is to calculate the inductance of the meander coil for a frequency range of 1 kHz to 10MHz, when placed in an environment. From the inductance the inductive reactance can be calculated and the plotted against the frequency to see their relationship.

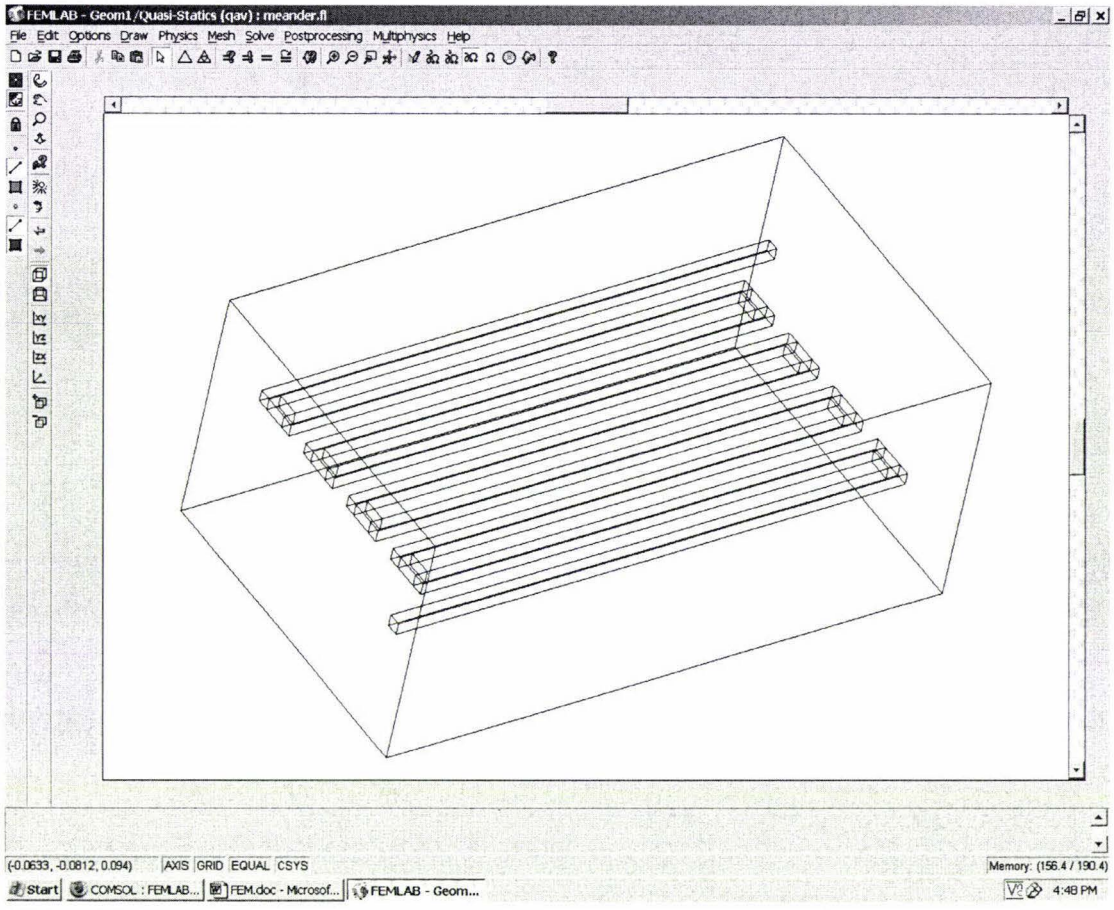

Figure 3.2: Model of meander type sensor

The Reactance is calculated by

$$X_L = 2 \bullet \pi \bullet f \bullet L \qquad [3.17]$$

where f is the frequency and L is the inductance calculated from the model

The meander sensor is modeled as shown above in figure 3.2. The large rectangular block that surrounds the sensor acts as the environment the sensor is exposed to. The sensor is initially modeled by individual blocks as shown in figure 3.3a. The individual blocks are then connected together by creating a composite object of all the individual objects as shown in figure 3.3b. The sensor block and the environment box are then made into one object as in figure 3.4.

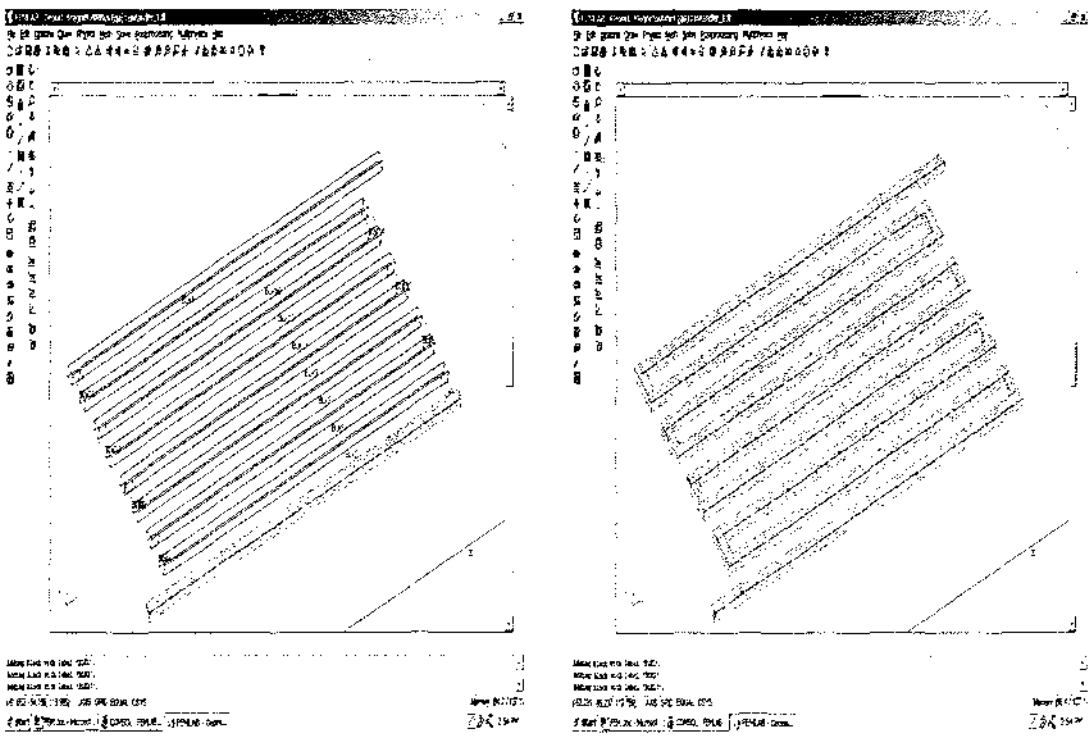

(a) (b)

Figure 3.3: Geometry of meander type sensor

In the "Boundary Settings" menu each boundary is defined according to the required condition. The two sides of the sensor are provided an electric potential; one is assumed to be at ground potential and the outer side is kept at a value of 1V. All plates in the rectangular box except the ones touching the sensor voltage and ground boundaries are set to "Electric Insulation". All boundaries are set to "Magnetic Insulation" in the Magnetic Parameters menu. The menu for setting the boundary conditions is shown in figure 3.4.

The electrical conductivity, relative permittivity and relative permeability are set in the "Subdomain Settings" menu. The model has two subdomains: the sensor and the rectangular box. Figure 3.5 shows the window for setting the subdomain. There are two main regions, copper and air. The frequency of operation can be set in the "Scalar Variables" dialog box. Figure 3.6 shows the model after the meshing.

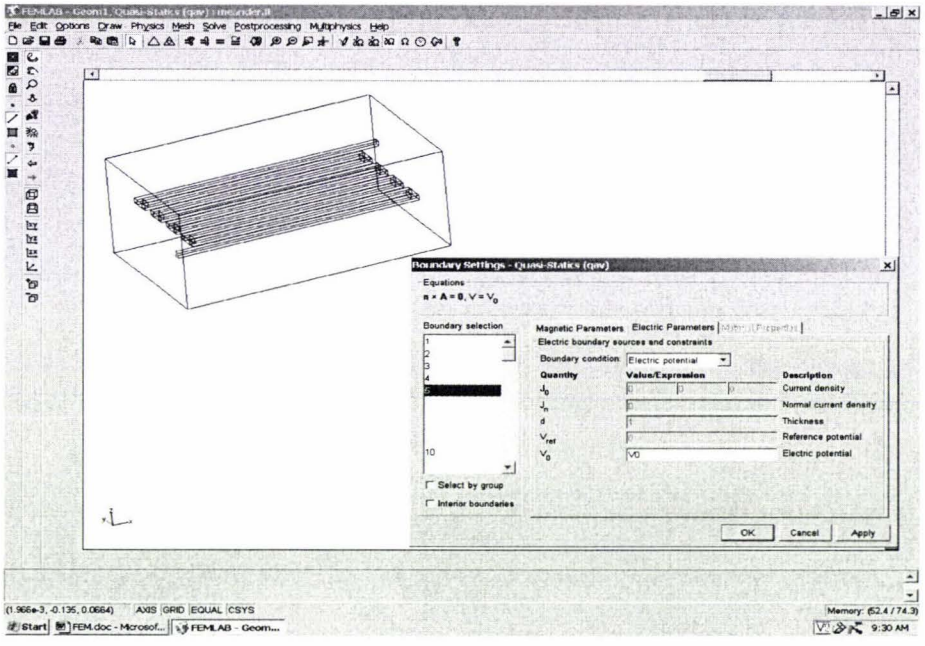

Figure 3.4: Window for boundary setting

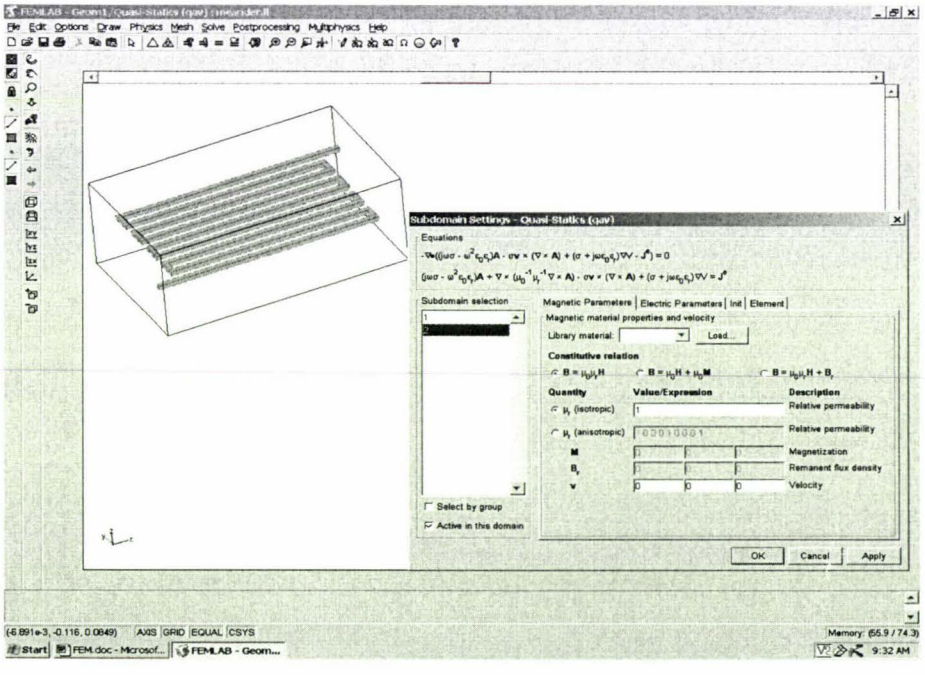

Figure 3.5: Window for subdomain setting

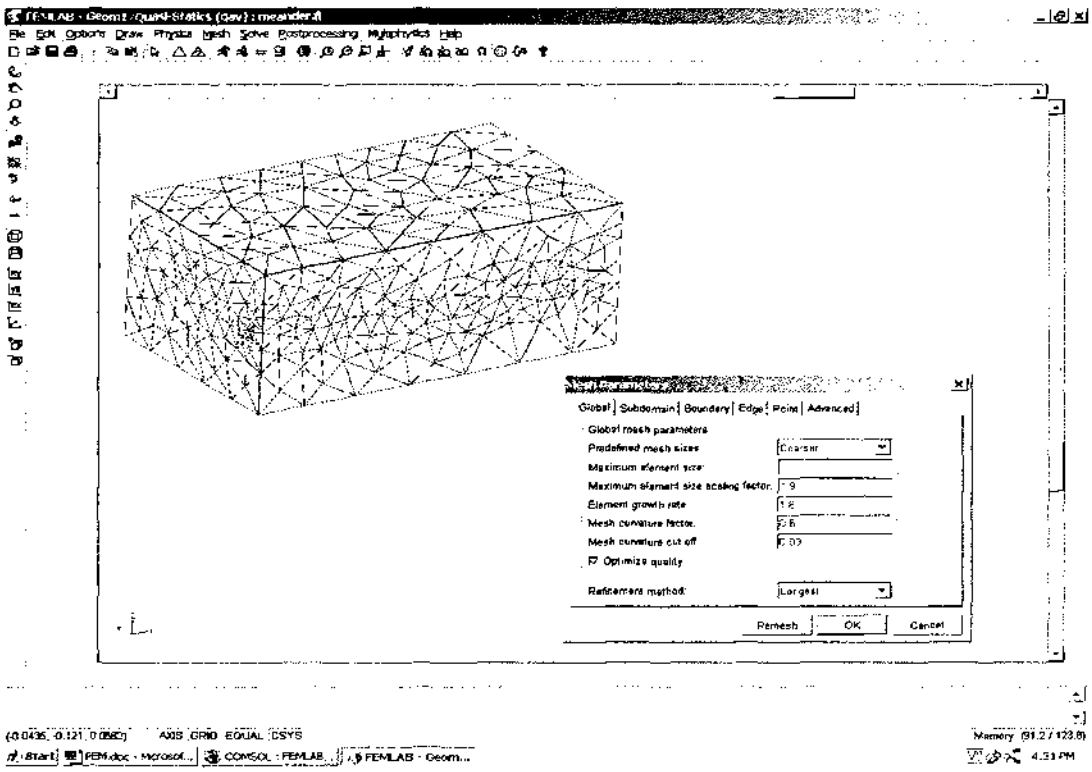

Figure 3.6: Mesh of the model

Figure 3.7 shows the required setting for solving the problem.

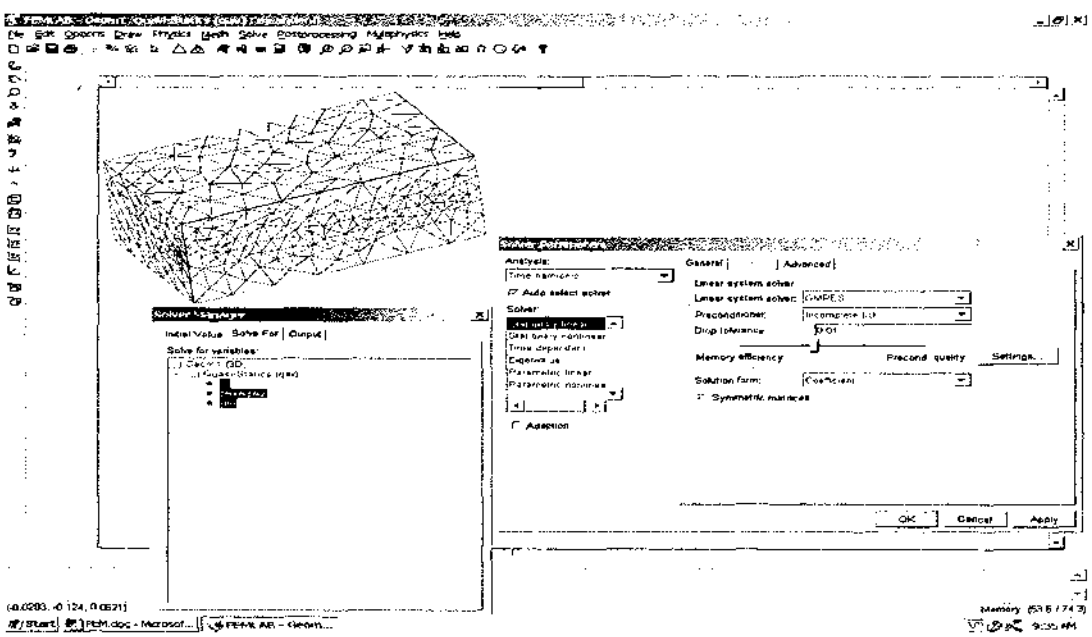

Figure 3.7: Solve menu

Figure 3.8 shows the solved meander sensor model for 500 kHz. The "tube streamlines" and the arrows represent the magnetic flux density while the electric potential distribution is shown on the surface of the sensor. While the electric potential ranges from 0 to 1 on the surface of the sensor the magnetic flux density has a range from 4.026e-7 Tesla to 1.073e-4 Tesla.

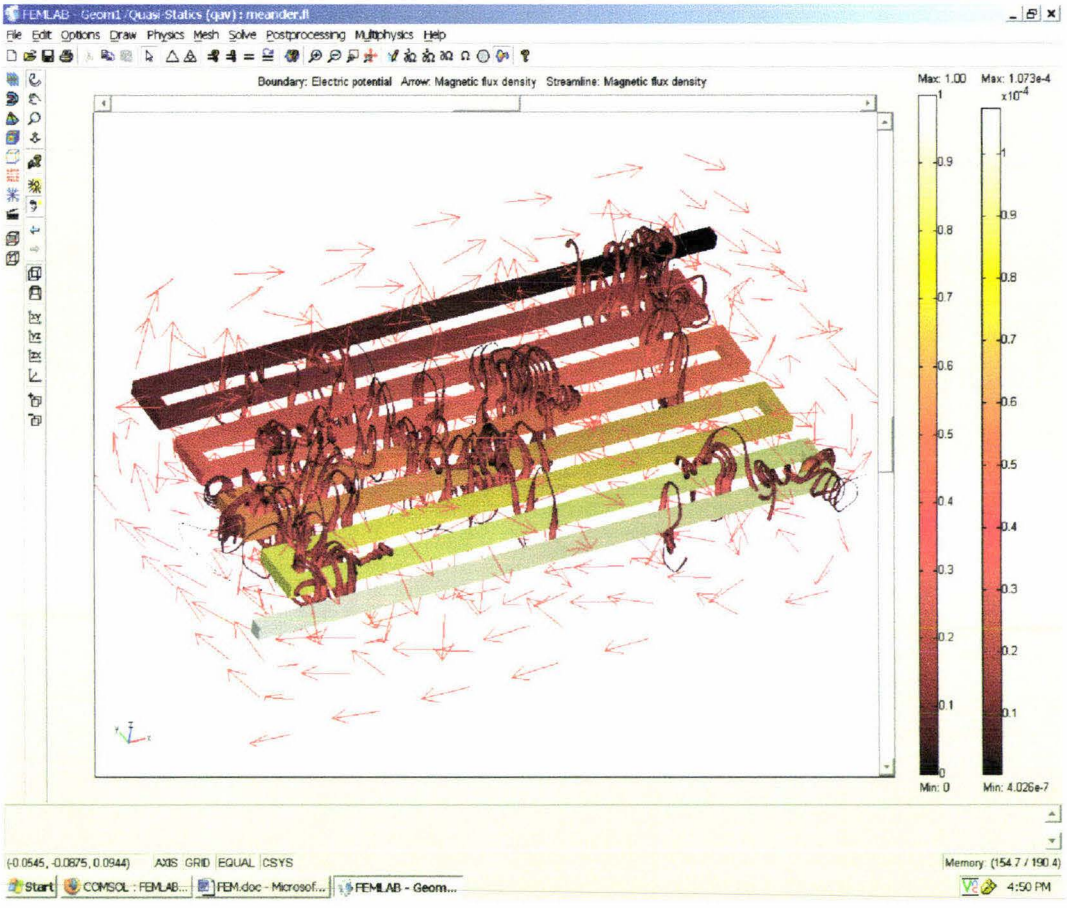

Figure 3.8: Solved meander model

Once the solution is obtained different parameters can be calculated. For the meander sensor the important parameter is the inductance. The inductance is calculated by

$$L = \frac{2W_m}{I^2} \qquad [3.18]$$

where W_m is the magnetic energy stored, and I is the current flowing in the sensor.

The calculation of magnetic energy and current are done using the postprocessing menu with the help of subdomain and boundary integration. Once the inductance is obtained, the operating frequency is changed. The solution and postprocessing is repeated to obtain the new value of inductance. The reactance of the sensor is plotted as a function of frequency. It is seen that the reactance increases with the increase in frequency. This indicates the meander sensor behaves as an inductive sensor.

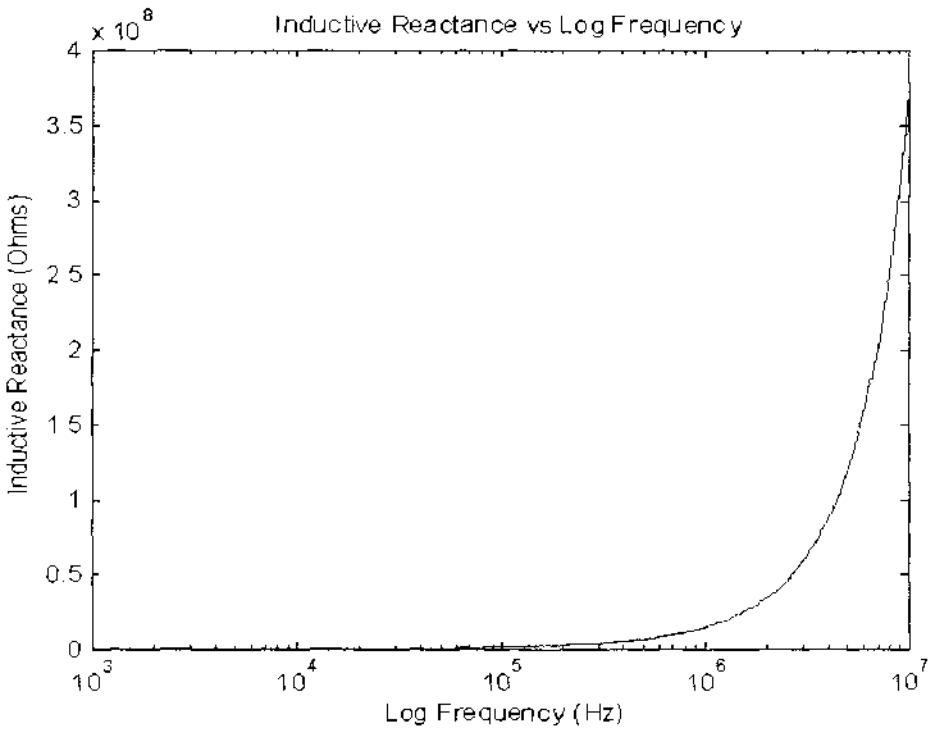

Figure 3.9: Variation of reactance with frequency

3.3 Analysis of Planar Mesh Sensor

The mesh sensor principles are very much similar to the meander sensor. The pattern of the windings [25, 26] is different to the meander sensor as shown in figure 3.10. The frequency range for calculating inductance remains the same, from 1 kHz to 10MHz. The inductance is calculated the same way as the meander sensor.

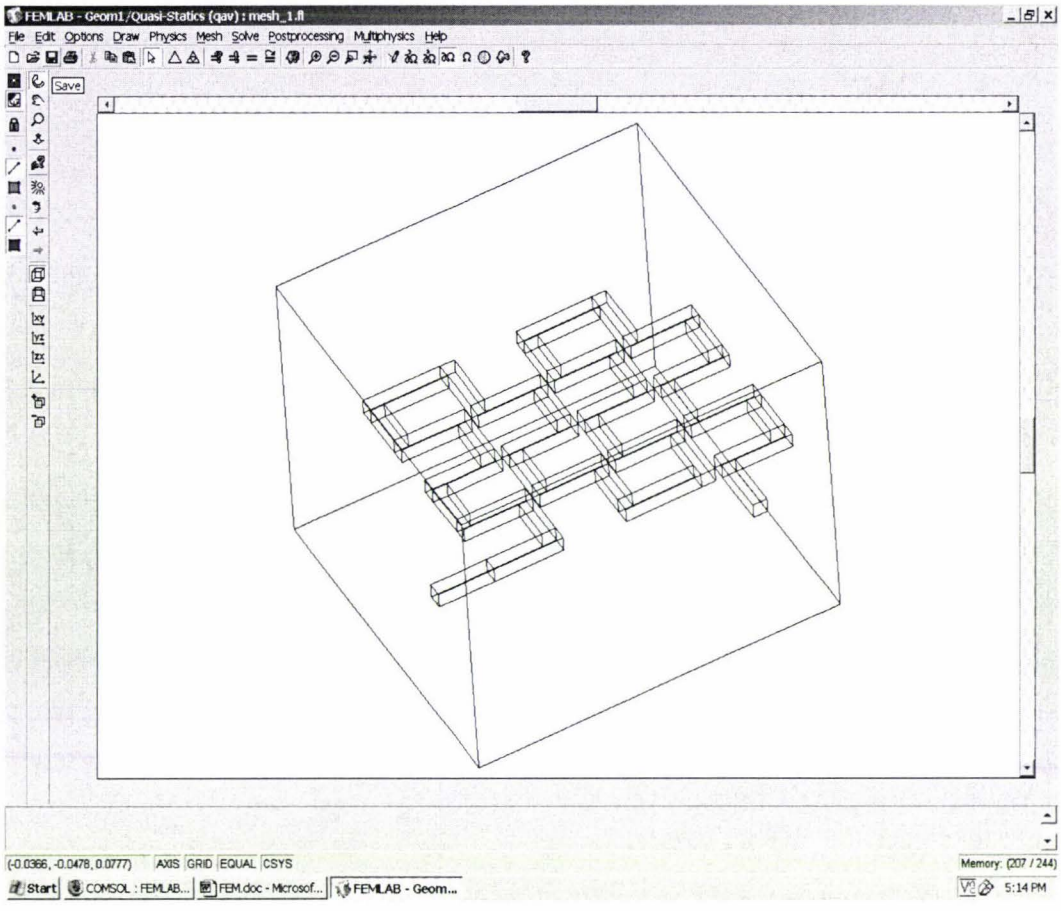

Figure 3.10: Model of mesh type sensor

The sensor block and the rectangular block are made into one. One end of the sensor is given an electric potential of 1 whereas the other end is set to ground. All plates in the rectangular box except the ones touching the sensor voltage and ground boundaries are set to "Electric Insulation". All boundaries are set to "Magnetic Insulation" in the Magnetic Parameters menu.

The electrical conductivity, relative permittivity and relative permeability can be set in the "Subdomain Settings" menu. The two subdomains are set exactly like in the meander sensor and meshed before solving. The "Solver Parameter" and "Solver Manager" settings are the same as for the meander sensor. Figure 3.11 shows the solution of the mesh sensor.

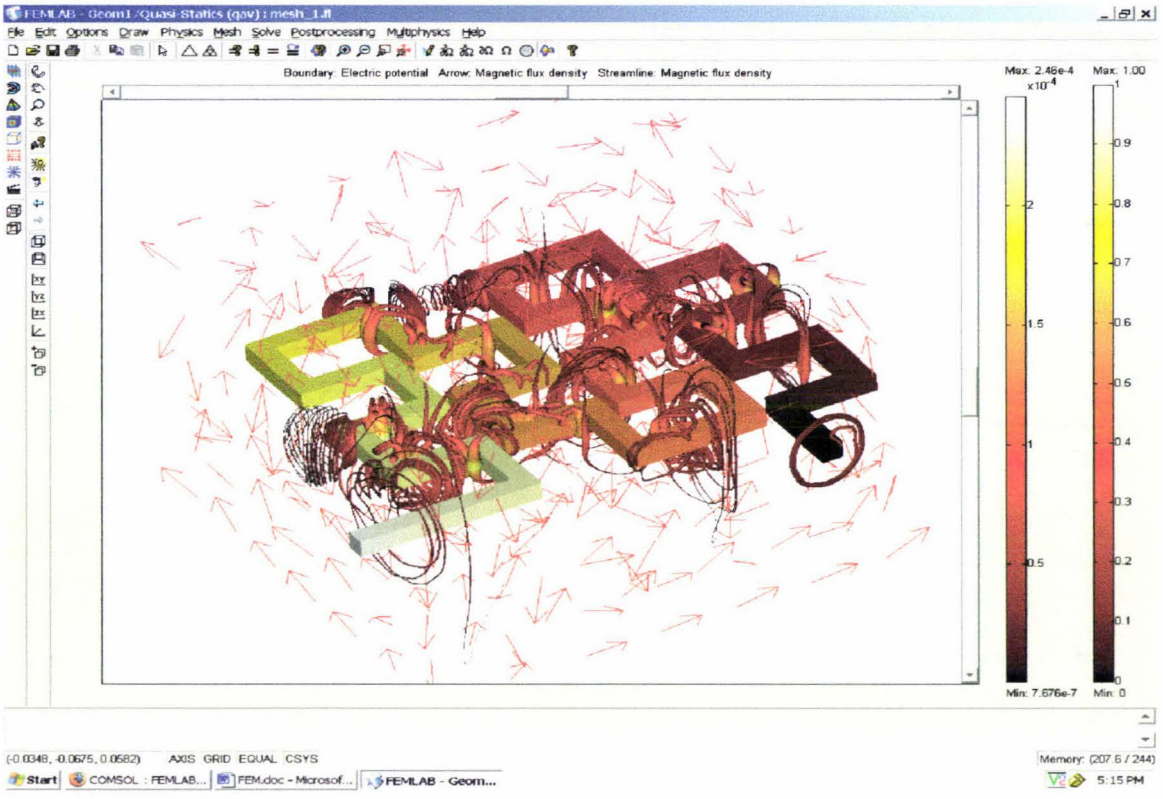

Figure 3.11: Solved mesh model

The mesh sensor results are similar to that of the meander sensor. The "tube streamlines" and the arrows represent the magnetic flux density while the color distribution on the sensor surface represents the electric potential. The results show how magnetic flux is distributed at a frequency of 500kHz. While the electric potential ranges from 0 to 1 along the sensor blocks the magnetic flux density has a range from 7.67e-7 Tesla to 2.46e-4 Tesla. The magnetic energy and the current are calculated the same way as in the meander sensor to get the inductance. Figure 3.12 shows the variation of reactance of the mesh sensor as a function of the frequency. The reactance increases with frequency which indicates that the planar mesh sensor is inductive type too.

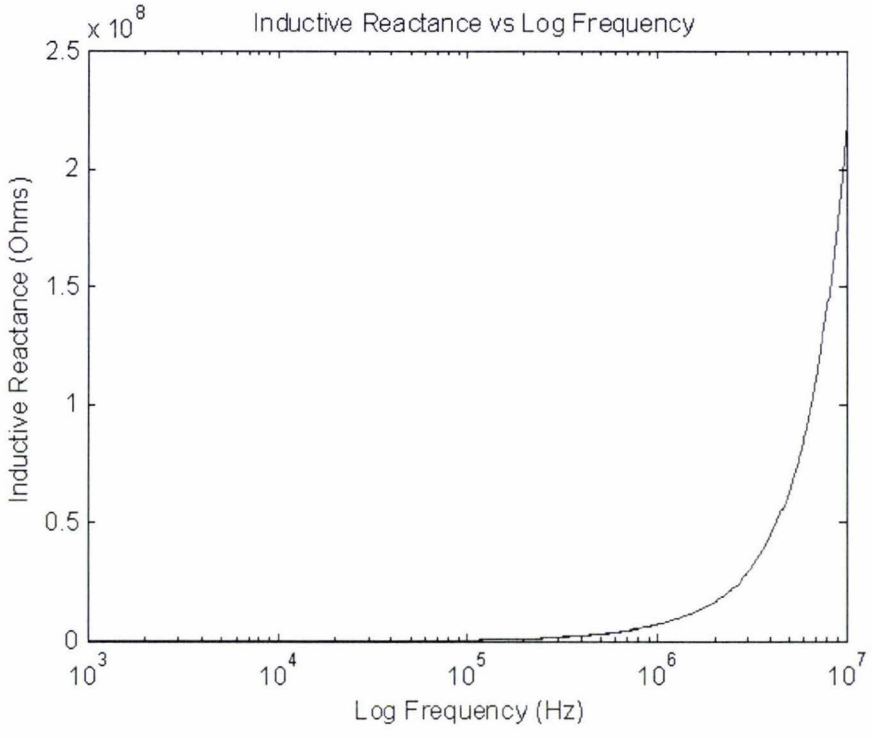

Figure 3.12: Variation of reactance with frequency

3.4 Analysis of Planar Interdigital Sensor

The interdigital orientation has one set of electrodes connected to a voltage and the others to ground. This forms the basis of a parallel plate capacitor [29]. As shown in figure 3.13a below the colored blocks are given a voltage of 1V whereas the white electrodes are set to ground. An electric field is thus formed between the voltage and the ground electrodes. The sensor blocks are made into one block. Then the sensor block along with the rectangular box is made into one block as shown in figure 3.13b.

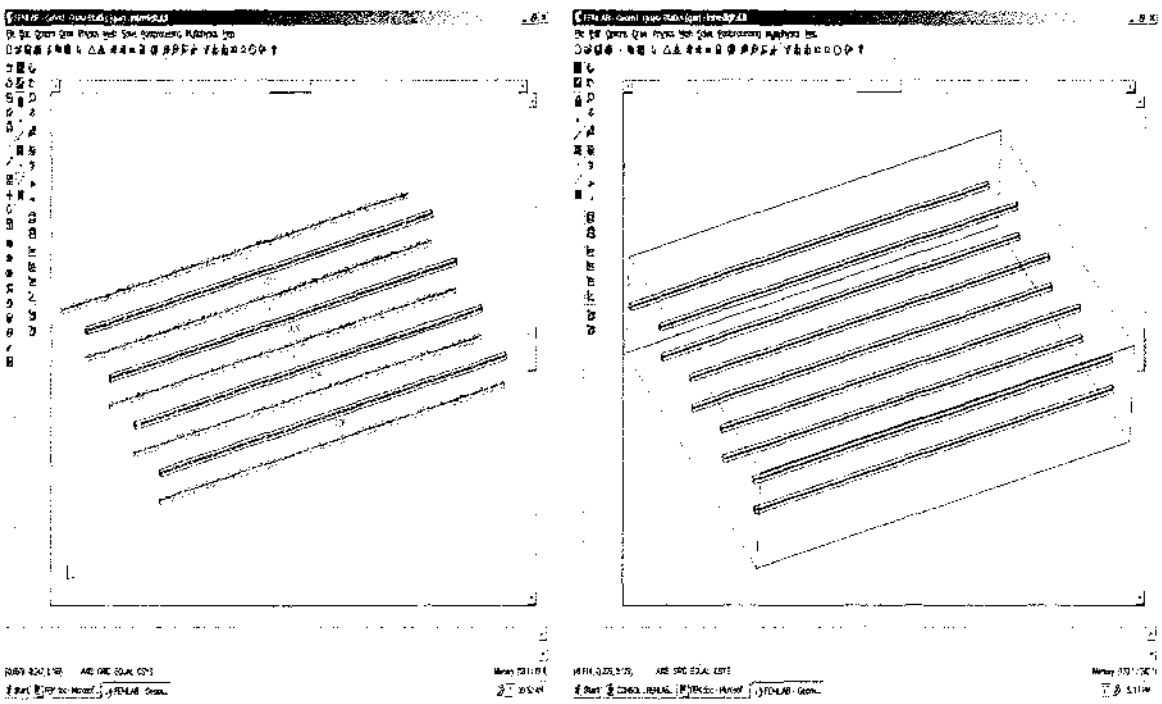

(a) (b)

Figure 3.13: Geometry of interdigital type sensor

The capacitance of the sensor electrodes can be calculated by

$$C = \frac{2W_e}{V_0^2} \qquad [3.19]$$

where W_e is the stored electrical energy and V_0 is the applied voltage

The capacitance is calculated for a frequencies ranging from 1kHz to 10MHz. From the capacitance the capacitive reactance (X_c) can be calculated by

$$X_c = \frac{1}{2\pi fc} \qquad [3.20]$$

where f is the frequency of operation and C is the capacitance calculated from the model

The permittivity value is also varied to see the effect of permittivity on the capacitanee and hence the capacitive reactance. In the "Subdomain Settings" permittivity of the rectangular box, which acts as the environment the sensor is exposed to, is set to 1 initially and then to 10

and 100. The capacitance is calculated for each setting and plotted. The conductivity of the electrodes is given a value of 5.8e7 S/m and a permittivity of 1 for all settings. The permeability remains at 1 for both the sensor and the rectangular box. The conductivity of the box also remains at 1 for all settings. The meshing procedure remains the same as meander and the mesh sensors. The "Solver Parameter" and "Solver Manager" settings are the same as for the mesh and meander sensors.

The electric field distribution of the interdigital sensor is shown by the arrows and the "tube streamlines" in figure 3.14. From the figure it is apparent that there is an electric field between the driven and ground electrodes that ranges from 0.396 to 1090.098 V/m.

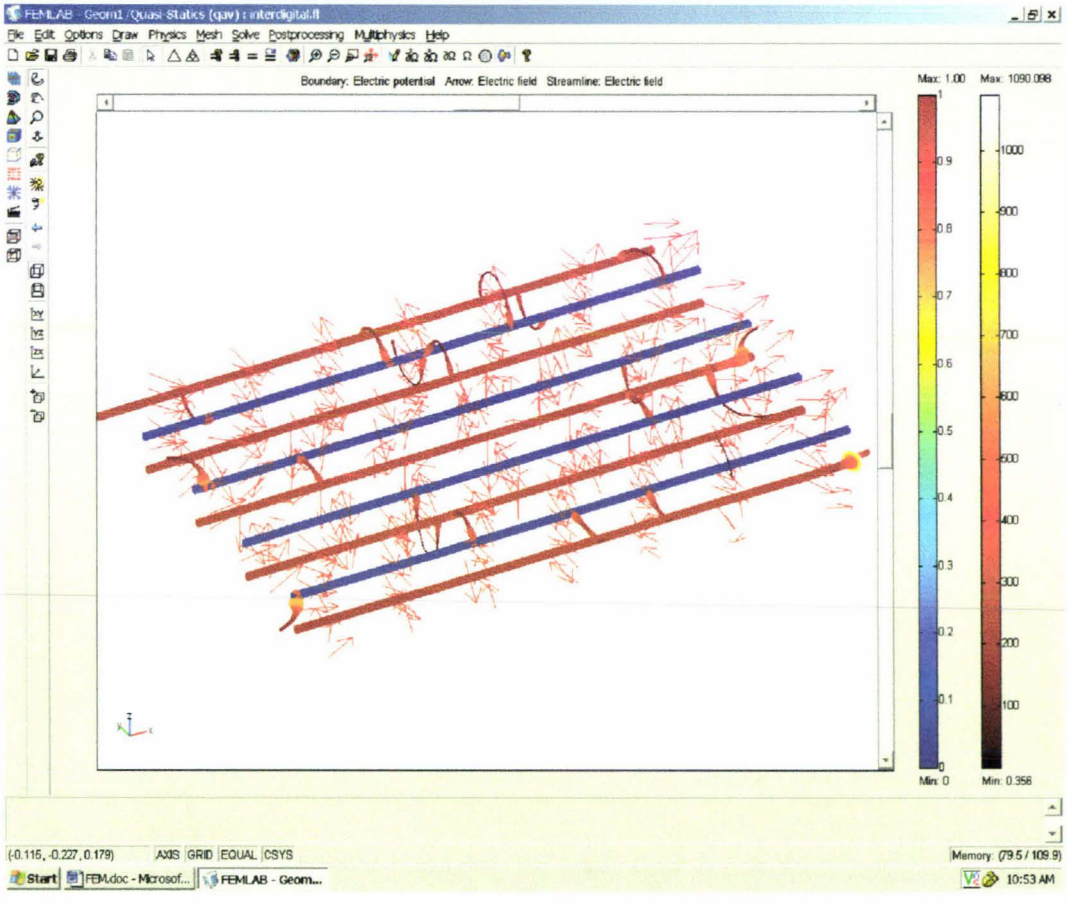

Figure 3.14: Solved interdigital model

The graph in figure 3.15 above shows variation of reactance with frequency. Unlike the meander and mesh sensors, capacitive reactance decreases with an increase in frequency. It can

also be deduced from the graph that the value of reactance decreases with an increase in permittivity. Since the interdigital sensor is the type of sensor used for the major experiments on this thesis, it is important to see how the permittivity affects the capacitive reactance.

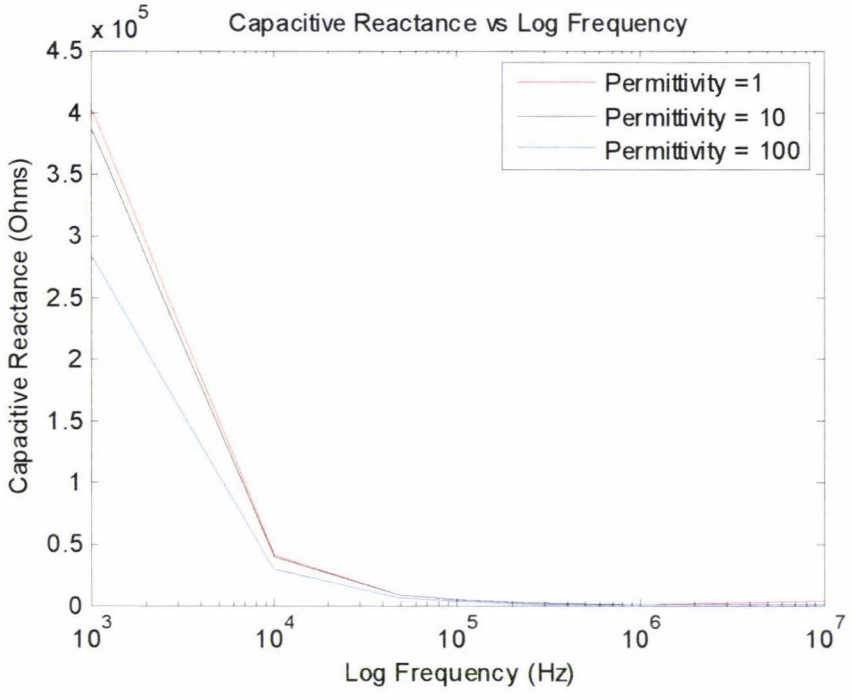

Figure 3.15: Variation of reactance with frequency

3.5 Conclusion

In this section the modeling of planar type sensors of meander, mesh and interdigital configuration have been carried out for the analysis of field distribution, using the finite element software package FEMLAB. The impedance of the sensors as a function of frequency has been calculated. It is seen that the impedance of meander and mesh type sensors increase with frequency, whereas it decreases with frequency for the interdigital type. Hence, it can be concluded that the meander and mesh type are of inductive type and will respond well to conducting and magnetic materials. The interdigital type is of capacitive type and will respond well to dielectric materials. The actual nature of their impedance characteristics has been discussed in the next chapter.

CHAPTER 4

EXPERIMENTAL CHARACTERIZATION OF PLANAR ELECTROMAGNETIC SENSORS

4.1 Introduction

In the previous chapter all three types of planar sensor, meander, mesh and interdigital configurations were modelled using finite element analysis and the impedance characteristics were presented. This section aims to support the results obtained from field modelling of the earlier chapter, by experimenting the sensors with materials of varying electric, magnetic and dielectric properties. The mesh, meander and interdigital sensors are characterized by actual experiment and the results are presented in this chapter.

4.2 Experimental Setup

The experimental set up is shown in figure 4.1 below.

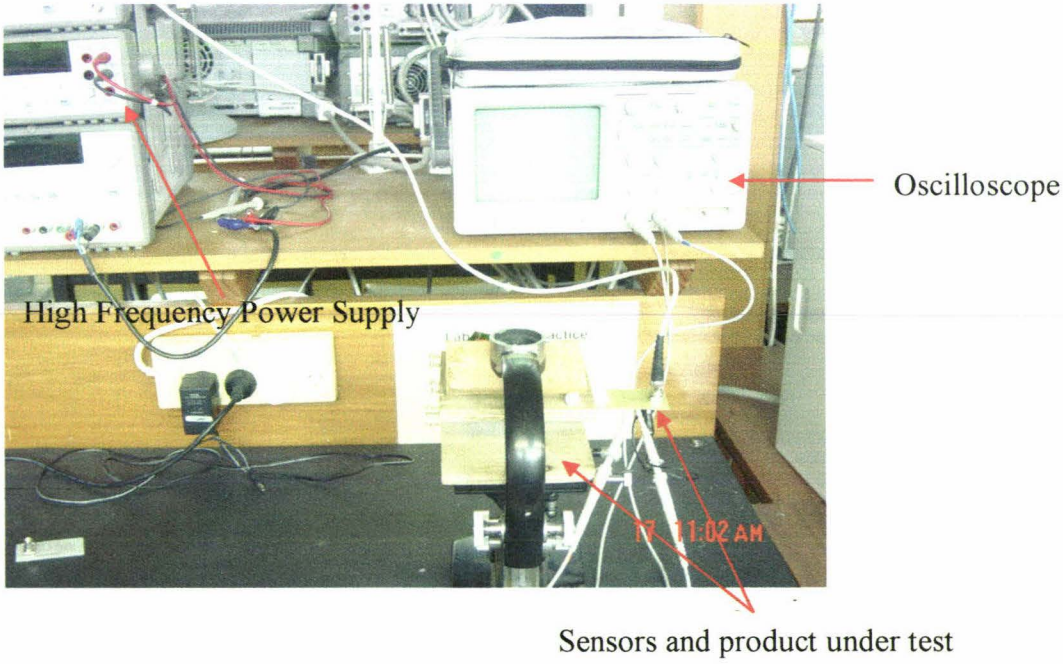

Figure 4.1: Experimental setup for planar sensor characterization

The setup has an Agilent 33120A waveform generator which provides the driving signal for excitation of the sensor. The different types of materials were tested at varying frequencies. An old microscope was used to fit the sensor on the top wooden plate as shown in figure 4.1,

and the material under test was on the bottom wooden plate. The sensor was lowered towards the material of interest using the microscope knobs. Hence, the sensor was able to get as close as possible to the material under test, without actually touching it. The Agilent 54622D mixed signal oscilloscope was used for analysis of input voltage, output current and the phase.

Materials of different electric and dielectric properties were chosen for experimentation. These are:

- Copper
- Aluminium
- Iron
- Milk
- Water

Copper, aluminium and iron have strong electric properties thus having high conductivity and permeability (for iron) values compared with milk and water. Alternatively milk and water have strong dielectric properties with high permittivity values. The three types of metal were cut into $10mm \times 5mm \times 0.1mm$ pieces, while the water and milk were put into a plastic container of the dimensions $10mm \times 5mm \times 2mm$. This was done in order to provide the sensors an appropriate area for sensing.

4.3 Experimental Results

4.3.1 Impedance Characteristics of Mesh, Meander and Interdigital Sensors

Both the meander and mesh type sensors consist of two coils: one used for excitation and another for sensing. The high frequency alternating supply is provided to the exciting coil and the voltage across the sensing coil is measured. The transfer impedance (the ratio of the sensing voltage to the exciting current) is used as the characterization parameter for the meander and mesh type sensors. In case of interdigital sensor the exciting voltage and the displacement current through the sensor is measured. The impedance (the ratio of the applied voltage to the current) is the characterization parameter used for the interdigital sensor. Different sizes of sensors of each meander, mesh and interdigital types have been experimented using the experimental set-up. The frequency of excitation has been varied

between 100 kHz to 100 MHz. The impedance characteristics of the sensors are shown in figures 4.2, 4.3 and 4.4.

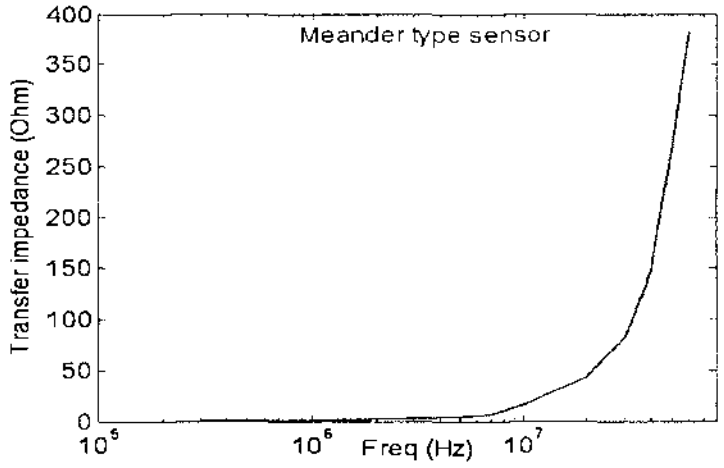

Figure 4.2: Transfer impedance characteristics of meander type sensor

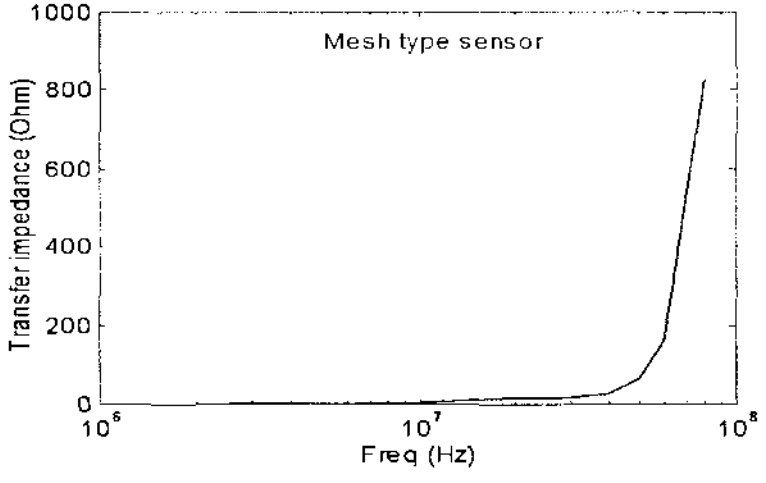

Figure 4.3: Transfer impedance characteristics of mesh type sensor

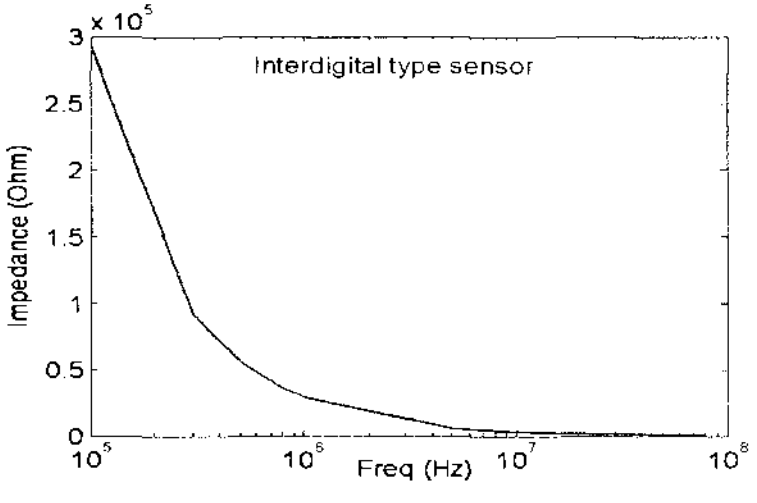

Figure 4.4: Impedance characteristics of interdigital type sensor

It is seen that the transfer impedance for both meander and mesh type increases with the increase in frequency whereas the impedance of interdigital type sensor decreases with frequency. With the same effective area the response of mesh type sensors is better than meander type. From the impedance characteristics is seen that both the meander and mesh types sensors are inductive type whereas the interdigital type sensor is capacitive type. It is also seen that both meander and mesh type sensors response well at high frequency whereas the response of the interdigital sensor is very good at low frequency and doesn't response well at high frequency. This is very important while the sensors are used for non-destructive testing. The selection of operating frequency is to be carefully chosen.

4.3.2 Experiments with Materials

The five types of materials are tested with all three types of sensors. Only the change of magnitude of impedance is shown here (the impedance with air is considered as unity), in practice the phase information is also used.

4.3.2.1 Interdigital Sensor

The results obtained at 84 MHz are shown in table 4.1. The value of "Air" (with no materials), were taken before each test. The start Air value was different for milk and water when compared to Copper, Aluminium and Iron. This due to metal tests and milk and water tests been done at different times on any given day. However, since only the change of magnitude of impedance is shown here, this effect can be ignored. This applies to all the tests that have been done in this chapter.

Table 4.1: Interdigital results at 84 MHz

Type	Start Air Voltage (V)	Output Voltage(V)	Ratio	Phase (Degrees)
Air	1.316	1.316	1	22
Copper	1.316	1.336	1.0151976	28
Aluminium	1.316	1.336	1.0151976	27
Iron	1.316	1.314	0.9984802	26
Milk	1.535	1.385	0.9022801	44
Water	1.457	1.348	0.9251887	37

Table 4.2: Interdigital percentage change compared to air at 84 MHz

Type	Change Percent (%)
Copper	1.5
Aluminium	1.5
Iron	0.15
Milk	9.8
Water	7.5

The interdigital sensor reacts well to milk and water, which are of the dielectric nature. The percentage change (table 4.2) of the milk and water is quite high compared and the ratios quite low compared to the metals. There is also a difference of percentage and ratio between milk and water due to their difference in permittivity values. There is also a noticeable phase change between the metals and milk and water.

Table 4.3: Interdigital results at 91 MHz

Type	Start Air Voltage(V)	Output Voltage(V)	Ratio	Phase (Degrees)
Air	0.832	0.832	1	5
Copper	0.832	0.837	1.0060096	3
Aluminium	0.832	0.847	1.0180288	3
Iron	0.832	0.839	1.0084135	3
Milk	0.925	0.846	0.9145946	7
Water	0.899	0.832	0.9254727	5

Table 4.4: Interdigital percentage change compared to air at 91 MHz

Type	Change Percent (%)
Copper	0.6
Aluminium	1.8
Iron	0.8
Milk	8.5
Water	7.5

Referring to table 4.3 and 4.4 it can be seen that the nature of ratio and the percentage changes between the metals and the liquids are very similar, to that observed at 84 MHz. However the change between milk and water is less. The phase difference between the different materials is not as clear compared to the results obtained at 84 MHz.

4.3.2.2 Mesh Sensor

The results obtained for the mesh sensor for the different types of materials at 84 and 91 MHz are shown in tables 4.5 and 4.6.

Table 4.5: Mesh results at 84 MHz

Type	Start Air Voltage(V)	Output Voltage(V)	Ratio	Phase (Degrees)
Air	2.104	2.104	1	92
Copper	2.104	1.844	0.8764259	96
Aluminium	2.104	1.824	0.8669202	95
Iron	2.104	1.629	0.7742395	103
Milk	1.912	1.816	0.9497908	95
Water	1.912	1.861	0.9733264	94

Table 4.6: Mesh results at 91 MHz

Type	Start Air Voltage(V)	Output Voltage(V)	Ratio	Phase (Degrees)
Air	1.994	1.994	1	49
Copper	1.994	1.76	0.8826479	54
Aluminium	1.994	1.77	0.887663	54
Iron	1.994	1.74	0.8726179	55
Milk	1.994	1.885	0.945336	49
Water	1.994	1.896	0.9508526	48

Table 4.7: Mesh percentage change compared to air at 84 MHz

Type	Change Percent (%)
Copper	12.4
Aluminium	13.3
Iron	22.6
Milk	5
Water	2.7

Table 4.8: Mesh percentage change compared to air at 91 MHz

Type	Change Percent (%)
Copper	11.7
Aluminium	11.2
Iron	12.7
Milk	5.5
Water	4.9

The mesh sensor reacts well to metals, which are good conductors. This is reflected by the low ratio and the high percentage changes, in tables 4.5-4.8. Even though the phase differences between the metals and the milk and water is not that significant, it can be seen that the phase of the metals are generally higher than the milk and water.

4.3.2.3 Meander Sensor

The results obtained for the meander sensor for the different types of materials at 84 and 91 MHz are shown in tables 4.9 and 4.10.

Table 4.9: Meander results at 84 MHz

Type	Start Air Voltage(V)	Output Voltage(V)	Ratio	Phase(Deg)
Air	2.395	2.395	1	49
Copper	2.395	2.186	0.9127349	55
Aluminium	2.395	2.184	0.9118998	54
Iron	2.395	2.174	0.9077244	52
Milk	2.352	2.471	1.0505952	26
Water	2.352	2.467	1.0488946	33

Table 4.10: Meander results at 91 MHz

Type	Start Air Voltage(V)	Output Voltage(V)	Ratio	Phase(Deg)
Air	2.084	2.084	1	21
Copper	2.084	1.859	0.8920345	21
Aluminium	2.084	1.869	0.896833	21
Iron	2.084	1.83	0.878119	24
Milk	2.205	2.207	1.000907	7
Water	2.205	2.238	1.014966	5

Table 4.11: Meander percentage change compared to air at 84 MHz

Type	Change Percent (%)
Copper	8.7
Aluminium	8.8
Iron	9.2
Milk	5
Water	4.9

Table 4.12: Meander percentage change compared to air at 91 MHz

Type	Change Percent (%)
Copper	10.8
Aluminium	10.3
Iron	12.2
Milk	0.1
Water	1.5

The meander sensor response to metals is very similar to that of the mesh sensor. The meander sensor reacts well to metals, compared to the milk and water. This is reflected by the low ratio and the high percentage changes, in tables 4.9-4.12. There is also a considerable difference in the measured phase for metals compared with milk and water. The measured phase for the metals is very much higher at both frequencies compared to the milk and water.

4.4 Conclusion

It can be concluded from the results that the meander and mesh type sensors respond very well to conducting and magnetic materials (copper, aluminium, iron). However their reaction to dielectric materials is not as good. On the other hand, the interdigital sensor acts in an opposite manner and responds well to dielectric materials. If the inspection is related to metal products it is recommended to use either meander or mesh type sensors. If the inspection is related to dielectric products the interdigital sensor is the better choice. In areas which require the inspection of materials comprising metal and dielectric compositions, mesh and/or meander sensors along with interdigital sensors can be used.

CHAPTER 5

EXPERIMENTS WITH MILK

5.1 Introduction

Dairy production is an important sector of the national economy of many countries in the world. For example, the national economy of New Zealand is significantly dependent on the export of dairy products; it is approximately 25% of the total foreign export earnings of the country. The major part of the New Zealand dairy industry is administered by Fonterra, which is the largest dairy cooperative in the world. Currently Fonterra employs the following procedure for analyzing and monitoring the quality of the milk - it measures the fat to protein ratio of milk using mid infrared spectroscopy prior to processing [33-38]. This provides a very accurate and rapid (1 reading/min) measurement with a standard deviation of 0.02% w/w from reference methods. In turn it allows precise milk standardization, which is vital to efficient milk processing.

The infrared spectrometers used by Fonterra and other large dairy companies in the world are very expensive. This makes it hard for small companies and individual farmers to use this technique to analyze the total solid content in milks. At the same time, such an analysis is very important since the dairy producers are paid based on the quality of their milk products. Hence there is a need to develop a low-cost high-efficiency sensing system aimed at applications in the dairy industry. The use of an electromagnetic sensor has the potential to offer a good solution leading to a robust instrument with high accuracy at a low capital cost. At the same time the testing system will be smart and light so that it can be carried easily to the testing site. The current system, based on infrared spectrometry, is heavy and is not flexible at all to do the test; the milk sample has to be sent through the test rig [33-38].

This sensing technique has the potential to be successfully employed in the quality inspection of dairy products such as milk, butter, cheese, curd and yogurt. This chapter presents the experiments done on milk by mesh, meander and interdigital sensors.

5.2 Experimental Setup

The three sensors were tested and the results were analyzed. The experimental setup was the same as explained in chapter 4. The experiment involved adding 1ml of cream to 79 ml of water. Some time is allowed in order to get a constant reading, so that the magnitude of the voltage across the series resistance attains a steady state. Prior to adding 1ml of cream each time, 1ml of the water and cream mix were taken out, to keep the depth of the mix constant. The total solution (cream and milk) was always kept at 80ml. The interdigital sensor was tested with a 100Ω as well as a 4.7 kΩ resistor in series with the sensor coil whereas the mesh and the meander had 100Ω resistors in series with the exciting coils. The operating frequency was set at 500 kHz. The transfer impedance was calculated for the mesh and the meander sensors and the impedance was calculated for the interdigital sensor.

For Mesh and Meander sensors:

Voltage across the sensing coil = $V1$ [5.1]

Current across the 100Ω resistor = $\frac{V2}{100}$ [5.2]

Transfer Impedance = $\frac{V1}{i} = \frac{i}{100} \bullet \frac{V1}{V2}$ [5.3]

For Interdigital sensors:

Voltage across the exciting coil = $V1$ [5.4]

Current through the sensing coil = $\frac{V2}{R}$ (100Ω or 4.7kΩ) [5.5]

Impedance = $\frac{V1}{i} = R \bullet \frac{V1}{V2}$ [5.6]

5.3 Experimental Results

5.3.1 Mesh and Meander Sensors

Figure 5.1 shows the variation of the magnitude of transfer impedance as a function of cream content. Figure 5.2 shows the phase of the transfer impedance as a function of cream content. It is seen from figures 5.1 and 5.2 that the mesh and the meander type sensor do not

react well to the cream solution. The sensors were only tested up to 10ml of cream in 70ml of water, but the impedance scarcely changed. The phase also followed a similar pattern, even though the mesh sensor changed a bit, it was insignificant, compared to the phase change observed during experiments with the interdigital sensor.

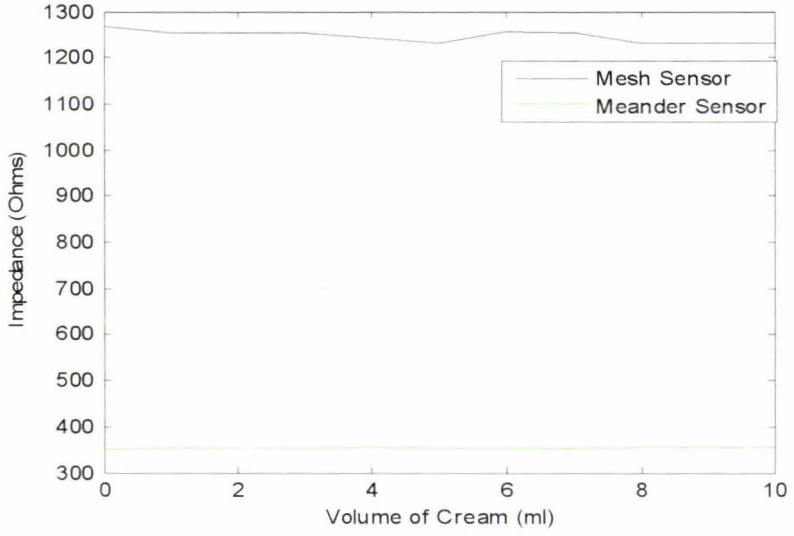

Figure 5.1: Impedance vs Cream graph for mesh and meander type sensor

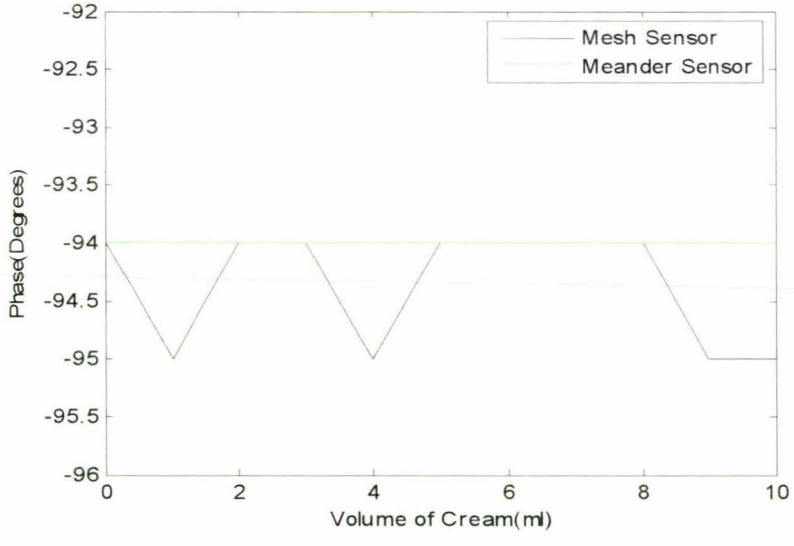

Figure 5.2: Phase vs Cream graph for mesh and meander type sensor

Figure 5.3 is a comparative response of the three types of sensors. It is clear that the interdigital sensor has a very good response to the percentage of fat, whereas the change of impedance of the mesh and meander sensors are pretty constant for the various percentages of

fat. More results with interdigital sensors are shown below, where a moderately low frequency signal is used.

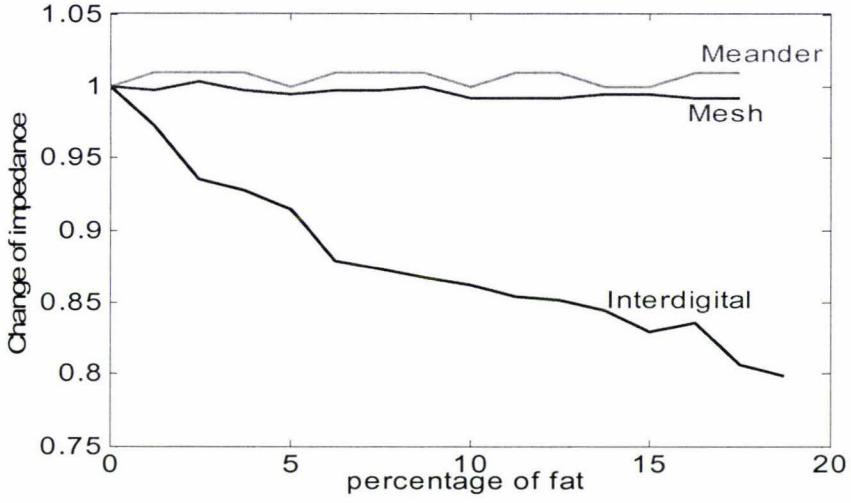

Figure 5.3: Impedance characteristics for three types of sensors at 100 kHz

5.3.2 Interdigital Sensor

The interdigital sensor responds well to the changing concentrations of cream that is added to water. Each time cream is added to water there is a change in the dielectric properties of the solution. Figure 5.4 and 5.6 show that the impedance decreases with increasing concentration of cream. The phase follows a similar pattern (figures 5.5 and 5.7). A relationship between the impedance and phase with the volume of cream is obtained by a cubic fit as shown in the figures 5.4-5.7.

- Sensor with 100Ω in series with the sensor coil

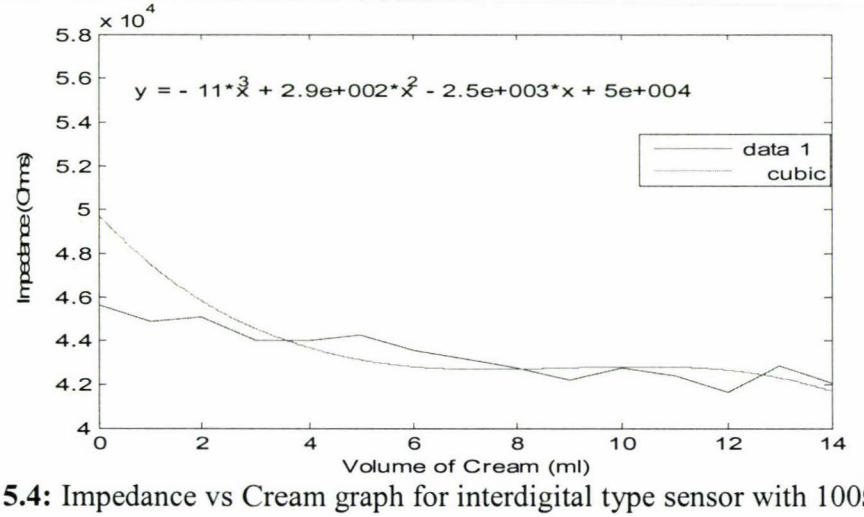

Figure 5.4: Impedance vs Cream graph for interdigital type sensor with 100Ω series resistance

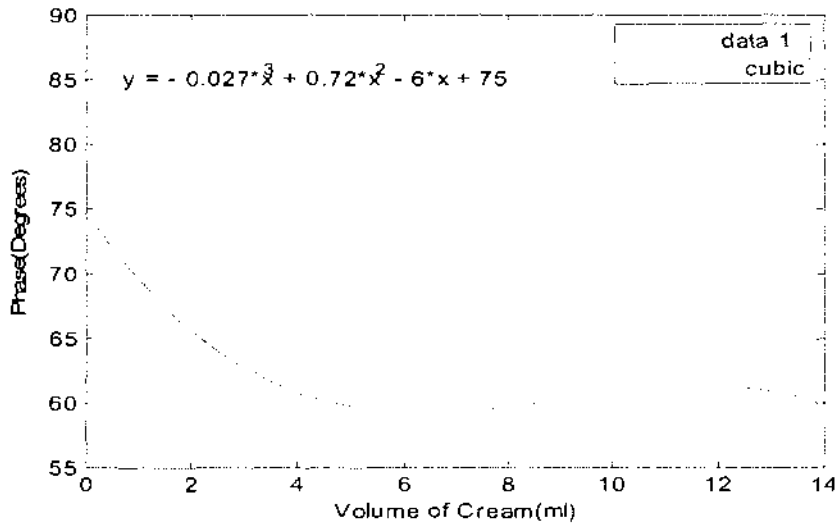

Figure 5.5: Phase vs Cream graph for interdigital type sensor with 100Ω series resistance

- Sensor with 4.7 kΩ resistor in series with the sensing coil

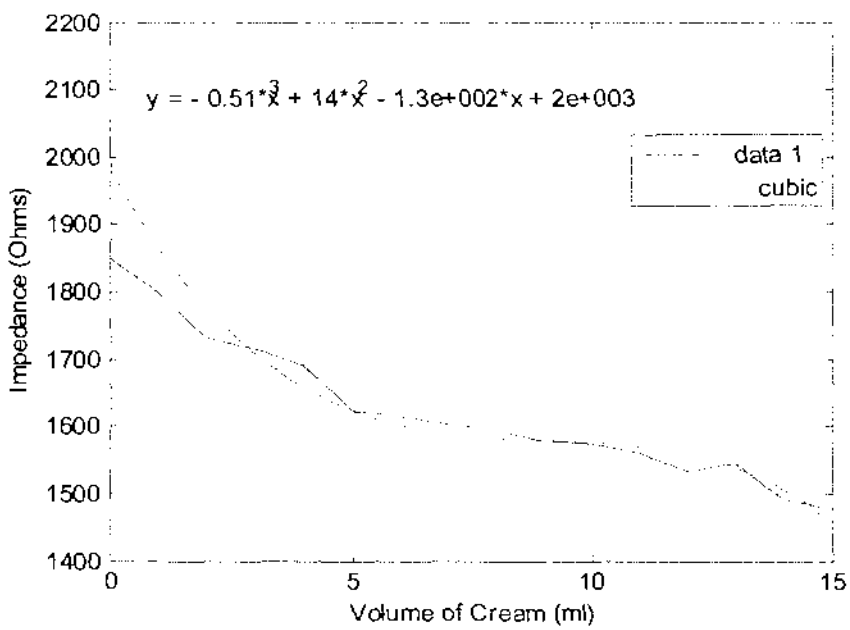

Figure 5.6: Impedance vs Cream graph for interdigital type sensor with 4.7kΩ series resistance

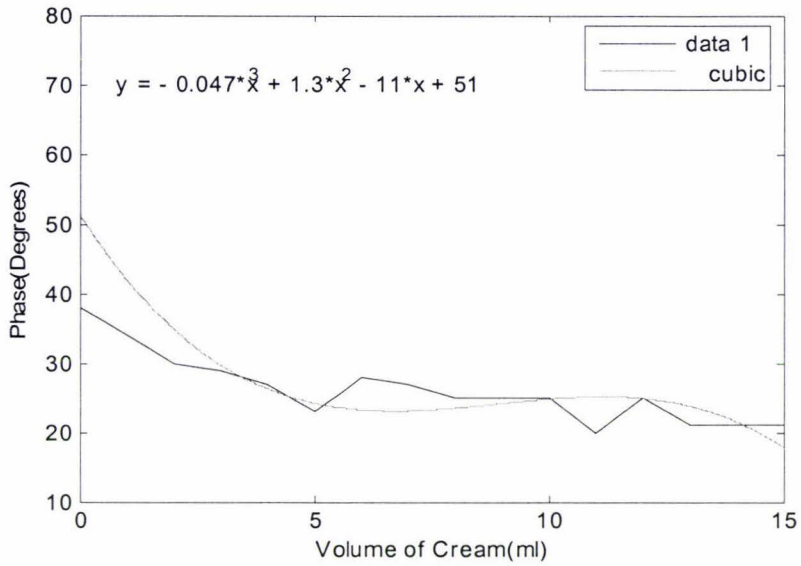

Figure 5.7: Impedance vs Cream graph for interdigital type sensor with 4.7kΩ series resistance

5.4 Data Analysis

5.4.1 Obtaining Linear and Quadratic Equations

The cream percentages were predicted from the sensor results. The cream percentages were estimated using a linear and a quadratic equation. Four percentages with known impedances were chosen to get the equations. Shown below in tables 5.1 and 5.2 are the four samples used for the two sensors.

Table 5.1: Sensor with 100Ω resistor in series with the sensing coil

Cream Volume(ml)	Cream Percentage (%)	Impedance, Z (Ohms)
1	1.25	44888
5	6.25	44283
10	12.5	42772
14	17.5	42055

- Linear Equation

$$\text{Cream (Estimated)} = -0.0054 \times Z + 240 \qquad [5.7]$$

- Quadratic Equation

$$\text{Cream (Estimated)} = -1.3e-7 \times Z^2 + 0.0061 \times Z - 5.9 \qquad [5.8]$$

Table 5.2: Sensor with 4.7kΩ resistor in series with the sensing coil

Cream Volume(ml)	Cream Percentage (%)	Impedance, Z (Ohms)
1	1.25	1797.4
5	6.25	1623.1
10	12.5	1572.7
14	17.5	1490.7

- Linear Equation

$$\text{Cream (Estimated)} = -0.053 \times Z + 95 \qquad [5.9]$$

- Quadratic Equation

$$\text{Cream (Estimated)} = -0.00014 \times Z^2 - 0.51 \times Z + 470 \qquad [5.10]$$

5.4.2 Estimated Results

Tables 5.3 and 5.4 show the cream percentage results obtained from linear and quadratic equations. Referring to tables 5.3 and 5.4 it can be seen that the cream percentage predicted using the quadratic equation using the interdigital sensor with 4.7kΩ, gives the smallest errors.

Table 5.3: Cream percentage estimation from sensor with 100Ω resistor in series with the sensing coil

Cream (%)	Predicted value using Linear equation	Predicted value using Quadratic equation	Error 1	Error 2
1.25	1.9071	1.8142	-0.6571	-0.5642
2.5	0.8206	0.6471	1.6794	1.8529
3.75	6.6831	6.8171	-2.9331	-3.0671
5	6.7315	6.8668	-1.7315	-1.8668
6.25	5.161	5.2453	1.089	1.0047
7.5	9.0227	9.1919	-1.5227	-1.6919
8.75	11.3085	11.4639	-2.5585	-2.7139
10	13.2878	13.3926	-3.2878	-3.3926
11.25	16.4234	16.375	-5.1734	-5.125
12.5	13.2878	13.3926	-0.7878	-0.8926
13.75	15.2348	15.255	-1.4848	-1.505
15	19.4945	19.2091	-4.4945	-4.2091
16.25	12.7984	12.919	3.4516	3.331
17.5	17.1441	17.0478	0.3559	0.4522

Table 5.4: Cream percentage estimation from sensor with 4.7kΩ resistor in series with the sensing coil

Cream (%)	Predicted value using Linear equation	Predicted value using Quadratic equation	Error 1	Error 2
1.25	0.1066	1.1276	1.1434	0.1224
2.5	3.6632	2.6174	-1.1632	-0.1174
3.75	4.4985	3.1498	-0.7485	0.6002
5	5.7173	4.0512	-0.7173	0.9488
6.25	9.2634	7.5145	-3.0134	-1.2645
7.5	9.7572	8.096	-2.2572	-0.596
8.75	10.3718	8.8538	-1.6218	-0.1038
10	10.8552	9.476	-0.8552	0.524
11.25	11.5906	10.4674	-0.3406	0.7826
12.5	11.9111	10.9163	0.5889	1.5837
13.75	12.5363	11.8213	1.2137	1.9287
15	13.9652	14.0359	1.0348	0.9641
16.25	13.3663	13.083	2.8837	3.167
17.5	16.2189	17.9417	1.2811	-0.4417
18.75	16.9597	19.3358	1.7903	-0.5858

5.5 Conclusions

The interdigital type sensor based approach proposed in this chapter can be a very promising alternative to the existing measurement techniques used in the dairy industry to monitor the quality of products. This sensing technique is non-destructive in nature. It is also safe and cost-effective. In addition, the approach does not involve any fragile sensing elements (such as glass probes) and it is quite stable (requires only infrequent periodic calibration).

The effect of dielectric materials such as milk, butter, cheese, curd, yogurt, etc., on the transfer impedance of planar electromagnetic sensors has been experimentally observed and is reported in this chapter. It is shown that the properties of dielectric materials have a great influence on the value of the impedance in interdigital sensors. The experimental results also showed that the sensor had a very good potential to be used to determine composition of dairy products.

CHAPTER 6

EXPERIMENTS WITH SAXOPHONE REEDS

6.1 Introduction

A saxophone reed, as shown in figure 6.1, is a small piece of bamboo that is attached to the mouthpiece of a saxophone. When the player blows into the saxophone, the reed vibrates, creating sound. The reed is therefore, in part, responsible for the tone and ease of use of a saxophone. There is nothing more frustrating for a saxophone player than playing on a bad reed. Reeds wear out after a few weeks of playing and must be replaced. The problem with reeds is that currently the quality is very variable: in a box of ten, three or four reeds are usually found to be 'bad' when played and are thus discarded. Since the reeds are expensive, and more importantly the quality of the music depends on them, this section looks at a novel way of evaluating reeds using interdigital sensors.

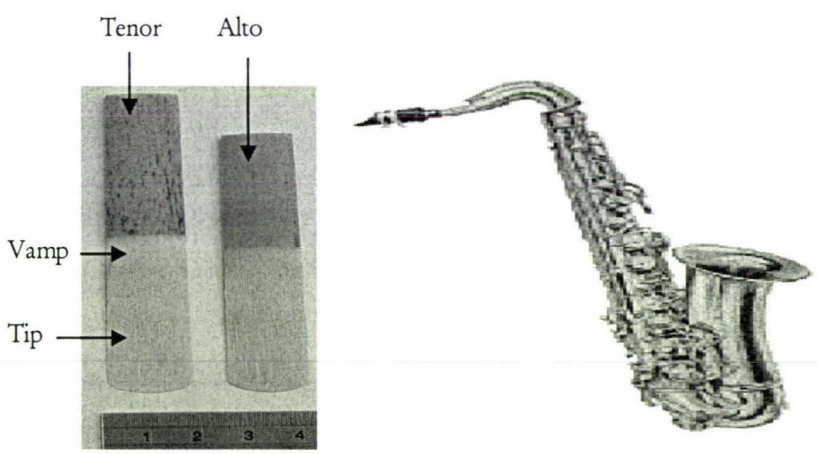

Figure 6.1: Tenor and Alto Saxophone reeds, different sections of the reeds, and a saxophone

6.2 Experimental Setup

A moderately high frequency alternating current supply has been used for the experiments on the interdigital type of planar sensors. A relatively large number of reed

samples, of which a few are known to be bad from the beginning, have been tested. Experiments have been carried out at five different frequencies to decide the optimum frequency for testing. Figure 6.2 below, shows how the reeds were tested with the interdigital sensor.

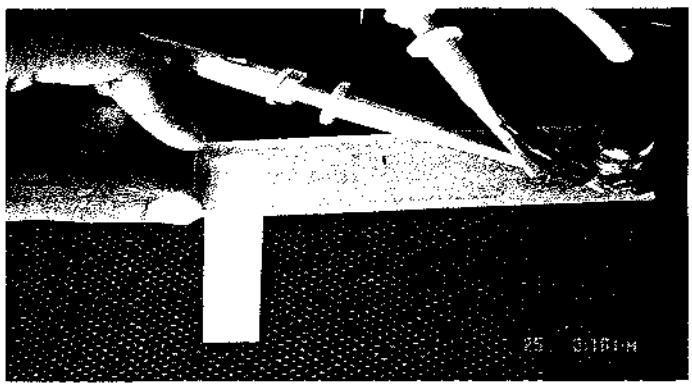

Figure 6.2: Experiment using interdigital type sensor

6.3 Experimental Analysis

Figures 6.3 – 6.7 show the impedance values of the interdigital type sensors with different reeds at operating frequencies of 40 kHz, 75 kHz, 100 kHz, 1 MHz and 10 MHz respectively. The sensors are tested by a saxophone player and divided into good and bad categories. The test results obtained corresponding to 75 kHz are very close to that.

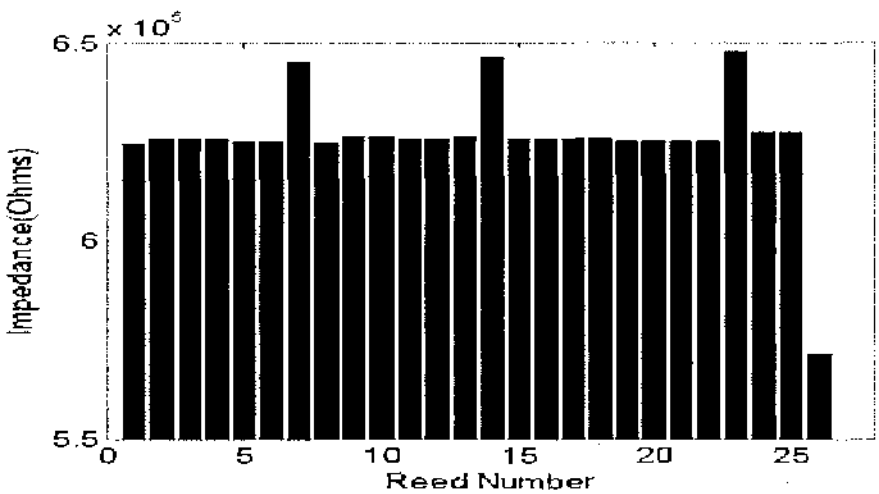

Figure 6.3: Impedance of interdigital sensor for different reeds at 40 kHz

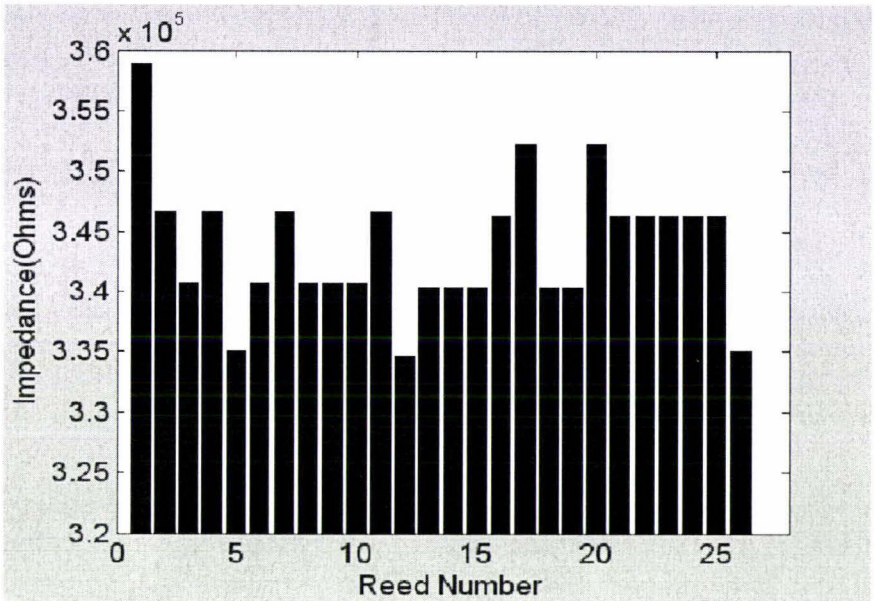

Figure 6.4: Impedance of interdigital sensor for different reeds at 75 kHz

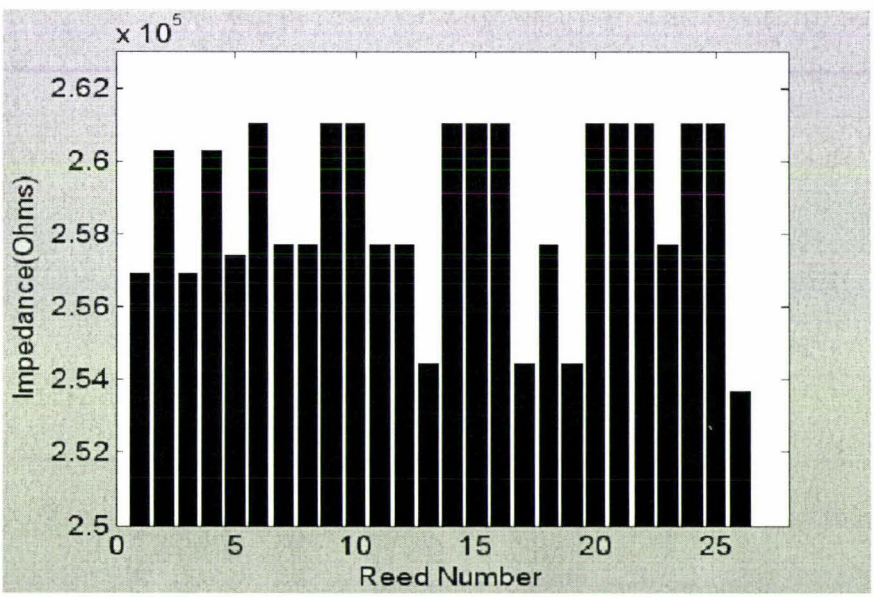

Figure 6.5: Impedance of interdigital sensor for different reeds at 100 kHz

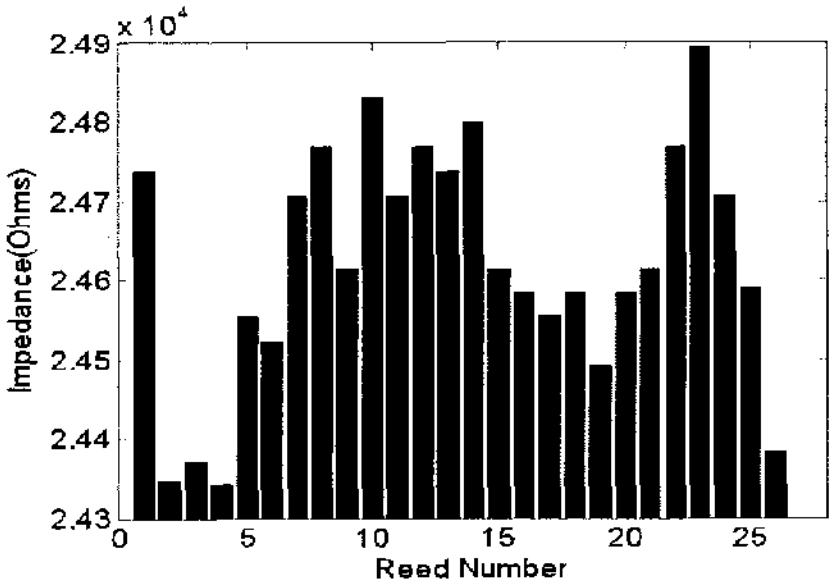

Figure 6.6: Impedance of interdigital sensor for different reeds at 1 MHz

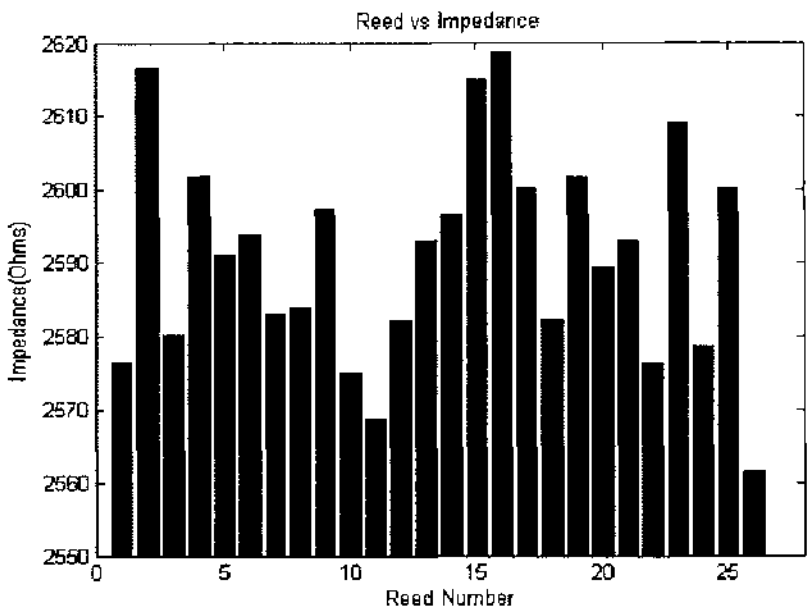

Figure 6.7: Impedance of interdigital sensor for different reeds at 10 MHz

6.3 Conclusion

This section looks as the specific case of saxophone reeds and how the interdigital sensor can be used to evaluate saxophone reeds. Initial results for quality inspection of saxophone reeds are promising. There appears to be a measurable difference given by the sensor between 'good' and 'bad reeds. More experimentation needs to be done with a larger sample size, to get a conclusive relationship between saxophone reeds and the signals of the interdigital sensor.

CHAPTER 7

ELECTROMAGNETIC INTERACTION OF PLANAR INTERDIGITAL SENSORS WITH PORK BELLY CUTS

7.1 Introduction

In this chapter the interaction of planar Interdigital sensors with pork belly cuts has been described. Electromagnetic field propagation in biological tissue, such as fat and muscle, mainly depends on permittivity and conductivity parameters of the tissue. The parameters are described in detail in [53]. Research work on the dielectric properties of meat has been mostly done at high frequencies [48-51], while research on low to high frequency analysis is reported in [52]. The aim is to determine the fat content in pork belly cuts in a non-invasive way. Pork belly, in simplest terms, is a side of fresh pork. It is the underside of the pig. The primal pork belly is located below the loin and it accounts for around 16% of the carcass weight. It is very fatty with only minute amounts of lean meat. There are many methods that are used to estimate parameters of the pork belly, mainly fat and protein:

- Chemical analysis [43]
- Physical dissection – Dissecting the different compositions (fat, muscle etc) and weighing them
- Subjective assessment [47]
- Grading measurements [39]
- Ultrasonic evaluation [46]
- Specific gravity [43]
- Electrical properties
    - Bioelectric Impedance Analysis (BIA) [42]
    - Total body electrical conductivity (TOBEC) [41]
- Magnetic Resonance Imaging (MRI) or Computer Tomography (CT) scans [45]
- Dual-energy X-ray Absorptiometry (DXA) scans [44]
- Video Image Analysis (VIA) [40]

7.2 Initial Experiments

A planar interdigital sensor (40mm×40mm area) as shown in figure 7.1 has been used to experiment with different types of pork using the experimental set-up as shown in figure 7.2.

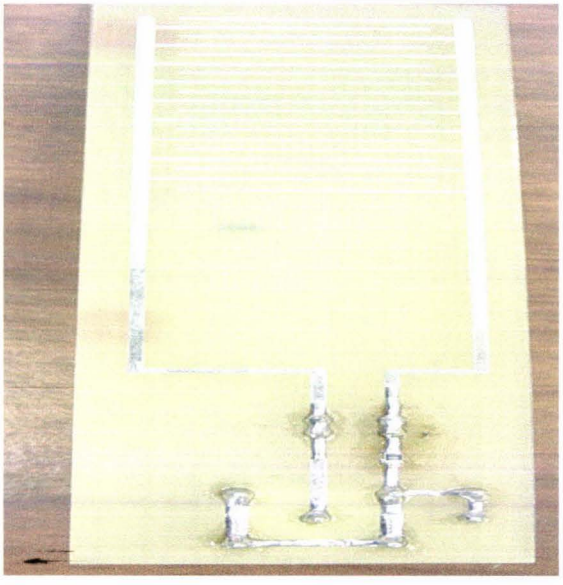

Figure 7.1: Fabricated interdigital type sensor

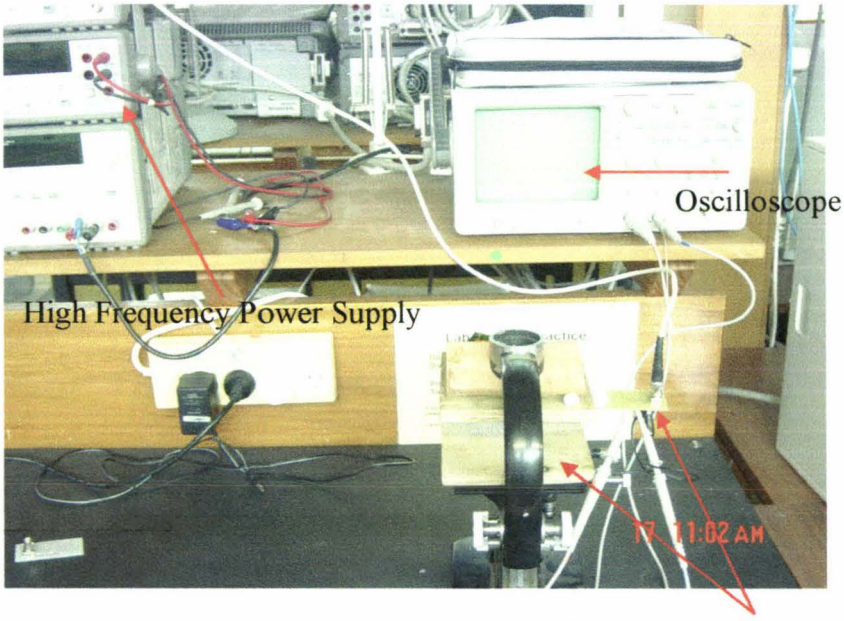

Figure 7.2: Experimental setup for fat measurement

There are mainly four main varieties in pork meat

- Fat
- Mixed
- Muscle
- Skin

The sensor was tested on 4 pieces of fat, 2 pieces of mixed meat, 4 pieces of muscle and 1 piece of skin. One piece of each type is shown in figure 7.3. All the pieces were of different shape and size. The experiment involved analyzing the sensor results, to see if the different amount of fat content affected the original signal.

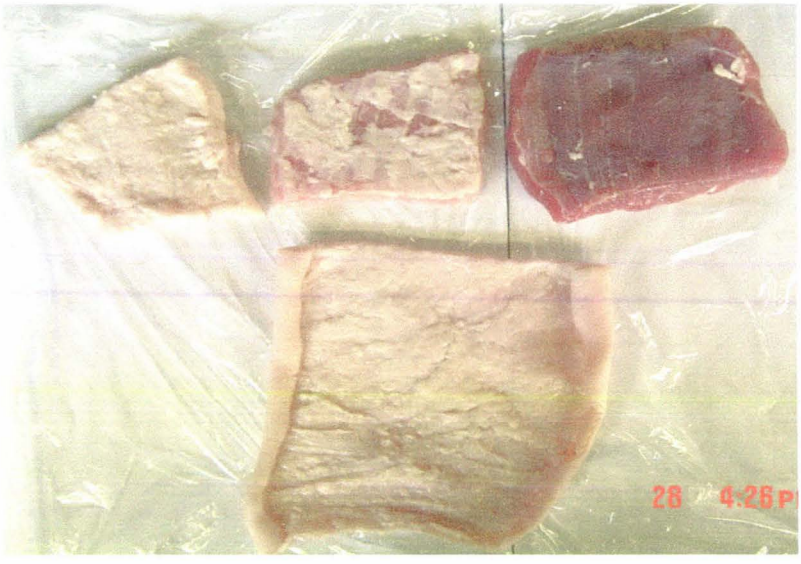

Figure 7.3: Pork samples for test

7.2.1 Experiment

Each piece was tested separately, and the sensor was placed as close as possible to the meat for all experiments bar experiment 1. In experiment 1 glad-wrap was placed on top of the meat, and the sensor lightly touched the top of the meat. During the last experiment (exp 4) the skin was put on top of a piece of fat, mixed and muscle. With the exception of experiment 1, the sensor had no direct contact with the meat, during all other experiments. The interdigital sensor was tested with a 4.7 kΩ resistor. The operating frequency was set at 500 kHz. The impedance was then calculated as shown below.

Voltage across the sensor coil = $V1$ [7.1]

Current through the sensing coil, i = $\frac{V2}{R}$; R is the series resistance [7.2]

Impedance of the sensor = $\frac{V1}{i}$ [7.3]

Operating conditions: Temperature = 16.1°C, Frequency = 500 kHz

Some experimental results are shown in figures 7.4 to 7.6. The signal#1 (top) corresponds to the applied excitation and signal#2 corresponds to the current through the sensor.

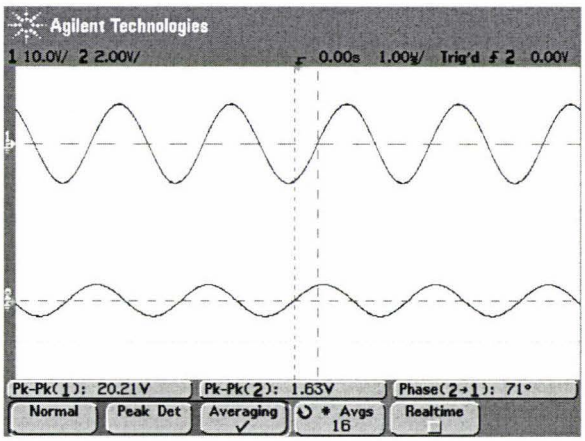

Figure 7.4: Signals corresponding to sensor in air

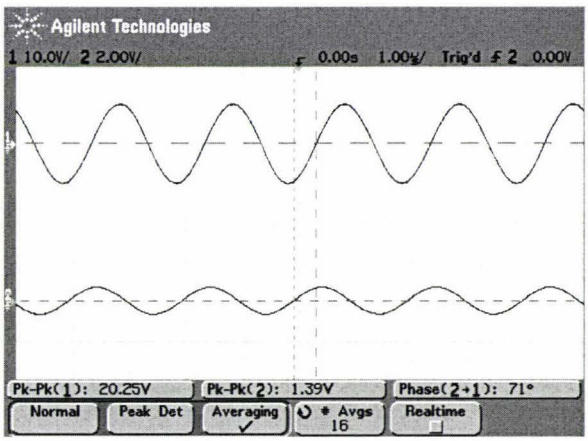

Figure 7.5: Signals corresponding to sensor placed on fat

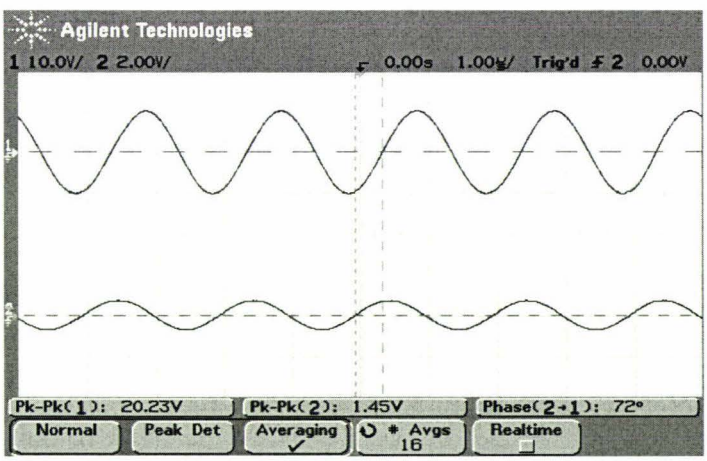

Figure 7.6: Signals corresponding to sensor placed on muscle

It is seen from figures 7.4 to 7.6 shows that there is an obvious difference in both signals, when the sensor is placed on fat and muscle, with respect to air. The signals obtained from the fat sample, also show difference when compared to the signals obtained from the muscle sample.

7.2.2 Analysis of Results

The variation of impedance of the sensor when exposed to different portions of pork are shown below in figures 7.7 to 7.10.

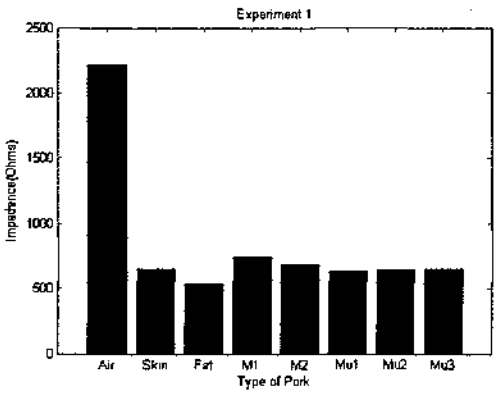

Figure 7.7: Impedance of the sensor obtained from Experiment 1

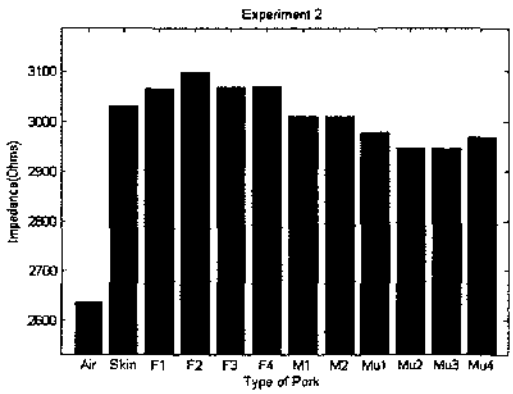

Figure 7.8: Impedance of the sensor obtained from Experiment 2

An initial measurement is obtained for the sensor with no materials under it, before each of the four experiments. In the graphs above this measurement is shown as "Air". The first experiment had low values of impedance compared to the other three experiments, for all types of meat. The direct contact the sensor had with the meat in experiment 1 gave a higher output signal which resulted in lower impedance. Looking closely at experiment 1 it can be seen that fat has the lowest impedance followed by muscle and finally mixed. This shows that the sensor can detect different types of pork based on the different fat content. Skin, which has the lowest thickness, fits in the middle. Experiment 2 shows that fat has the highest impedance, followed by mixed and muscle.

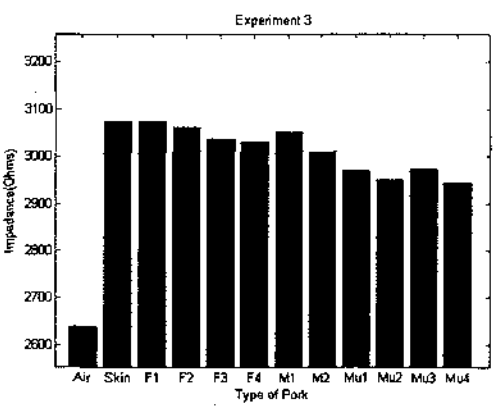

Figure 7.9: Impedance of the sensor obtained from Experiment 3

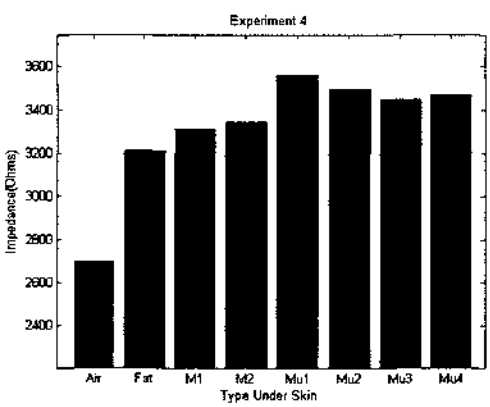

Figure 7.10: Impedance of the sensor obtained from Experiment 4

7.2.3 Discussion

The results show the sensor responds in a different way to muscle fat and skin. A clear cut analysis of skin is hard to obtain since it is very thin comparatively. In experiment 4 we put the skin on top and analyze the results. Experiment 4 shows fat once again having the lowest impedance followed by mixed and finally muscle. In all but one (experiment1) of the cases fat and muscle are the two extremes and mixed is in the middle.

The sensor used in the experiment is not the optimum one required for the best result. But observing the results it can be concluded that the planar interdigital sensor has the potential to be used for the estimation of fat content in pork meat. The experiments show that the sensor can detect different types of pork and hence can be used to estimate fat content in pork. In order to obtain better results some more experiments have been carried out which are reported in the next section.

7.3 Second Set of Experiments

7.3.1 Sensors and Pork Samples

The initial experiments in the previous section showed the planar type electromagnetic sensors have responded well to fat content of pork belly cuts. However it was observed in the initial experiments that the size of the sensor used for experimentation was not sufficient to cover the sample of meat tested. In practice the bellies are cut into particular sizes and the possibility of testing them by doing experiments only once are preferred. Three Interdigital sensors of varying periodicity as shown in table 7.1 were fabricated and tested on six pork belly pieces (A1, B1, C1, A2, B2, and C2). To simulate the factory situation, the pork pieces were placed on top of each sensor as shown in figure 7.11. The pieces of pork were placed on the sensor according to four different orientations as explained below using figure 7.12. The pork bellies were around 20-30 mm deep with skin.

Figure 7.11: Experimental setup for second experiment

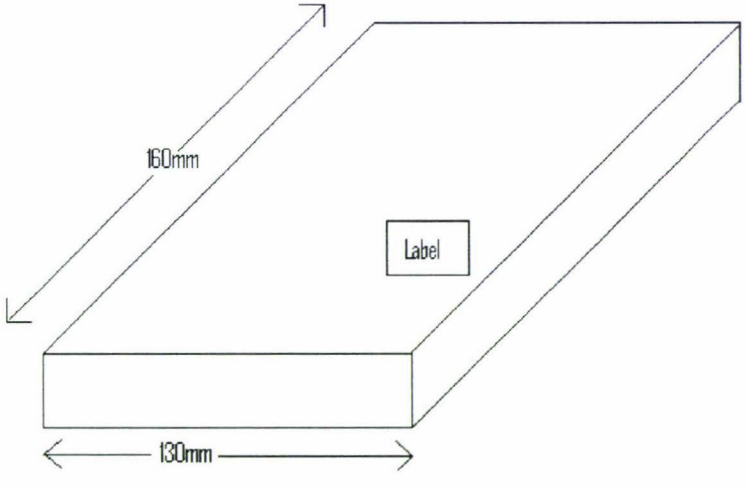

Figure 7.12: Pork belly sample dimensions

Orientation 1 = [skin side up, label at front] – as shown above
Orientation 2 = [skin side up, label at back] – Rotate 180°
Orientation 3 = [skin side down, label at front but underneath] – Flip over
Orientation 4 = [skin side down, label at back underneath] - Rotate 180°

The interdigital sensors used for experimentation has one sided access to the material under test (MUT). Electric field lines pass through the MUT, and the capacitance between the two electrodes, depend on the material dielectric properties as well as on the electrode and material geometry. Three sensors of differing periodicity were used for experimentation.

Table 7.1: Sensor parameters

Sensor	Periodicity(cm)	Finger-length(cm)
1	15	120
2	20	120
3	30	120

7.3.2 Experimental Setup

The interdigital sensors were driven by a 10V Sine wave. The measurements were made at frequencies in the range from 5 kHz to 1 MHz. The pork belly pieces had skin on top and muscle at the bottom, where the personal view of top and bottom is contradictory. The sensors were rested on a table with an insulating mat underneath, with the electrodes facing up. Glad wrap was placed on top of the sensor to prevent direct contact with the pork. This is done to keep up the high standards of hygiene required when testing meat. Each of the six pieces of pork was tested for all four orientations at the same frequency range mentioned above. The driving signal for the sensors were provided by the Agilent 33120A waveform generator and the Agilent 54622D mixed signal oscilloscope, analyzed the input voltage, output current and the phase. All efforts were done to make sure the pork pieces were all tested at similar temperatures, varying between 16-18°C.

7.3.3 Analysis of Results

The results obtained are shown below. Since different pork samples may have different effective permittivity, the imaginary component of impedance will be mainly affected. The figures 7.13 to 7.24 show the variation of the reactive part of impedance of all three sensors, as a function of frequency, for all four orientations, for all six samples. It is seen that there is a distinct difference in the magnitude of impedance in the frequency range 5 kHz to 40 kHz. The difference in magnitude between samples decreases with increasing frequency. The three sensors also give different results when compared with each other. Even though the results are quite distinct for all six samples, the results obtained for orientation 1 and 2 differ from orientations 3 and 4. This is due to the fact that the response of the sensors depends on its penetration depth [29]. If the thickness of the pork belly exceeds the penetration depth of the electric field lines, the sensors may not be able to respond to fat if the fat lies on the top surface of the meat sample. The impedance of the

sensors provides an average indication of the fat, to the depth of penetration and the part of the meat within the electric field.

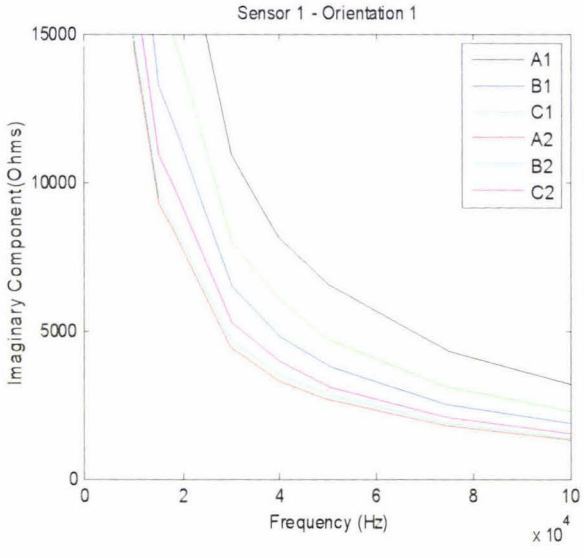

Figure 7.13: Sensor 1 characteristics for pork belly samples at orientation 1

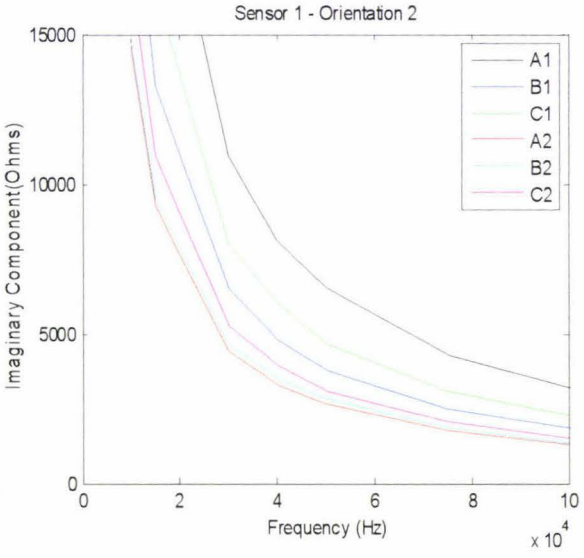

Figure 7.14: Sensor 1 characteristics for pork belly samples at orientation 2

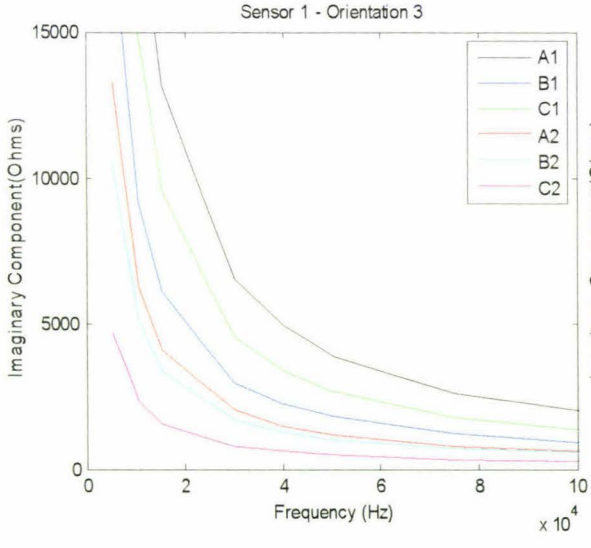

Figure 7.15: Sensor 1 characteristics for pork belly samples at orientation 3

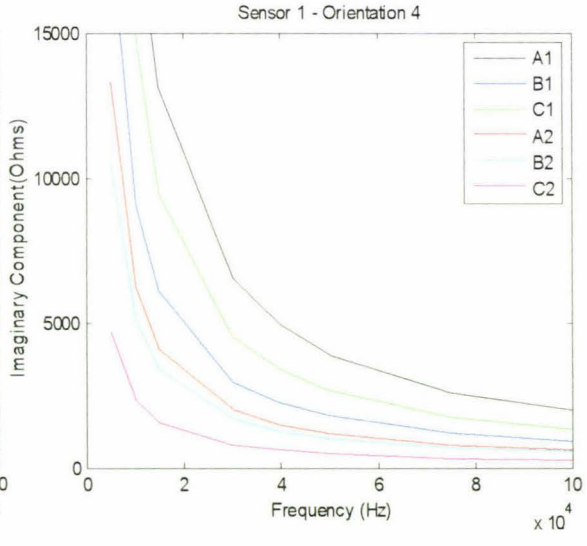

Figure 7.16: Sensor 1 characteristics for pork belly samples at orientation 4

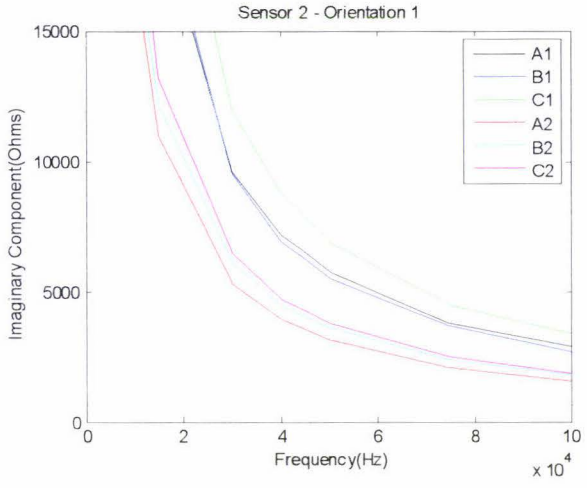

Figure 7.17: Sensor 2 characteristics for pork belly samples at orientation 1

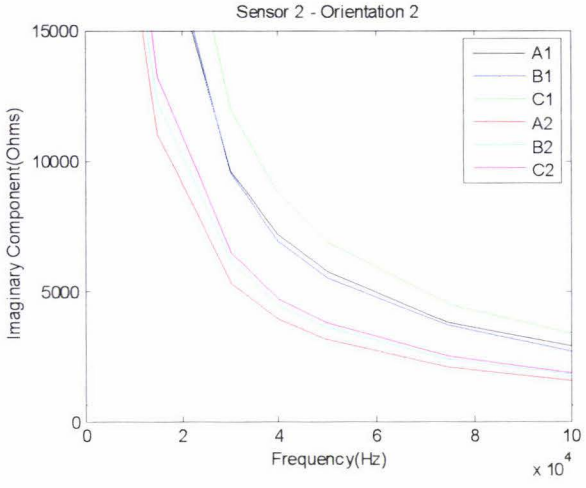

Figure 7.18: Sensor 2 characteristics for pork belly samples at orientation 2

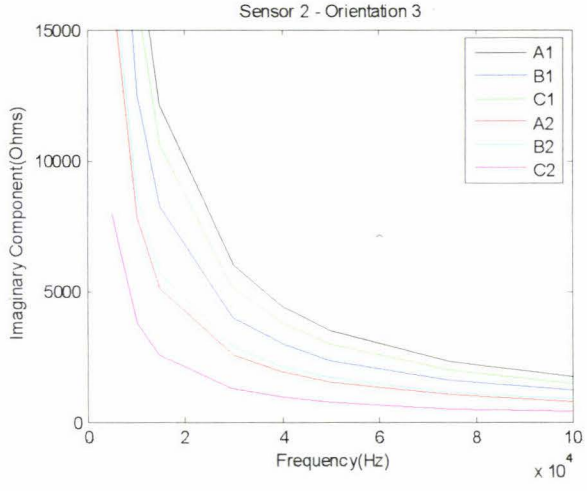

Figure 7.19: Sensor 2 characteristics for pork belly samples at orientation 3

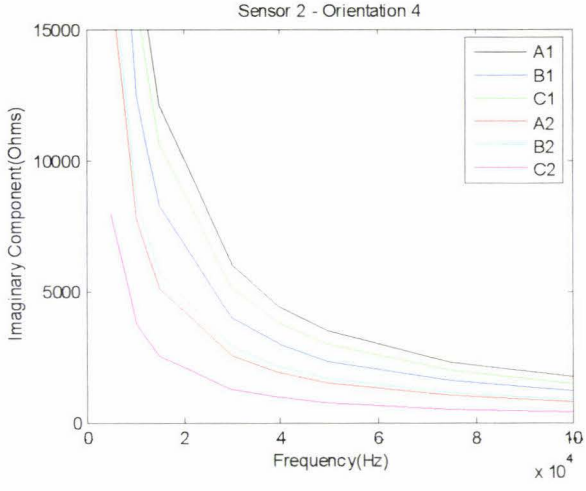

Figure 7.20: Sensor 2 characteristics for pork belly samples at orientation 4

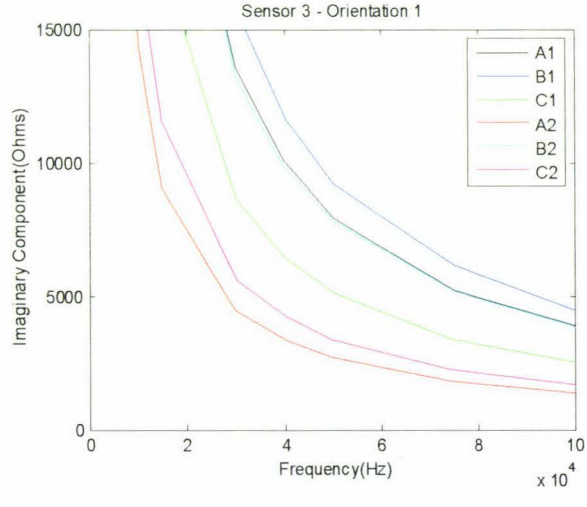

Figure 7.21: Sensor 3 characteristics for pork belly samples at orientation 1

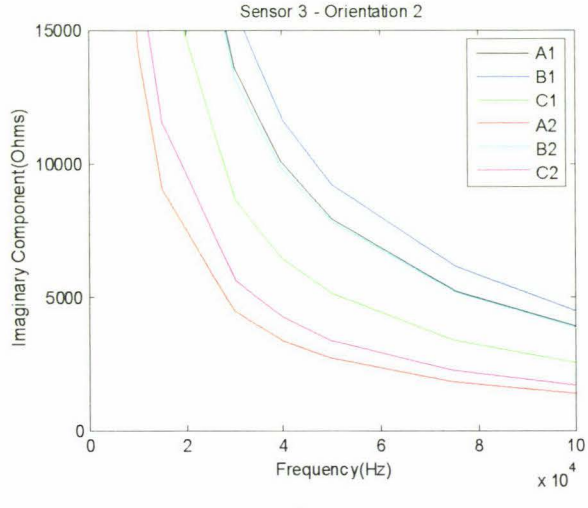

Figure 7.22: Sensor 3 characteristics for pork belly samples at orientation 2

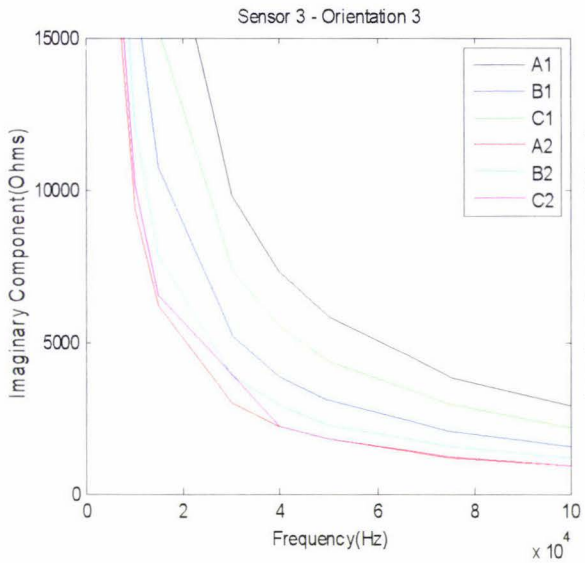

Figure 7.23: Sensor 3 characteristics for pork belly samples at orientation 3

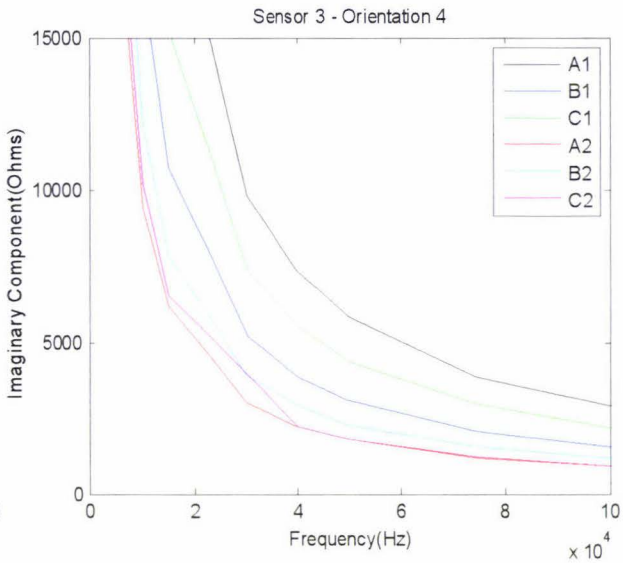

Figure 7.24: Sensor 3 characteristics for pork belly samples at orientation 4

In practice, measurement for one frequency or at only a few frequencies is required. The bar graphs (figures 7.25 – 7.36) show the reactive impedance values of different samples for all sensors and all orientations, at an operating frequency of 5 kHz. It can be seen that the impedance values are quite distinct from each other. Sample A1 has got the highest impedance and sample A2 has the lowest impedance. The measurement at 5 kHz provides the opportunity for the development of a low cost instrumentation and measurement system based on a Cygnal C8051F020 microcontroller.

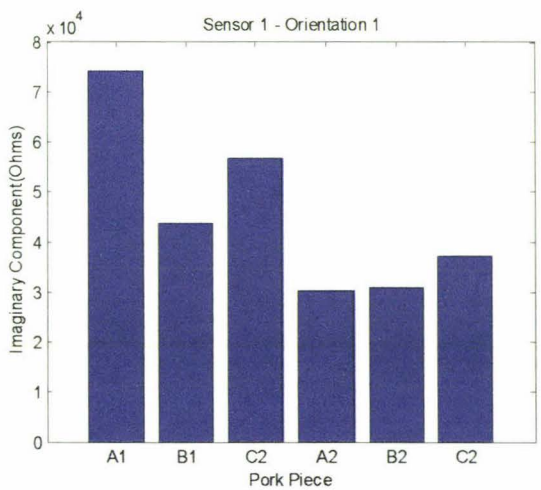

Figure 7.25: Sensor 1 characteristics at 5 kHz for pork belly samples at orientation 1

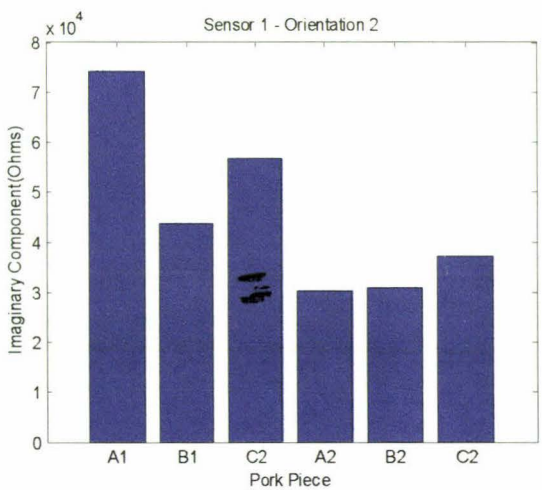

Figure 7.26: Sensor 1 characteristics at 5 kHz for pork belly samples at orientation 2

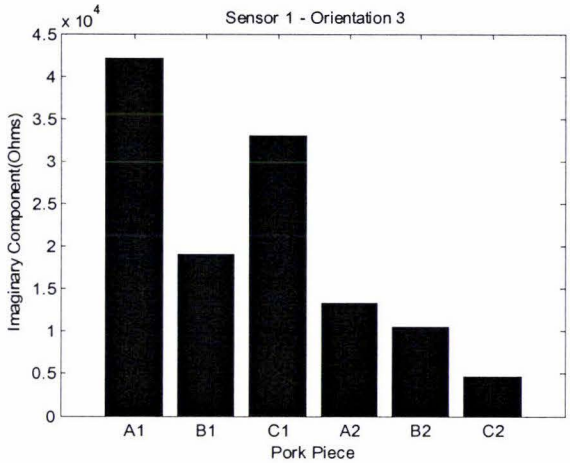

Figure 7.27: Sensor 1 characteristics at 5 kHz for pork belly samples at orientation 3

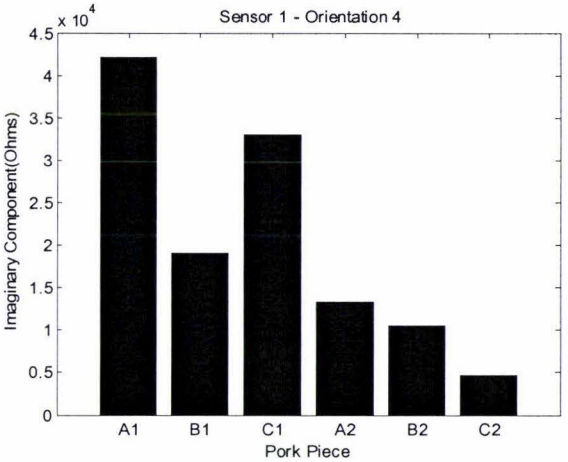

Figure 7.28: Sensor 1 characteristics at 5 kHz for pork belly samples at orientation 4

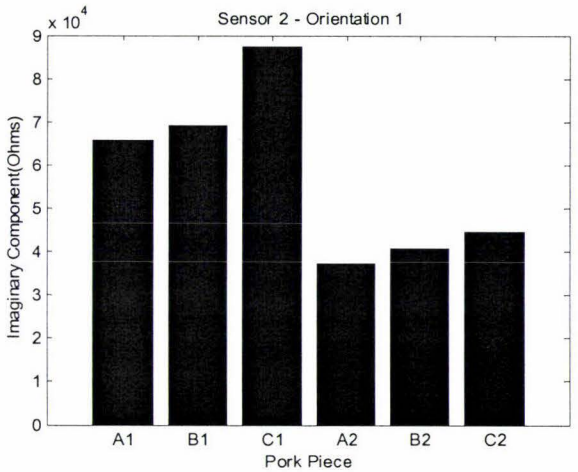

Figure 7.29: Sensor 2 characteristics at 5 kHz for pork belly samples at orientation 1

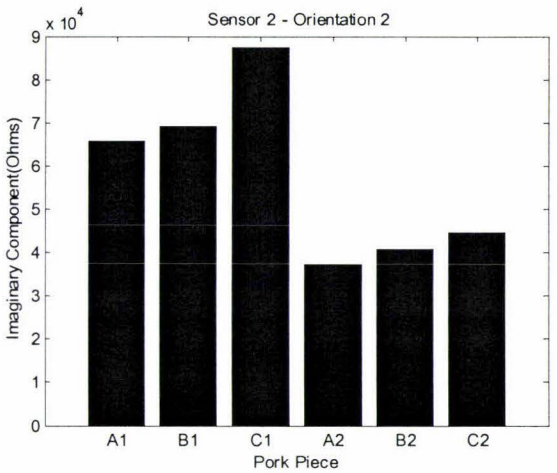

Figure 7.30: Sensor 2 characteristics at 5 kHz for pork belly samples at orientation 2

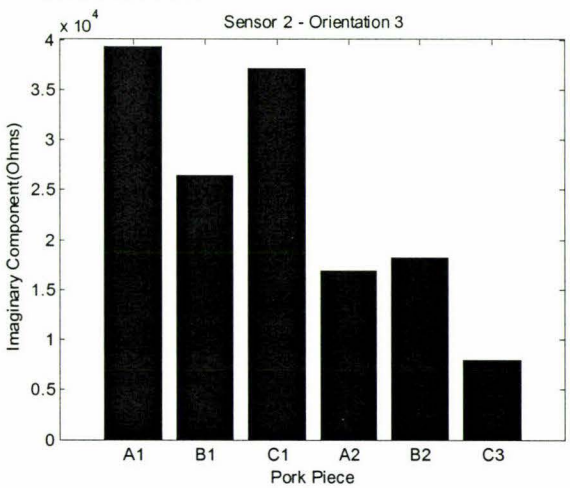

Figure 7.31: Sensor 2 characteristics at 5 kHz for pork belly samples at orientation 3

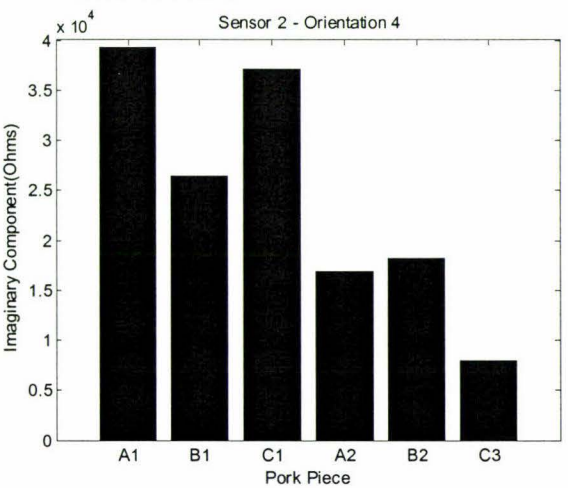

Figure 7.32: Sensor 2 characteristics at 5 kHz for pork belly samples at orientation 3

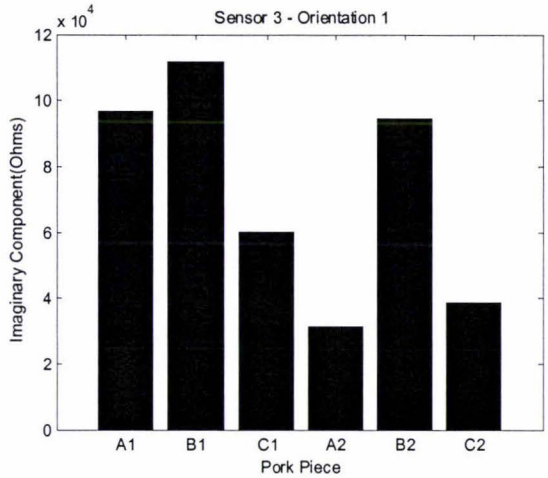

Figure 7.33: Sensor 3 characteristics at 5 kHz for pork belly samples at orientation 1

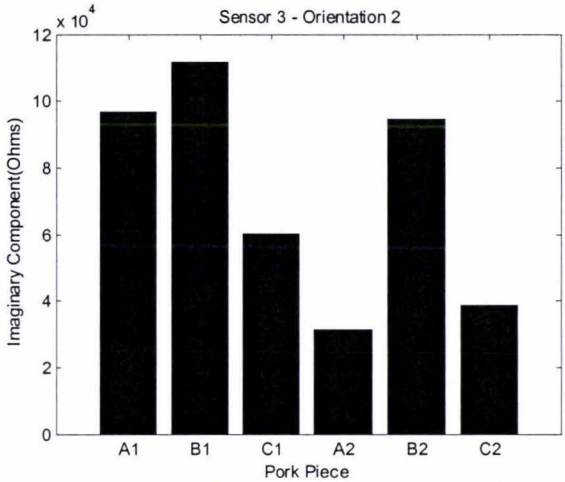

Figure 7.34: Sensor 3 characteristics at 5 kHz for pork belly samples at orientation 2

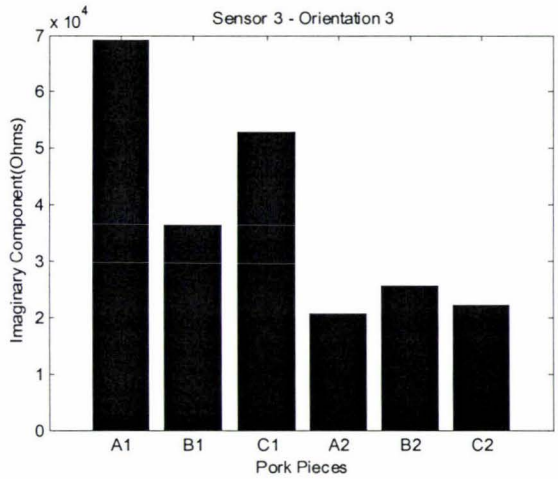

Figure 7.35: Sensor 3 characteristics at 5 kHz for pork belly samples at orientation 3

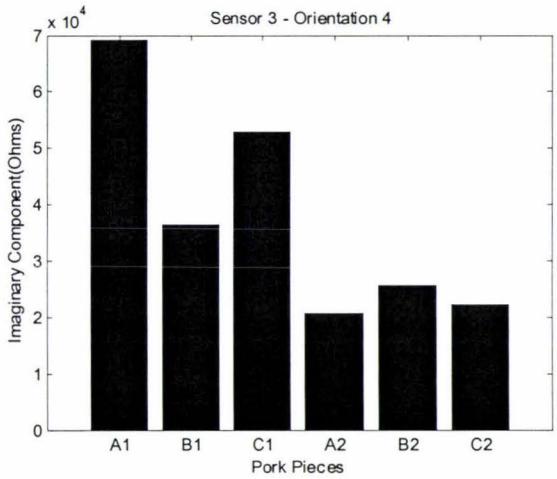

Figure 7.36: Sensor 3 characteristics at 5 kHz for pork belly samples at orientation 4

7.3.4 Data Analysis

The results are analyzed to determine whether the reactive impedance values have a relationship with the fat content of the pork belly. To compare the performance of the sensors, 3 test samples were analyzed by Soxhlet extraction of homogenized sample (including the skin) using petroleum ether (Bp 40 - 60°C) and the results are shown in Table 7.2. The maximum fat content is for sample A1, which matches the result obtained from sensor 1. From figure 7.25 it is seen that the average fat content of B2 is slightly higher than A2. From the results obtained from the sensors it can be safely concluded, that the planar interdigital sensors has a good potential for the on-line determination of fat content and pork meat.

Table 7.2: Fat content from chemical analysis

Chemical Test	Sample A1	Sample A2	Sample B2
	30.09	19.96	17.36

The fat content is estimated by mathematical analysis and can be compared to the results obtained by the chemical analysis. The magnitude and phase of the impedance of the sensor without meat samples (air) and with meat under test (MUT) are measured. The reactance impedances are calculated as follows

$$X_{air} = Z_{air} \times \sin(\phi_{air}) \qquad [7.4]$$

where Z_{air} and ϕ_{air} are the impedance magnitude and phase of the sensors without meat.

$$X_{MUT} = Z_{MUT} \times \sin(\phi_{MUT}) \qquad [7.5]$$

where Z_{MUT} and ϕ_{MUT} are the impedance magnitude and phase of the sensors with pork belly under test.

The effective permittivity of the sample is calculated as

$$\varepsilon_{eff} = \frac{X_{air}}{X_{MUT}}; \qquad [7.6]$$

The inverse of the effective permittivity is taken as the parameter of index, κ, and is used for the analysis to determine the fat and protein content. Tables 7.3 to 7.5 show the parameter of index of the three sensors for four different orientations corresponding to six different meat samples. It is seen that the orientation 1 and 2 are quite uniform and are used for the estimation of fat content.

Table 7.3: ε_{eff} and Κ for sensor 1

Sample	Effective Permittivity (ε_{eff})	Parameter of Index (Κ)
	Orientation 1	
A1	2.7871	0.3588
B1	4.7246	0.2117
C1	3.6407	0.2747
A2	6.1203	0.1634
B2	6.0075	0.1665
C2	4.9867	0.2005
	Orientation 2	
A1	2.7871	0.3588
B1	4.7246	0.2117
C1	3.6407	0.2747
A2	6.1203	0.1634
B2	6.0075	0.1665
C2	4.9867	0.2005
	Orientation 3	
A1	4.9093	0.2037
B1	10.8659	0.0920
C1	6.2759	0.1593
A2	14.0014	0.0714
B2	17.7739	0.0563
C2	40.1206	0.0249
	Orientation 4	
A1	4.9093	0.2037
B1	10.8659	0.0920
C1	6.2759	0.1593
A2	14.0014	0.0714
B2	17.7739	0.0563
C2	40.1206	0.0249

Table 7.4: ε_{eff} and K for sensor 2

Sample	Effective Permittivity (ε_{eff})	Parameter of Index (K)
	Orientation 1	
A1	3.0841	0.3242
B1	2.9338	0.3409
C1	2.3215	0.4308
A2	5.4505	0.1835
B2	4.9945	0.2002
C2	4.5442	0.2201
	Orientation 2	
A1	3.0841	0.3242
B1	2.9338	0.3409
C1	2.3215	0.4308
A2	5.4505	0.1835
B2	4.9945	0.2002
C2	4.5442	0.2201
	Orientation 3	
A1	5.1710	0.1934
B1	7.6872	0.1301
C1	5.4653	0.1830
A2	12.0070	0.0833
B2	11.1804	0.0894
C2	25.6018	0.0391
	Orientation 4	
A1	5.1710	0.1934
B1	7.6872	0.1301
C1	5.4653	0.1830
A2	12.0070	0.0833
B2	11.1804	0.0894
C2	25.6018	0.0391

Table 7.5: ε_{eff} and Κ for sensor 3

Sample	Effective Permittivity (ε_{eff})	Parameter of Index (Κ)
	Orientation 1	
A1	2.5090	0.3986
B1	2.1737	0.4600
C1	4.0400	0.2475
A2	7.7207	0.1295
B2	2.5647	0.3899
C2	6.2797	0.1592
	Orientation 2	
A1	2.5090	0.3986
B1	2.1737	0.4600
C1	4.0400	0.2475
A2	7.7207	0.1295
B2	2.5647	0.3899
C2	6.2797	0.1592
	Orientation 3	
A1	3.5069	0.2851
B1	6.6751	0.1498
C1	4.5888	0.2179
A2	11.7028	0.0854
B2	9.4633	0.1057
C2	10.9665	0.0912
	Orientation 4	
A1	3.5069	0.2851
B1	6.6751	0.1498
C1	4.5888	0.2179
A2	11.7028	0.0854
B2	9.4633	0.1057
C2	10.9665	0.0912

Only sensor 1 and orientation 1 has been used for the estimation of fat and protein. For the calculation of fat the following equation is used

$$\text{Fat}_{cal} = 48.1 \times (\kappa - 0.15) + 18.1 \qquad [7.7]$$

and for the calculation of protein the following equation is used

$$\text{Protein}_{cal} = 16.5 - 16.1 \times (\kappa - 0.15) \qquad [7.8]$$

The parameters of the above equations are obtained from two test samples which correspond to the calibration of the sensor. Based on equations 7.7 and 7.8 the fat and the protein content of the samples are obtained and are shown in table 7.6. It can be seen from table 7.6 that the predicted results are very close to the experimental one. In reality it is impossible to get exactly the same results using a planar sensor to that obtained from chemical analysis. The planar sensor provides an average result of a large sample of pork belly whereas the result from chemical analysis is based on 5 grams of homogenized sample.

Table 7.6: Estimation of fat and protein content

Sample	Parameter of Index (K)	Calculated Fat content	Calculated protein content
A1	0.3987	30.06	12.49
A2	0.1633	18.74	16.28
B1	0.2353	22.20	15.12
B2	0.1644	18.80	16.26
C1	0.3053	25.57	13.99
C2	0.2005	20.53	15.68

7.4 Final Experiments on Pork Belly

7.4.1 More Experiments

Further experiments were carried out using the three sensors on thirteen pork belly samples. The new pork belly samples were different to the previous ones in the sense that they were smaller, shallower and skinless. The skin was removed so that the samples would correspond more favourably to the electric field penetration. Like the earlier experiments the readings were taken for four different orientations. Figures 7.37 – 7.48 show the variation of the reactive part of impedance of the three sensors as a function of frequency, for all orientations. The results are shown up to a maximum operating frequency of 50 kHz. The difference in readings between samples is not noticeable for higher frequencies. Figures 7.49 to 7.60 show the results at 5 kHz.

7.4.2 Analysis of Results

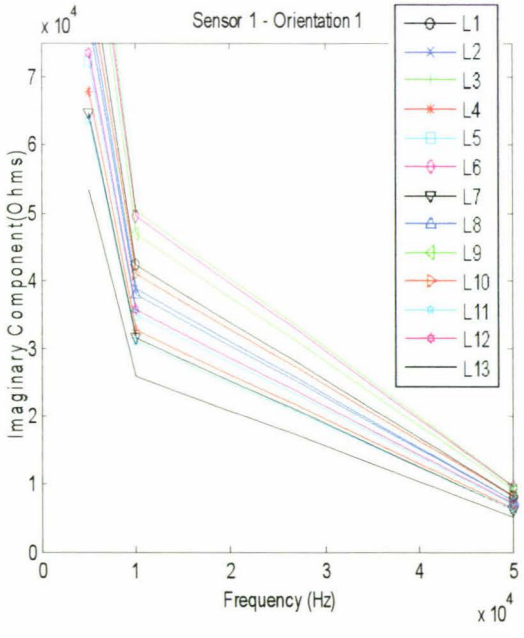

Figure 7.37: Sensor 1 characteristics for pork belly samples at orientation 1

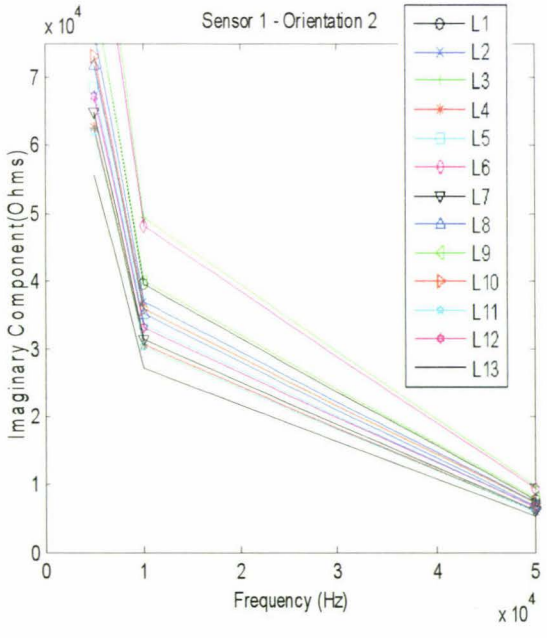

Figure 7.38: Sensor 1 characteristics for pork belly samples at orientation 2

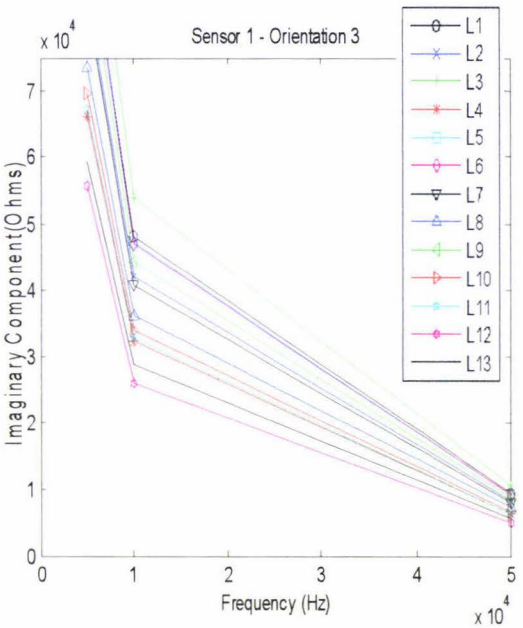

Figure 7.39: Sensor 1 characteristics for pork belly samples at orientation 3

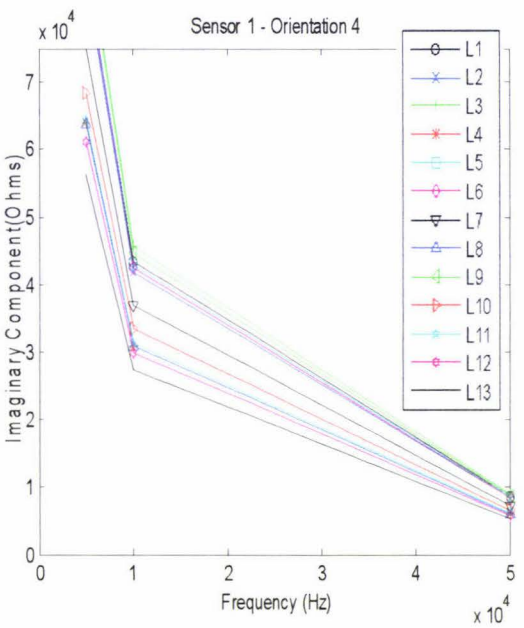

Figure 7.40: Sensor 1 characteristics for pork belly samples at orientation 4

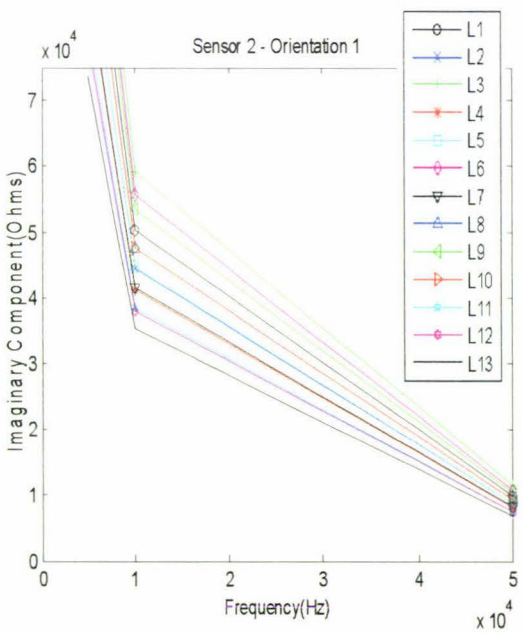

Figure 7.41: Sensor 2 characteristics for pork belly samples at orientation 1

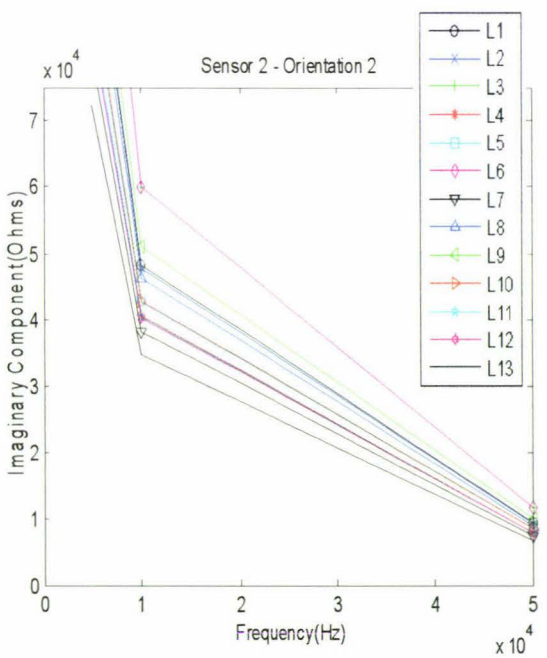

Figure 7.42 Sensor 2 characteristics for pork belly samples at orientation 2

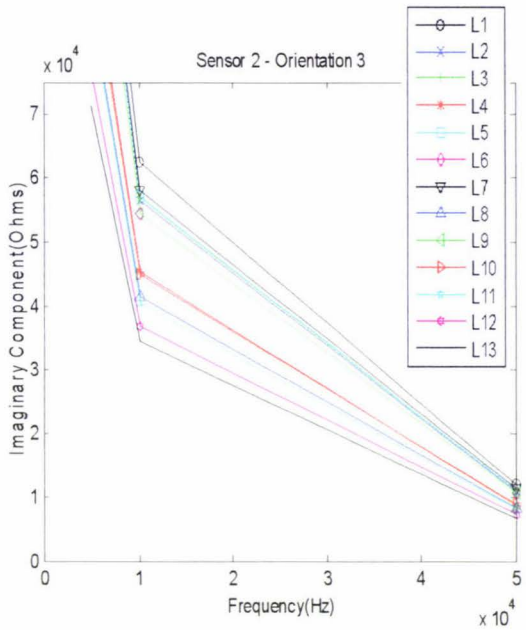

Figure 7.43: Sensor 2 characteristics for for pork belly samples at orientation 3

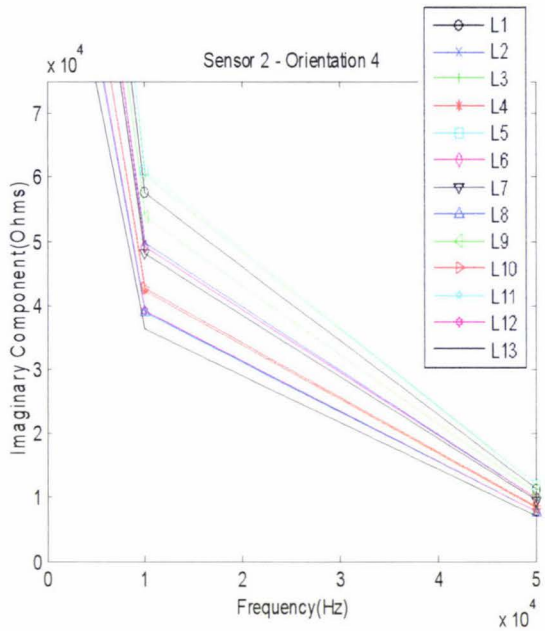

Figure 7.44: Sensor 2 characteristics for pork belly samples at orientation 4

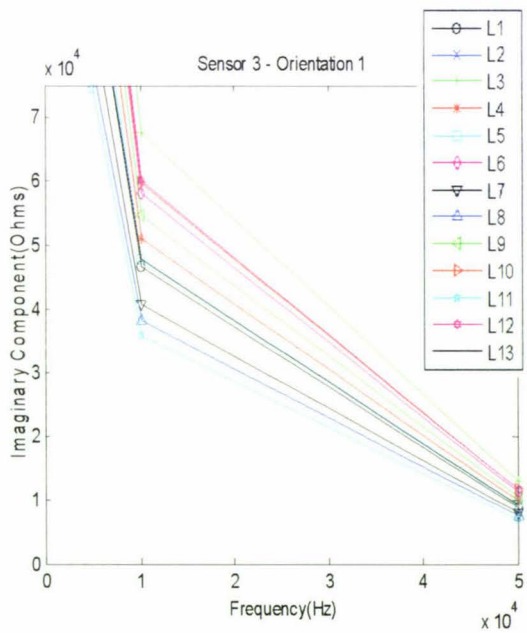

Figure 7.45: Sensor 3 characteristics for for pork belly samples at orientation 1

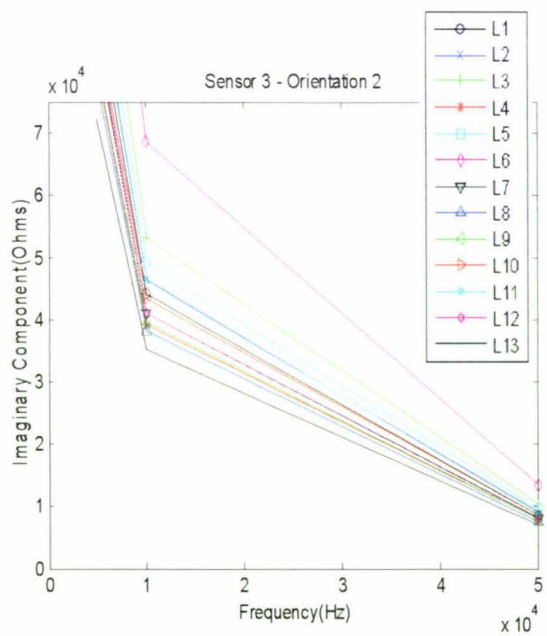

Figure 7.46: Sensor 3 characteristics for pork belly samples at orientation 2

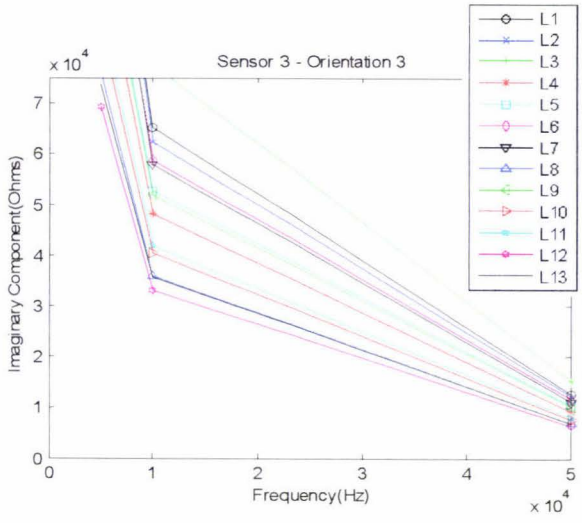

Figure 7.47: Sensor 3 characteristics for for pork belly samples at orientation 3

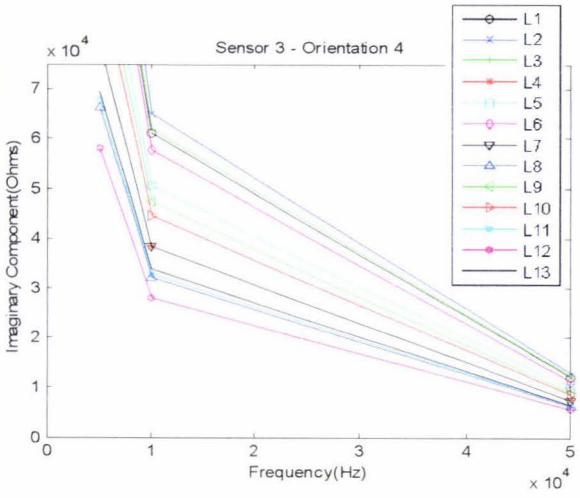

Figure 7.48: Sensor 3 characteristics for pork belly samples at orientation 4

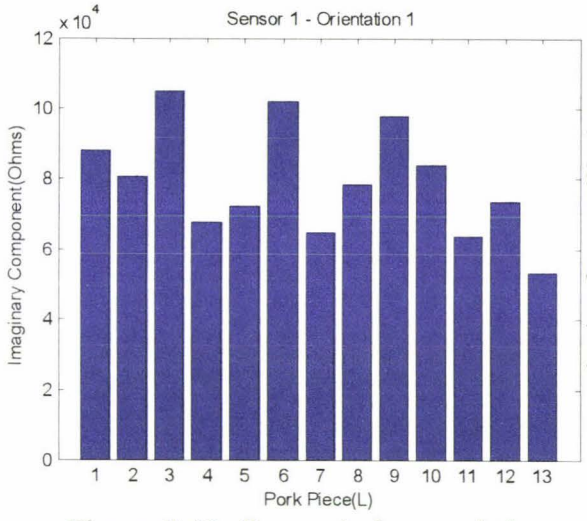

Figure 7.49: Sensor 1 characteristics at 5 kHz for pork belly samples at orientation 1

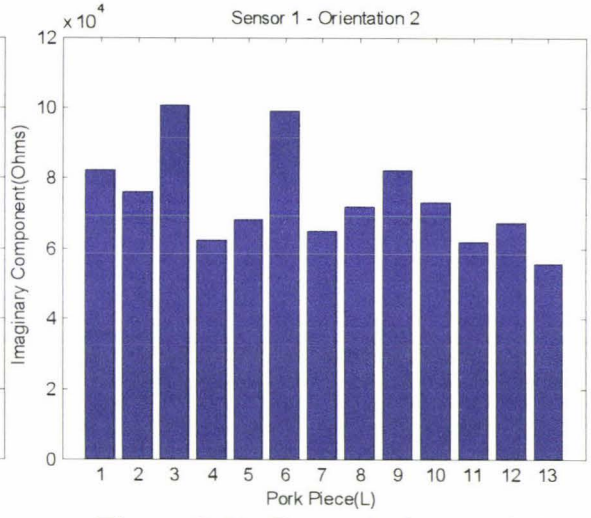

Figure 7.50: Sensor 1 characteristics at 5 kHz for pork belly samples orientation 2

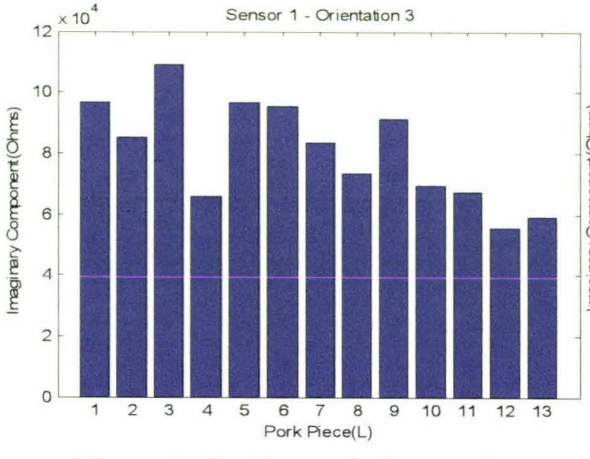

Figure 7.51: Sensor 1 characteristics at 5 kHz for pork belly samples at orientation 3

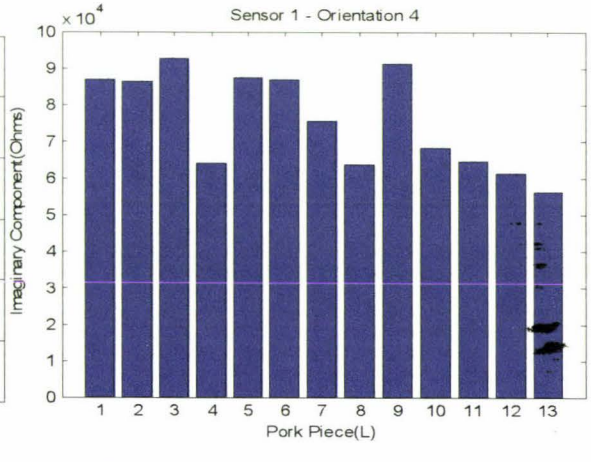

Figure 7.52: Sensor 1 characteristics at 5 kHz for pork belly samples at orientation 4

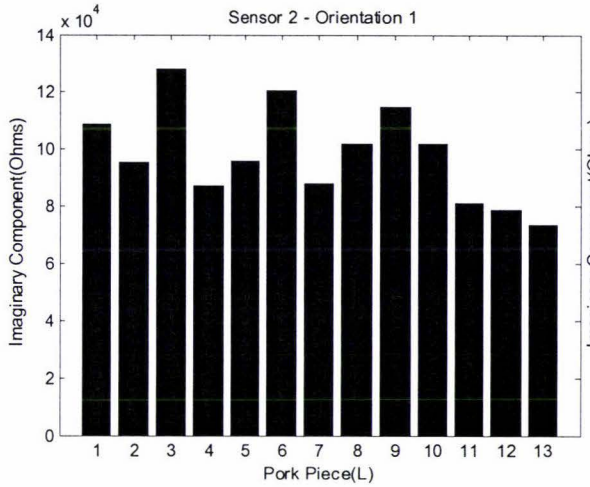

Figure 7.53: Sensor 2 characteristics at 5 kHz for pork belly samples at orientation 1

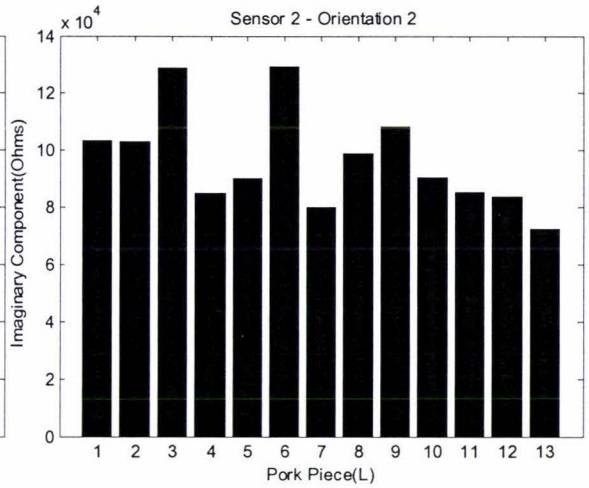

Figure 7.54: Sensor 2 characteristics at 5 kHz for pork belly samples at orientation 2

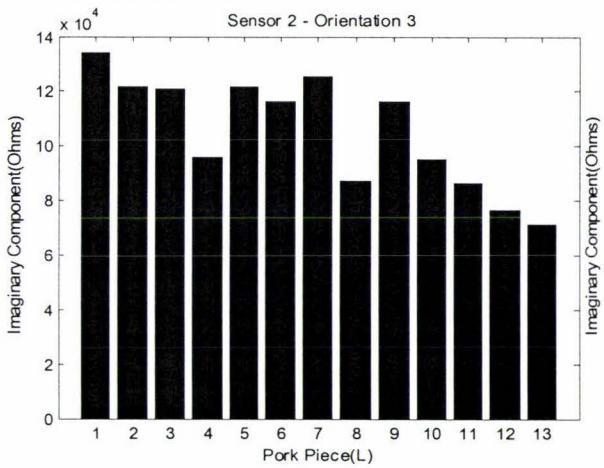

Figure 7.55: Sensor 2 characteristics at 5 kHz for pork belly samples at orientation 3

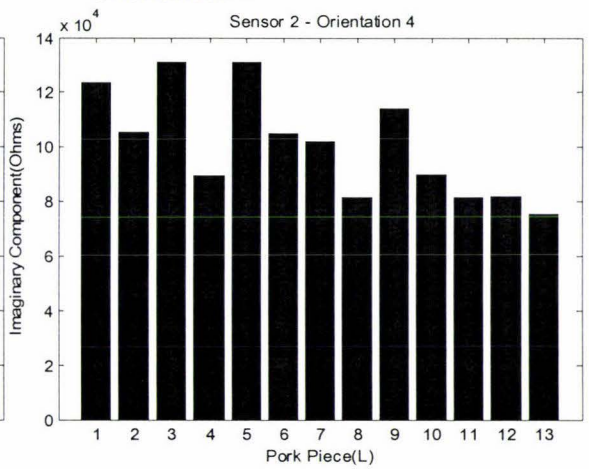

Figure 7.56: Sensor 2 characteristics at 5 kHz for pork belly samples at orientation 4

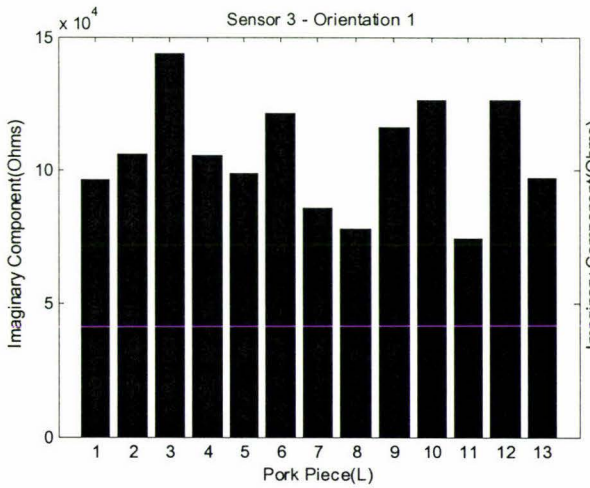

Figure 7.57: Sensor 3 characteristics at 5 kHz for pork belly samples at orientation 1

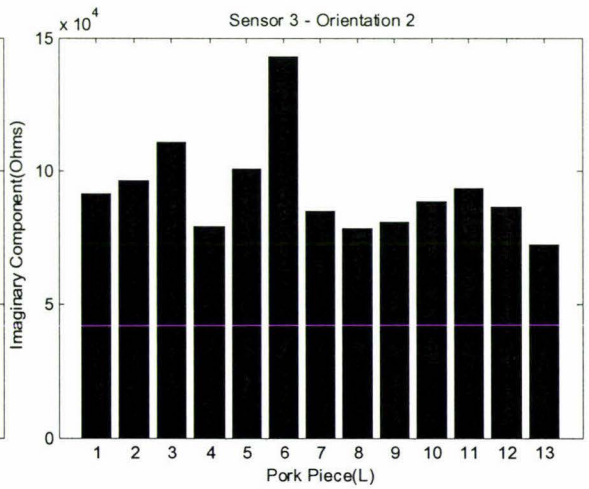

Figure 7.58: Sensor 3 characteristics at 5 kHz for pork belly samples at orientation 2

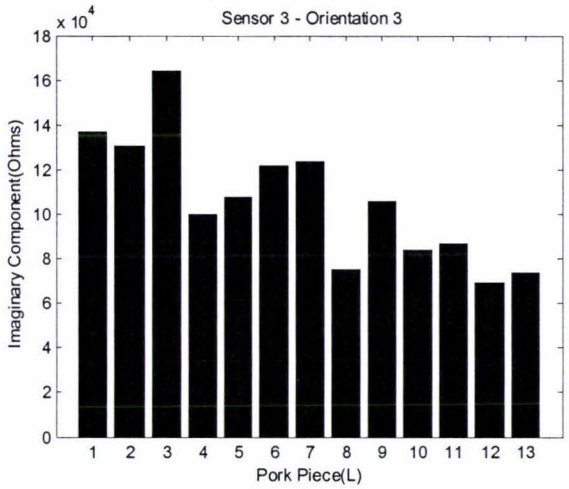

Figure 7.59: Sensor 3 characteristics at 5 kHz for pork belly samples at orientation 3

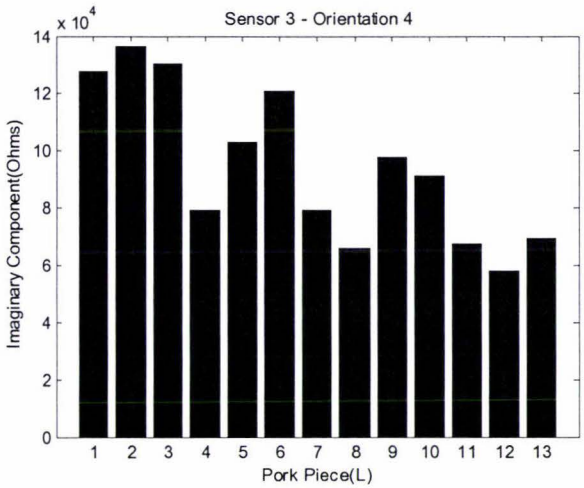

Figure 7.60: Sensor 3 characteristics at 5 kHz for pork belly samples at orientation 4

7.4.3 Data Analysis

The fat content of the thirteen pork belly samples were predicted from the sensor results at 5 kHz (tables 7.7 to 7.9). The fat content of the samples were estimated using a linear and a quadratic equation, for each orientation and for each sensor. The linear equations are obtained by choosing two samples from the extremes of the Parameter of Index spectrum, while the quadratic equation is obtained from three samples where the extremes as well as a sample in the middle of the spectrum are chosen for calculation. An example calculation is shown below for sensor 1 orientation 1.

- Linear Calculation

  Sample 6 (Ķ=0.5047, Fat Actual = 43.78) and sample 13 (Ķ=0.2632, Fat Actual = 25.3) chosen for calculation

$$\text{Fat (Estimated)} = \frac{43.78 - 25.3}{0.5047 - 0.2632} \times (\kappa - 0.2632) + 25.3$$

$$= 76.52 \times (\kappa - 0.2632) + 25.3 \qquad [7.9]$$

- Quadratic Calculation

  Sample 6 (Ķ=0.5047, Fat Actual = 43.78), sample 12 (Ķ=0.3632, Fat Actual = 25.22) and sample 13 (Ķ=0.2632, Fat Actual = 25.3) chosen for calculation

From the above three simultaneous equations can be formed and can be used to solve for the three unknown variables a, b and c

$$0.4378 = 0.2547a + 0.5057b + c$$
$$0.2522 = 0.1319a + 0.3632b + c$$
$$0.253 = 0.0693 + 0.2632b + c$$

The final quadratic equation is

$$\text{Fat (Estimated)} = 5.4566\kappa^2 - 3.4239\kappa + 0.7760 \qquad [7.10]$$

Table 7.7 Fat estimation from sensor 1 results

Parameter of Index (K)	Predicted value using Linear Equation	Predicted value using Quadratic Equation	Actual value	Error 1	Error 2
		Orientation 1			
0.264	25.3918	25.22	25.3	-0.0918	0.08
0.315	29.2331	23.89	22.57	-6.6631	-1.32
0.321	29.7076	23.92	26.48	-3.2276	2.56
0.335	30.8018	24.14	25.66	-5.1418	1.52
0.356	32.4317	24.88	32.78	0.3483	7.9
0.363	32.952	25.22	25.22	-7.732	0
0.388	34.8497	26.9	15.76	-19.09	-11.14
0.398	35.6225	27.77	21.86	-13.763	-5.91
0.414	36.8622	29.41	17.17	-19.692	-12.24
0.436	38.5074	32.02	30	-8.5074	-2.02
0.484	42.2186	39.76	36.16	-6.0586	-3.6
0.505	43.7796	43.79	43.78	0.0004	-0.01
0.519	44.8432	46.79	39.35	-5.4932	-7.44
		Orientation 2			
0.275	25.3	25.3	25.3	0	0
0.306	27.9992	29.2	22.57	-5.4292	-6.63
0.309	28.2364	29.53	25.66	-2.5764	-3.87
0.322	29.3041	30.94	26.48	-2.8241	-4.46
0.332	30.2341	32.12	25.22	-5.0141	-6.9
0.339	30.768	32.78	32.78	2.012	0
0.355	32.163	34.42	15.76	-16.403	-18.66
0.362	32.7485	35.07	17.17	-15.579	-17.9
0.377	34.0316	36.44	21.86	-12.172	-14.58
0.406	36.589	38.88	36.16	-0.429	-2.72
0.407	36.6321	38.92	30	-6.6321	-8.92
0.49	43.7792	43.78	43.78	0.0008	0
0.498	44.5284	44.12	39.35	-5.1784	-4.77

		Orientation 3			
0.276	25.22	25.22	25.22	0	0
0.293	25.8612	21.83	25.3	-0.5612	3.47
0.327	27.1436	17.3	25.66	-1.4836	8.36
0.332	27.3375	16.88	22.57	-4.7675	5.69
0.344	27.7811	16.16	17.17	-10.611	1.01
0.364	28.5193	15.76	15.76	-12.759	0
0.414	30.3609	19.07	26.48	-3.8809	7.41
0.421	30.6554	20.17	21.86	-8.7954	1.69
0.451	31.7626	25.72	36.16	4.3974	10.44
0.473	32.5716	31.18	43.78	11.208	12.6
0.478	32.7804	32.78	32.78	-0.0004	0
0.479	32.8139	33.04	30	-2.8139	-3.04
0.54	35.0656	55.49	39.35	4.2844	-16.14
		Orientation 4			
0.278	25.3	25.3	25.3	0	0
0.302	26.8221	20.49	25.22	-1.6021	4.73
0.316	27.6455	18.75	15.76	-11.886	-2.99
0.317	27.7016	18.65	25.66	-2.0416	7.01
0.319	27.8264	18.45	22.57	-5.2564	4.12
0.338	29.0615	17.17	17.17	-11.892	0
0.373	31.2448	18.23	26.48	-4.7648	8.25
0.427	34.5821	28.06	21.86	-12.722	-6.2
0.43	34.7506	28.82	30	-4.7506	1.18
0.431	34.8192	29.13	43.78	8.9608	14.65
0.433	34.9876	29.93	32.78	-2.2076	2.85
0.452	36.1604	36.16	36.16	-0.0004	0
0.458	36.5304	38.21	39.35	2.8196	1.14

Table 7.8: Fat estimation from sensor 2 results

Parameter of Index (K)	Predicted value using Linear Equation	Predicted value using Quadratic Equation	Actual value	Error 1	Error 2
		Orientation 1			
0.288	25.3	25.31	25.3	0	-0.01
0.309	26.68	25.54	25.22	-1.46	-0.32
0.317	27.25	25.7	22.57	-4.68	-3.13
0.34	28.74	26.34	25.66	-3.08	-0.68
0.344	29.01	26.48	26.48	-2.53	0
0.373	30.91	27.79	21.86	-9.05	-5.93
0.374	31	27.86	32.78	1.78	4.92
0.398	32.6	29.35	15.76	-16.84	-13.59
0.399	32.64	29.39	17.17	-15.47	-12.22
0.425	34.39	31.42	30	-4.39	-1.42
0.449	35.95	33.57	36.16	0.21	2.59
0.47	37.36	35.78	43.78	6.42	8
0.5	39.35	39.35	39.35	0	0

		Orientation 2			
0.282	25.3	25.3	25.3	0	0
0.313	27.2353	28.93	26.48	-0.7553	-2.45
0.327	28.152	30.46	25.22	-2.932	-5.24
0.332	28.4321	30.9	25.66	-2.7721	-5.24
0.333	28.5403	31.07	22.57	-5.9703	-8.5
0.352	29.7116	32.78	32.78	3.0684	0
0.354	29.8835	33.01	17.17	-12.714	-15.84
0.386	31.8824	35.43	15.76	-16.122	-19.67
0.402	32.9456	36.48	21.86	-11.086	-14.62
0.404	33.0729	36.59	30	-3.0729	-6.59
0.424	34.2952	37.58	36.16	1.8648	-1.42
0.503	39.3498	39.35	39.35	0.0002	0
0.505	39.4834	39.35	43.78	4.2966	4.43
		Orientation 3			
0.278	25.3	25.3	25.3	0	0
0.299	26.0944	24.83	25.22	-0.8744	0.39
0.337	27.5578	24.75	22.57	-4.9878	-2.18
0.341	27.6908	24.79	15.76	-11.931	-9.03
0.372	28.8767	25.55	17.17	-11.707	-8.38
0.375	28.9908	25.66	25.66	-3.3308	0
0.454	31.9746	30.69	43.78	11.805	13.09
0.454	32.005	30.77	36.16	4.155	5.39
0.473	32.6967	32.55	39.35	6.6533	6.8
0.475	32.769	32.75	21.86	-10.909	-10.89
0.475	32.7804	32.78	32.78	-0.0004	0
0.49	33.3429	34.42	26.48	-6.8629	-7.94
0.524	34.6581	38.84	30	-4.6581	-8.84
		Orientation 4			
0.294	25.3	25.3	25.3	0	0
0.318	26.8094	20.93	22.57	-4.2394	1.64
0.319	26.8936	20.72	15.76	-11.134	-4.96
0.319	26.926	20.65	25.22	-1.706	4.57
0.349	28.8176	17.3	25.66	-3.1576	8.36
0.35	28.9342	17.17	17.17	-11.764	0
0.398	31.9918	16.69	26.48	-5.5118	9.79
0.41	32.7691	17.49	43.78	11.011	26.29
0.412	32.8922	17.65	21.86	-11.032	4.21
0.445	35.0559	22.03	36.16	1.1041	14.13
0.482	37.4851	30.42	30	-7.4851	-0.42
0.511	39.3508	39.35	39.35	-0.0008	0
0.511	39.3637	39.42	32.78	-6.5837	-6.64

Table 7.9: Fat estimation from sensor 3 results

Parameter of Index (K)	Predicted value using Linear Equation	Predicted value using Quadratic Equation	Actual value	Error 1	Error 2
		Orientation 1			
0.215	14.4088	14.42	22.57	8.1612	8.15
0.226	15.76	15.76	15.76	0	0
0.248	18.5615	18.56	26.48	7.9185	7.92
0.278	22.2679	22.26	30	7.7321	7.74
0.281	22.651	22.61	25.3	2.649	2.69
0.285	23.1356	23.13	32.78	9.6444	9.65
0.306	25.6768	25.67	25.66	-0.0168	-0.01
0.307	25.8256	25.81	21.86	-3.9656	-3.95
0.336	29.47	29.46	36.16	6.69	6.7
0.351	31.317	31.31	43.78	12.463	12.47
0.365	33.0276	33.02	17.17	-15.858	-15.85
0.365	33.0772	33.07	25.22	-7.8572	-7.85
0.416	39.3496	39.36	39.35	0.0004	-0.01
		Orientation 2			
0.209	25.3	25.3	25.3	0	0
0.218	26.4215	25.29	22.57	-3.8515	-2.72
0.227	27.5052	25.46	15.76	-11.745	-9.7
0.23	27.8958	25.57	25.66	-2.2358	0.09
0.234	28.4881	25.78	36.16	7.6719	10.38
0.245	29.8616	26.48	26.48	-3.3816	0
0.25	30.4286	26.85	25.22	-5.2086	-1.63
0.256	31.1973	27.44	17.17	-14.027	-10.27
0.264	32.2558	28.4	30	-2.2558	1.6
0.279	34.0451	30.42	21.86	-12.185	-8.56
0.291	35.658	32.67	32.78	-2.878	0.11
0.321	39.3501	39.35	39.35	-1E-04	0
0.413	51.0312	74.51	43.78	-7.2512	-30.73
		Orientation 3			
0.2	25.22	25.22	25.22	0	0
0.213	25.5312	25.1	25.3	-0.2312	0.2
0.217	25.6357	25.08	15.76	-9.8757	-9.32
0.243	26.2702	25.07	17.17	-9.1002	-7.9
0.251	26.4549	25.11	22.57	-3.8849	-2.54
0.29	27.4006	25.66	25.66	-1.7406	0
0.306	27.7993	26.06	36.16	8.3607	10.1
0.312	27.9476	26.23	32.78	4.8324	6.55
0.353	28.9394	27.73	43.78	14.841	16.05
0.358	29.0488	27.93	26.48	-2.5688	-1.45
0.378	29.5375	28.93	21.86	-7.6775	-7.07
0.397	29.9993	30	30	0.0007	0
0.475	31.9028	35.81	39.35	7.4472	3.54

		Orientation 4			
0.168	25.22	25.22	25.22	0	0
0.191	26.8149	25.41	15.76	-11.055	-9.65
0.196	27.092	25.48	22.57	-4.522	-2.91
0.201	27.4569	25.59	25.3	-2.1569	-0.29
0.229	29.3627	26.46	25.66	-3.7027	-0.8
0.23	29.3897	26.48	26.48	-2.9097	0
0.265	31.7617	28.28	17.17	-14.592	-11.11
0.282	32.9647	29.5	36.16	3.1953	6.66
0.298	33.9986	30.71	32.78	-1.2186	2.07
0.35	37.5331	35.96	43.78	6.2469	7.82
0.37	38.8576	38.39	30	-8.8576	-8.39
0.377	39.351	39.35	39.35	-0.001	0
0.395	40.5674	41.87	21.86	-18.707	-20.01

7.5 Effect of Temperature

Temperature is an important factor to consider when experimenting with food materials [54, 55]. Thermal effects on meat have been reported in [48, 53, 56, and 57]. The impedance of a pork sample was measured for a range of temperatures as shown in figure 7.61. The experiment was run for nearly four hours, in which time the temperature of the pork sample changed from 2°C to around 12°C. It can be seen from figure that the impedance decreases with increasing temperature. Around 15 minutes were taken for each sample during experimentation (experimentation done in a "cold" room), and there was no appreciable change in temperature during this time. All other samples were kept in a cooler and all samples that were experimented on were immediately put into the cooler after. Hence, we can assume that the temperature doesn't have a significant effect on the results obtained. However if experiments were conducted in a warm or hot environment the temperature will play a significant part in the results obtained.

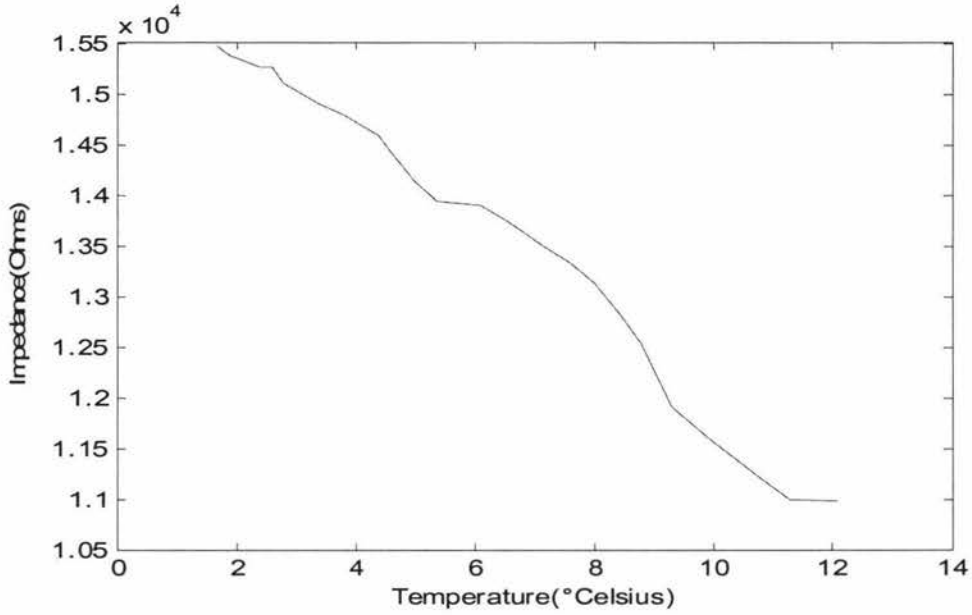

Figure 7.61: Variation of impedance of the sensor with temperature

7.6 Conclusion

This section has described the interaction of planar electromagnetic sensors with pork belly cuts. The sensors show quite distinctive results with different pork belly samples. The response of the sensors indicates a strong possibility of using this type of sensor for the prediction of fat content in pork belly in a non-invasive way. The development of a low cost instrumentation and sensing system configured around a Cygnal 8051CF020 microcontroller has been investigated and has been reported in the next chapter.

CHAPTER 8

DEVELOPMENT OF A LOW COST SENSING SYSTEM

8.1 Introduction

This chapter deals with necessary instrumentation that is essential for the development of an overall sensing system, that is efficient, cost-effective and reliable. Smart sensing microsystems employing an array of capacitive sensors have been reported in [59, 60]. Research has also been done in building electromagnetic sensor microsystems for environment monitoring [61] and in the separation of non-ferrous scrap metals [58]. The instrumentation used for the experiments throughout this thesis is very expensive. Several possibilities have been explored for the development of a low-cost smart sensing system. The following areas are identified:

(i) Sensors
(ii) Excitation system
(iii) Data Acquisition system

Since the role of the sensors that will be used in a low-cost system have been explained during various chapters of the thesis, this chapter will concentrate on the excitation system and the data acquisition system.

8.2 Excitation System

A smart power supply and associated instrumentation to provide the controlled excitation to the exciting coil of the sensor is very important for the target development. A controlled variable frequency power supply has been designed and developed for the supply of excitation voltage. The frequency can be controlled from tens of kHz to 1 GHz. The important components of the system are briefly discussed here.

Figure 8.1a shows the sensor connected to the power supply. Figure 8.1b shows the different component of the power supply unit. The total frequency range has been obtained by switching between different Voltage Controlled Oscillators (VCO)

corresponding to different frequency ranges. Figure 8.1c shows the VCO unit of the power supply.

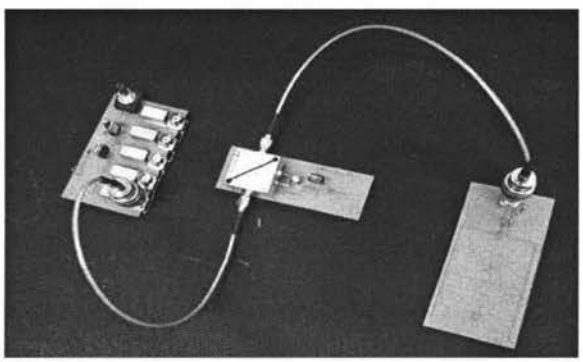

(a)

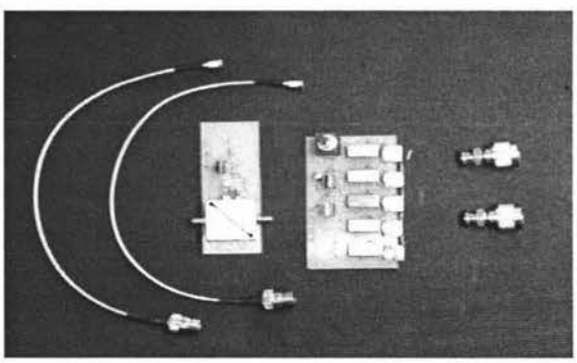

(b)

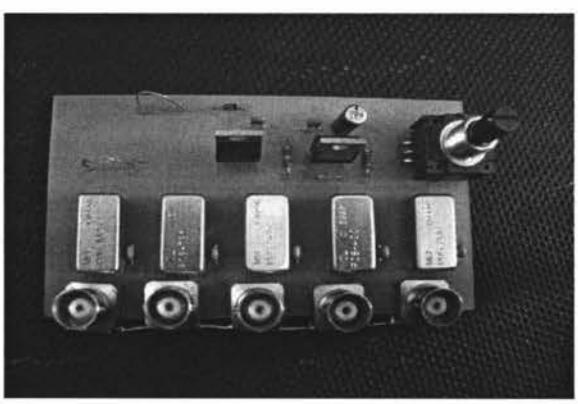

(c)

Figure 8.1: Sensors and instrumentation

The graph in figure 8.2 depicts the tuning voltage versus VCO operating frequency. The graph corresponds to one of the VCOs used to generate the exciting signal feeding the power amplifier. The straight dash line shows an ideal characteristic. It can be seen that the actual characteristic (solid line) is not too far from the ideal one.

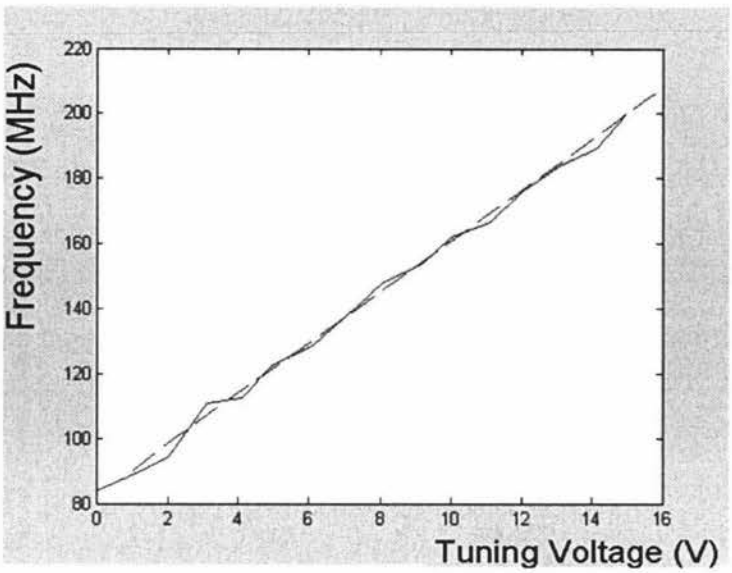

Figure 8.2: Frequency vs Tuning Voltage

The output of the power amplifier is connected to all the sensors and the effect of different materials in close proximity of the sensors is observed. Table 8.1 shows the experimental results for all the sensors at an operating frequency of 84 MHz. Only the amplitude change of the sensor output signal is shown in the table. However, in practice the phase information will also be used.

Table 8.1: Sensor experimental results

System Under Inspection	Sensor Output Amplitude Change at 84 MHz		
	Meander	Mesh	Interdigital
Air	1	1	1
Copper	0.9127349	0.8764259	1.0151976
Aluminum	0.9118998	0.8669202	1.0151976
Iron	0.9077244	0.7742395	0.9984802
Milk	1.0205952	0.9697908	0.9022801
Water	1.0188946	0.9733264	0.9251887

8.3 Data Acquisition System

For the collection of voltage and current signals, an efficient data acquisition system is very important. The analog data is captured using an analog-to-digital converter. A Silicon Lab microcontroller C8051F020 has been considered at the first instant as shown in Figure 8.3. The SiLab C8051F020 has two ADCs operating at 100 kHz and 500 kHz respectively. So an operating frequency of up to 50 kHz can be very well used using this system. The system has already been used and provides good results for single frequency measurement.

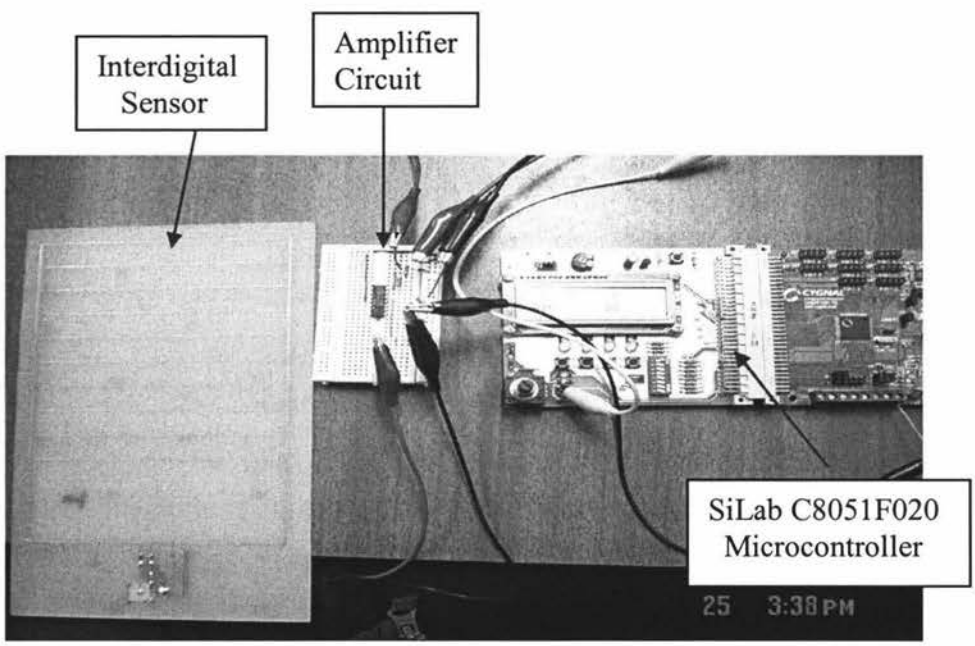

Figure 8.3: SiLab microcontroller C8051F020 based data acquisition system

The material to be tested can be placed on top of the sensor. In the case of liquids it can be put in a container and placed directly on top of the sensor. However pork meat requires a high level of hygiene requirements. Hence, before placing the pork one or two layers of gladwrap can be placed on top of the sensor. This prevents the pork directly touching the sensor.

The amplifier circuit used for this setup is shown in figure 8.4. The sensor output is fed into the non-inverting input through a capacitor and the voltage divider is used to offset the signal. The sensor input needs to have an offset since the 12-Bit Analog to Digital Converter (ADC) cannot process values less than zero. A LM324 Low Power Quad Operational Amplifier is used in the circuit. The sensor signal is amplified by a gain of around 4.3. VCC is set to 5V, and the Zener diode makes sure the signal into the ADC input in the microcontroller doesn't exceed 3.3Volts.

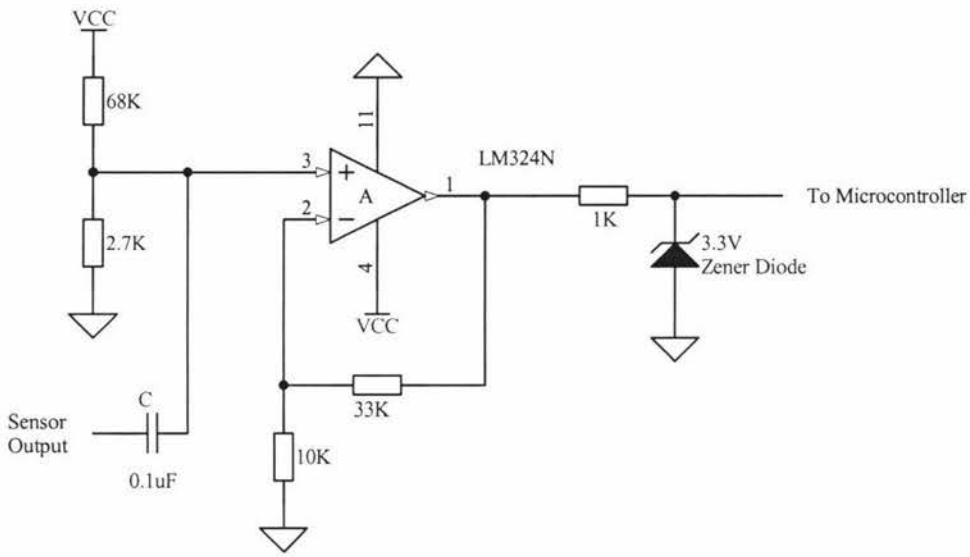

Figure 8.4: Amplifier circuit used in experimental setup

The analog signal from the sensor output is inputted into the ADC pin in the microcontroller. The program stores the highest and the lowest peak of the signal, hence calculating the peak to peak value. The value is outputted as a digital value. So as the response of the sensor changes with the type of material under test, the output digital value will change accordingly.

8.3.1 Experimental Results

Thirteen samples of pork belly were tested at 5 kHz with the setup in figure 8.3. Results were obtained for all thirteen samples and for all four orientations. Four readings were taken for each sample and orientation and the results were averaged. Figures 8.5 – 8.8 shows that the results obtained from the setup in figure 8.3, distinguishes between the thirteen samples quite well. The results are still different for each orientation implying that the interdigital sensor used is not penetrating through the pork sample well enough.

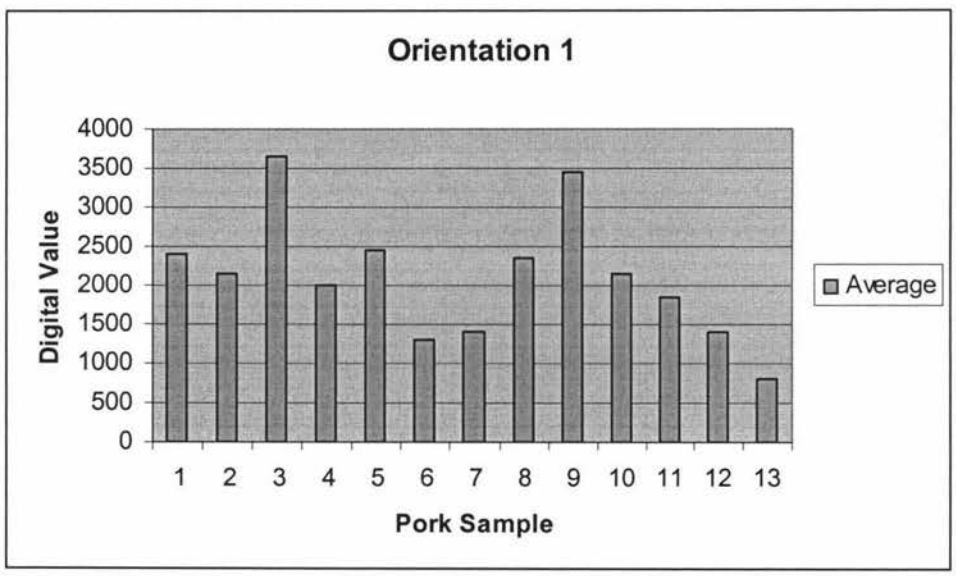

Figure 8.5: Pork belly samples at 5 kHz at orientation 1

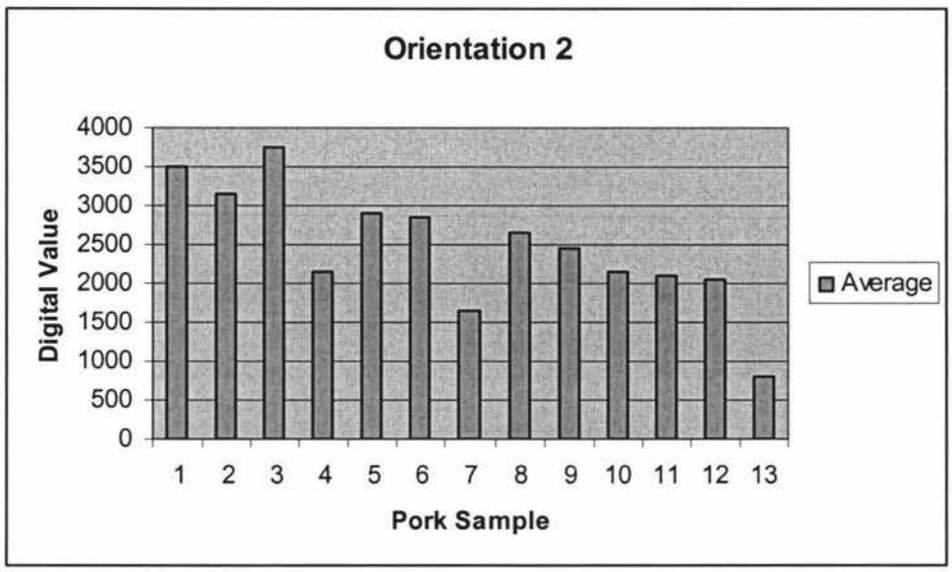

Figure 8.6: Pork belly samples at 5 kHz at orientation 2

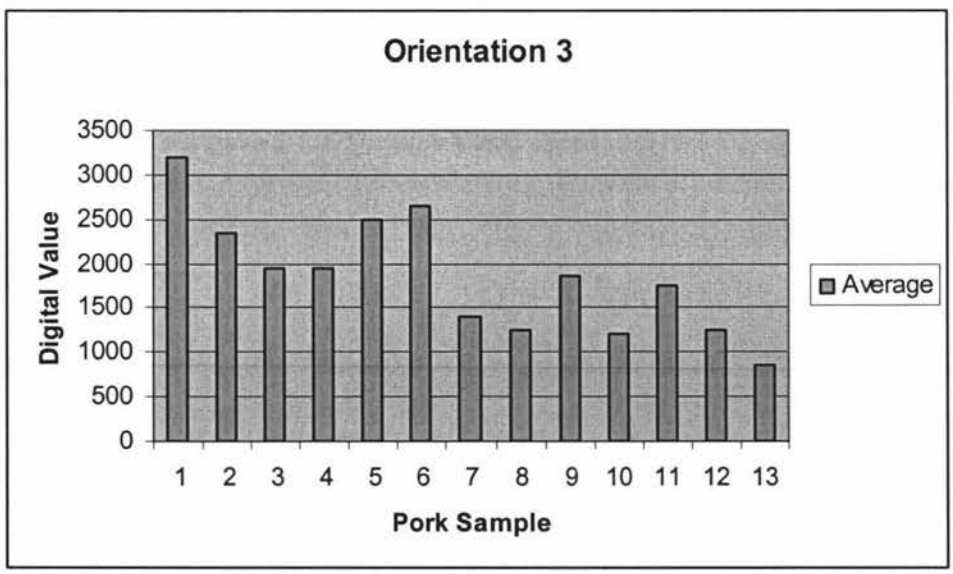

Figure 8.7: Pork belly samples at 5 kHz at orientation 3

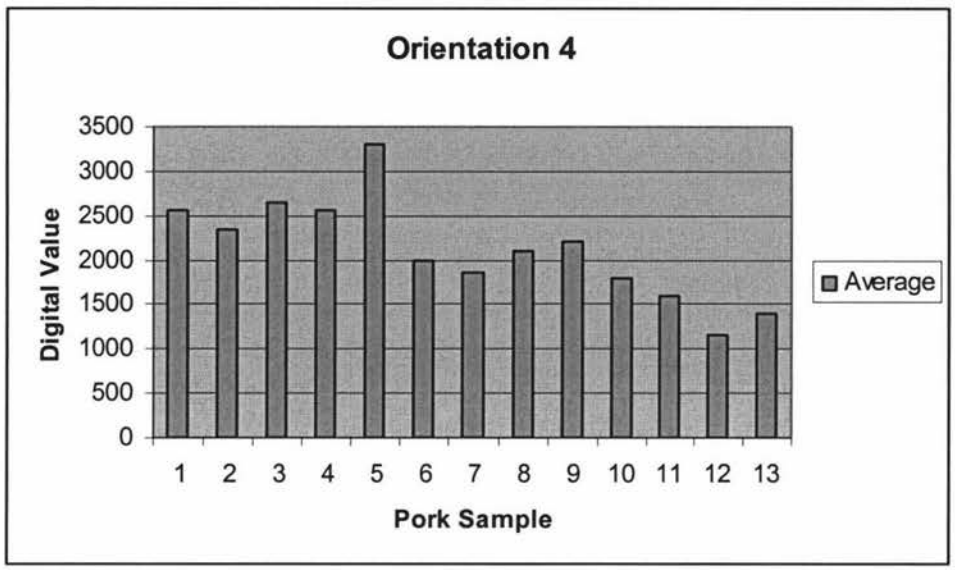

Figure 8.8: Pork belly samples at 5 kHz at orientation 4

8.4 Conclusion

Sensor technology in this age relies on small, smart and cost-effective sensing systems. This chapter has explained the development of an excitation system for the sensor, and the incorporation of an efficient data acquisition system in the SiLab C8051F020 microcontroller. These embody the heart of a low-cost smart sensing system. Experimental results obtained from both systems show a great potential in developing such a system in the near future.

CHAPTER 9

CONCLUSIONS AND FUTURE WORK

9.1 Conclusions

The works in this report include the characterization and experimental results on three types of planar electromagnetic sensors. The principles behind planar electromagnetic sensors have been used in many new technologies in many areas. The rapid rise of non-destructive evaluation has paved the way for planar electromagnetic sensors to play an important role in society today. Three types of planar electromagnetic sensors have been designed and fabricated. These are namely mesh type, meander type and interdigital type sensors. The sensors fabricated were of different pitches and lengths. The principles behind the design of mesh and meander type sensors are of electromagnetic fields and eddy currents. The interdigital sensors on the other hand are based on the electric field. The design of these sensors has been explained in Chapter 2. The sensors were then fabricated.

The three types of planar sensors were then modeled using the finite element software FEMLAB. The inductance and the inductive Reactance characteristics for a range of frequencies were calculated for the mesh and meander type sensors, while the capacitance and the capacitive reactance were calculated for interdigital type sensors. The mesh and meander type sensors were shown to be of the inductive type, while the interdigital sensors were known to be of capacitive type. In practice it is better to know the characteristics before putting the sensors to use.

Hence, the sensors were characterized by experiments. The three types of planar electromagnetic sensors were tested on different types of materials. The materials were metals and liquids of varying electric and dielectric properties. The response of the three types of sensors to these materials has been shown in the report. It can be concluded that mesh and meander type sensors respond well to metals, which have strong electrical properties but poor dielectric properties, and the interdigital type sensors have a strong

response to liquids, which have strong dielectric properties. Hence, the conclusion observed in the modeling chapter that mesh and meander type sensors are of the inductive type, and that the interdigital sensors are of the capacitive type, is well supported by experimentation.

All three types of sensors were used for the estimation of fat content in milk. Different amounts of cream were added to water to simulate different fat contents in milk. The three types of sensors were used for detecting the different percentages of cream added to water. The mesh and the meander type sensors' response was poor, reiterating the fact that they are of the inductive type and thus not reacting well to dielectric materials. The interdigital sensors, which have been concluded to be of the capacitive type by finite element modeling and experimental characterization, had a good response to the different percentages of cream added to the water. Based on these results the interdigital type sensors were used for further experimentation with cream and water. A relationship between impedance and frequency has been fitted with a linear and quadratic equation. The errors obtained from such a fit have been shown. The results obtained from these experiments show that there is a great potential of interdigital type sensors and associated instrumentation being used in the dairy industry by dairy farmers.

Saxophone reed integrity has been evaluated using the interdigital type sensor. The results show that the sensor is competent in evaluating reeds that are considered "bad". The experimental results show that these "bad" reeds are picked out consistently and comprehensively.

The meat industry currently employs expensive and heavy instrumentation to assess the composition of meat samples. The three types of planar interdigital sensors were tested on pork belly samples. The mesh and meander type sensors response to the initial set of pork samples, which ranged from fat, mixed (fat and muscle) and muscle, were unsubstantial to be considered for further experimentation. However the interdigital type sensors responded well to the initial set of pork samples. A new set of interdigital type sensors, whose parameters (pitch and length) match the pork samples tested, were

fabricated. Further experiments were conducted with the new interdigital sensors and results obtained. The results show that the interdigital type sensors are able to distinguish well between different samples of pork belly. Each pork belly sample is different to each other in composition and the sensors respond well to these changes. The sensor results were compared to the results obtained by chemical analysis. A linear and quadratic fit has been used to obtain the relationship between fat content, protein content and frequency.

The building blocks for a low-cost smart sensing system have been fabricated, tested and experimented on. A power supply to provide the excitation voltage to the sensor has been fabricated. The power supply has been tested and experiments have been conducted using it. The experiments were performed with all three types of sensors, on different types of materials. A data acquisition system based on the SiLab C8051F020 microcontroller has been used for the collection of voltage and current signals. The power supply and the microcontroller are essential components of a low-cost smart system. The development work is continuing in order to make it a low cost stand alone system.

The thesis has described three types of planar electromagnetic sensors in mesh, meander and interdigital types. The sensors have been characterized by finite element modeling and experimentation. Experiments were carried out with saxophone reeds, cream and pork belly. The response of the mesh and meander type sensors to the mentioned experimental material was insignificant. This was due to the fact that they were of inductive type and hence the response was poor for dielectric materials. However interdigital type sensors which are of the capacitive type, thus having very good response to dielectric materials, were used for experimentation. Results were obtained and compared with actual results and errors were reported. A power supply was fabricated and the SiLab C8051F020 microcontroller was employed, in an effort to build a low-cost smart sensing system.

9.2 Recommendations and Future Work

The interdigital type sensors used for experimentation needs to be calibrated. The results obtained during experimentation could be improved with proper calibration. This will however increase the complexity of the problem. The pitch of the interdigital type sensors used for the pork belly experiments need to be increased or the pork belly depth decreased. The pork belly samples gave varying results for the different orientations they were tested on. This most probably indicates that the electric field is not penetrating through the whole sample. Even though the pork belly samples were cut very well to the measurements given, some samples were not as deep as the others. This meant that even though it had more or less fat the results would indicate otherwise, since the electric field from the sensor has penetrated the whole material. The pork belly is composed mainly of fat, some protein, moisture and ash. All these different compositions have different permittivity values. Hence the depth of penetration is very important. Increasing the pitch of the interdigital sensor is easier than cutting the pork belly samples to a smaller depth. The interdigital sensor that is used for experimentation can then be calibrated and tested.

The SiLab C8051F020 microcontroller is currently used for measuring the magnitude of the output signal from the sensor. The microcontroller can be programmed to detect the phase difference between the input and the output signal as well. Currently the microcontroller also is limited to around 50 KHz operating frequency. This frequency is ideal for conducting experiments with the interdigital sensor but falls short when experiments with mesh and meander type sensors has to be performed. Mesh and meander type sensors respond well to high frequencies, so the data acquisition system needs to be able to perform at such frequencies. For relatively higher frequency of operation, as well as multi-frequency excitation, work on the DAC card PCI-9812 card is under development. The operating frequency can go up to 20MHz.

Taking into account the favorable response of the mesh and meander type sensors to conducting materials and the response of interdigital type sensors to dielectric materials,

a multi-sensor array detection system can be built to detect unexploded ordnance (UXO). The major aim would be in the detection of landmines amongst other unexploded ordnance. The latest mines are mostly made of plastic and a small amount of metal. The basic metal detector is easy and cheap to use and has a decent success rate. However the problem lies in the fact that the detectors identify all metallic objects; they cannot differentiate a mine or UXO from other debris. When using more sensitive detectors for plastic mines with little metal (which is the type of mine that is currently used extensively in warfare), the problem gets worse. However, an array of sensors employing mesh and meander type sensors can be developed to detect the metals or conducting materials in landmines and the interdigital type sensor can be used for the detection of plastic.

CHAPTER 10

REFERENCES

[1] W. Göpel and K.D. Schierbaum, "Sensors: A Comprehensive Survey (City Publishers)", vol. 2, pp. 5, 9, 1991

[2] J. Fraden, "Handbook of Modern Sensors: Physics, Designs, and Applications (American Institute of Physics Press)", Second Edition, pp. 1,5,28,33, 1997

[3] S. Semancik, J.R. Whetstone, "NIST (National Institute of Standards Technology)Workshop on Chemical Sensors: Strategies for Future Technologies", (Washington, D.C.: NIST), pp. 39, 1992

[4] J.W. Gardner, "Microsensors: Principles and Applications (John Wiley and Sons)" pp. 14, 1994

[5] A. Konig, P. Windirsch, M. Gasteier, and M. Glesner, "Visual Inspection in Indstrial Manufacturing," IEEE Micro, vol. 15, pp. 26-31, Mar. 1995

[6] G. Gauglitz, "Direct Optical Sensors: Principles and Selected Applications", Anal Bioanal Chem, vol. 381, pp. 141-155, Nov. 2005

[7] V.V. Nagarkar, J.S. Gordon, S. Vasile, P. Gothoskar, and F. Hopkins, "High Resolution X-ray sensor for Non-destructive Evaluation", IEEE Transactions on Nuclear Science, vol. 43, pp. 1559-1563, Mar. 1996

[8] J. Blitz, "Electrical and Magnetic Methods of Non-destructive Testing (Chapman and Hall)", Second Edition, pp. 48-52, 1997

[9] G. Hayward, "Developments in Transducer Technology for Ultrasonic Non-destructive Testing Applications, "IEE Proceedings – Science, Measurement and Technology, vol. 145, no. 5, pp. 227-228, 1998

[10] I.I. Loktev, V.V. Rozkhov, A.B. Aleksandrov, I.A. Tichomirov, "Leak Testing of Products Under Transient Condition", Proceedings of the 16th WCNDT (World Conference on Non-destructive Testing), pp. 49-52, 2004

[11] J.F. Vaerman, "Fluorescent Penetrant Inspection Process, Automatic Method for Sensitivity Quantification", Proceedings of the 11th WCNDT, vol. 3, pp. 1920-1927, Nov. 1985

[12] M.N. Bassim, M.P. Dudar, R. Rifaat, and R. Roller, "Application of Acoustic

Emission for Non-destructive Evaluation of Utility Inductive Reactors", IEEE Transactions on Power Delivery, vol. 8, pp. 281-284, Jan. 1993

[13] T. Takagi, M. Uesaka, and K. Mia et al., "Electromagnetic NDE Research Activities", JSAEM Electromagnetic Nondestructive Evaluation, T. Takagi et al., Eds. Amsterdam, The Netherlands: IOS, pp. 9-16, 1997

[14] Y. Shi and D. Jiles, "Finite Element Analysis of the Influence of Fatigue Crack on Magnetic Properties of Steel", Journal of Applied Physics, pp. 6353-6355, Jun. 1998

[15] N. Goldfine, "Near Surface Material Property Profiling for Determination of SCC Susceptibly", Fourth EPRI Balance-of-Plant Heat Exchanger NDE (Non-destructive Evaluation) Symposium, Jackson Hole, WY, pp. 1-11, Jun. 1996

[16] S. Baglio, S. Castorina and N. Savalli, "Integrated inductive Sensors for the Detection of Magnetic Microparticles", IEEE Sensors Journal, vol. 5, No. 3, pp. 372-384, Jun. 2005

[17] N.J. Goldfine, "Magnetometers for Improved Material Characterization in Aerospace Application", Material Evaluation, pp. 396-405, Mar. 1993

[18] N.J. Goldfine, D. Clark, and T. Lvett, "Material Characterization using Model based Meandering Winding Eddy Current Testing (MW-ET)", EPRI Topical Workshop: Electromagnetic NDE Applications in the Electric Power Industry, Charlotte, NC, pp. 1-9, Aug. 1995

[19] N.J. Goldfine, "Conformable Meandering Winding Magnetometer (MWM) for Flaw and Material Characterization in Ferrous and Nonferrous Metals", ASME (American Society of Mechanical Engineers) Pressure Vessels and Piping Conference, Proceedings on International Advancement in PVP Technology", Orlando, FL, pp. 131-138, Jul. 1997

[20] S. Yamada, H. Fujiki, M. Iwahara, S.C. Mukhopadhyay, and F.P. Dawson, "Investigation of Printed Wiring Board Testing By Using Planar Coil Type ECT Probe", IEEE Transactions on Magnetics, Vol. 33, No. 5, pp. 3376-3378, Sept. 1997

[21] S.C. Mukhopadhyay, "Quality Inspection of Electroplated Materials Using Planar Type Micro-Magnetic Sensors With Post Processing from Neural Network Model", IEE Proceedings – Science, Measurement and Technology, vol. 149, No. 4, pp. 165-171, Jul. 2002

[22] S.C. Mukhopadhyay, S. Yamada, and M. Iwahara, "Experimental Determination of Optimum Coil Pitch for a Planar Mesh Type Micro-magnetic Sensor", IEEE Transactions on Magnetics, vol. 38, No. 5, pp. 3380-3382, Sep. 2002

[23] S.C. Mukhopadhyay, S. Yamada, and M. Iwahara, "Optimum Coil Pitch Selection for Planar Mesh Type Micro-magnetic sensor for the Estimation of Near-Surface Material Properties", JSAEM Studies in Applied Electromagnetics and Mechanics Vol. 14, pp. 1-9, 2003

[24] S.C. Mukhopadhyay, " High Performance Planar Electromagnetic Sensors – A Review of Few Applications", Proceedings of the 2004 New Zealand National Conference on Non-Destructive Testing", pp. 33-41, Jun. 2004

[25] S.C. Mukhopadhyay, "A Novel Planar mesh Type Micro-electromagnetic Sensor: Part I – Model Formulation", IEEE Sensors Journal, vol. 4, No. 3, pp. 301-307, Jun. 2004

[26] S.C. Mukhopadhyay, "A Novel Planar mesh Type Micro-electromagnetic Sensor: Part II – Estimation of System Properties", IEEE Sensors Journal, vol. 4, No. 3, pp. 308-312, Jun. 2004

[27] E. Fratticcioli, M. Dionigi and R. Sorrentino, "A Planar Resonant Sensor for the Complex Permittivity Characterization of Materials", IEEE MIT-S Digest, paper no. WE1B-3, pp. 647-649, 2002

[28] K. Toda, Y. Komatsu, S. Oguni, S. Hashiguchi, and I. Sanemesa, "Planar Gas SensorCombined with Interdigitated Array Electrodes", Analytical Sciences, vol. 15, pp. 87-89, Jan. 1999

[29] A. Mamishev, K. Sundara-Rajan, F. Yang, Y. Du, and M. Zahn, "Interdigital Sensors and Transducers", Proceedings of the IEEE, vol 92, No.5, pp. 808-845, May 2004

[30] B.H. Timmer, W. Sparreboom, W. Olthuis, P. Bergveld, A. van den Berg, "Planar Interdigitated Conductivity Sensors for Low Electrolyte Concentrations, Proceedings of SeSens, pp. 878-883, Nov. 2001

[31] K. Sundara-Rajan, "Estimation of Moisture Content in Paper Pulp Containing Calcium Carbonate Using Fringing Filed Impedance Spectroscopy", Appita Journal, pp. 413-419, 2004

[32] K. Sundara-Rajan, L. Byrd II, and A.V. Mamishev, "Moisture Content Estimation in Paper Pulp Using Fringing Field Impedance Spectroscopy", IEEE Sensors Journal, vol. 4, No. 3, pp. 378-383, Jun 2003

[33] F.R. van de Voort, "Fourier transform infrared spectroscopy applied to food analysis", Food Research International, vol. 25, pp. 397-403, 1992.

[34] D. Firestone and A. Sheppard, "Determination of Trans Fatty Acids (Oily Press)", Advances in Lipid Methodology, vol. 1, pp 274-289, 1992.

[35] D. Lefier, R. Grappin and S. Pochet, "Determination of fat, protein and lactose in raw milk by Fourier Transform Infrared Spectroscopy and by analysis with a conventional filter-based milk analyser", Journal of the AOAC (Association of Official Analytical Chemists) International, vol. 79, pp. 711-717, 1996.

[36] A. Hewavitharana and B. Van Brakel, "Fourier Transform Infrared Spectrometric method for the rapid determination of casein in raw milk", The Analyst, vol. 122, , pp. 701-704, Jul. 1997.

[37] F.R. Van De Voort, K.P. Menon, J. Sedman, and A.A. Ismail, "Determination of solid fat for index by fourier transform infrared spectroscopy", Journal of the American Oil Chemists' Society, vol. 73, pp. 411-416, 1996.

[38] F.R. Van De Voort, J. Sedman, G. Emo, and A.A. Ismail, "Assessment of Fourier Transform Infrared Analysis of Milk", Journal of the AOAC (Association of Official Analytical Chemists) International, vol. 75, pp. 780-785, 1992.

[39] K. Swensen, M. Ellis, M.S. Brewer, J. Novakofsi, and F.K. McKeith, "Pork Carcass Composition: II. Use of Indicator Cuts for Predicting Carcass Composition, Journal of Animal Science, vol. 76, pp. 2405-2414, 1998

[40] E.K. McClure, J.A. Scanga, K.E. Belk, and G.C. Smith, "Evaluation of the E+V Video Image Analysis System as a Predictor of Pork Carcass Meat Yield", Journal of Animal Science, vol. 81, pp. 1193-1201, 2003

[41] P. Allen, B. McGeehin, "Prediction of Lean Meat Percentage in Pigs using TOBEC", Proceedings: 43rd International Congress of Meat Science & Technology, pp. 254-255, 1997

[42] M.J. Marchello, W.D. Slanger, J.K. Karlson, "Bioelectrical Impedance: Fat Content of Beef and Pork from Different Size Grinds", Journal of Animal Science, vol. 77, pp. 2464-2468, 1999

[43] B.G. Schroeder, and R.E. Rust, "Composition of Pork Bellies, II. Compositional Variations between and within Animals and the Relationship of Various Carcass Measurements with Chemical Compositions of the Belly", Journal of Animal Science, vol. 39, pp. 1037-1044, 1974

[44] D. Suster, B.J. Leury, C.D. Hofineyr, D.N.D'Souza, and F.R. Dunshea, "The Accuracy of Dual Energy X-ray Absorptiometry (DXA), Weight, and P2 Back Fat To Predict Half-carcass and Primal-cut Composition in Pigs within and across Research Experiments", Australia Journal of Agricultural Research, vol. 55, pp. 973-982, 2004

[45] A.D. Mitchell, A.M. Scholz, P.C. Wange and H. Song, "Body Composition Analysis of the Pig by Magnetic Resonance Imaging", Journal of Animal Science, vol. 79, pp. 1800-1813, 2001

[46] Y. Liu, and J.R. Stoufer, "Pork Carcass Evaluation with an Automated and Computerized Ultrasonic System", Journal of Animal Science, vol. 73, pp. 29-38, 1995

[47] A.P. Schinckel, J.R. Wagner, J.C. Forrest, and M.E. Einstein, "Evaluation of Alternative Measures of Pork Carcass Composition", Journal of Animal Science,Vol. 79, pp. 1093-1119, 2001

[48] O. Sipahioglu, S.A. Barringer, I. Taub, and A.P.P. Yang, "Characterization and Modeling of Dielectric Properties of Turkey Meat", Journal of Food Science, vol. 68, pp. 521-527, 2003

[49] V.N. Tran, and S.S. Stuchly, "Dielectric Properties of Beef liver, Chicken and Salmon at Frequencies from 100 to 2500 MHz", Journal of Microwave Power, vol. 22, pp. 29-33, 1987

[50] S. Ryynanen, "The Electromagnetic Properties of Food Materials: A Review of the Basic Principles", Journal of Food Engineering, vol. 26, pp. 409-429, 1995

[51] M.C. Steel, and R.J. Sheppard, "The Dielectric Properties of Rabit Tissue, Pure Water and Various Liquids suitable for Tissue Phantoms at 35 GHz", Phy.Med.Biol, vol. 33, No. 4, pp. 467-472, 1988

[52] B. Bodakian, F.X. Hart, "The Dielectric Properties of Meat", IEEE Transactions on Dielectrics and Electrical Insulation, vol. 1, No. 2, pp. 181-187, Apr. 1994

[53] C. Gabriel, S. Gabriel, R.W. Lau, and E. Corthout, "The Dielectric Properties of Biological Tissues: I. Literature Survey. II. Measurements in the Frequency range 10 Hz to 20 GHz. III. Parametric Models for the Dielectric Spectrum of Tissues", Phy.Med.Biol., vol. 41, pp. 2231-2293, 1996

[54] S.O. Nelson, and P.G. Bartley, "Measuring Frequency and Temperature-dependent permittivities of food materials", IEEE Transactions on Instrumentation and Measurement, vol. 51, No. 4, pp. 589-592, Aug. 2002

[55] S.O. Nelson, " Dielectric Spectroscopy of Fresh Fruits and Vegetables", Proceedings of 22nd IEEE Instrumentation and Measurement Technology Conference, pp. 360-364, May. 2005

[56] R.W. Dickerson Jr, and B.R. Read, "Thermal Conductivity of Meats", ASHRAE (American Society of Heating, Refrigerating and Air-conditioning Engineers) Transactions, vol. 81, pp. 356-360, 1975

[57] J.E. Hill, J.D. Leitman, and J.E. Sunderland, "Thermal Conductivity of Various Meats", vol. 21, pp. 1143-1151, 1967

[58] M.B. Mesina, T.P.R. de Jong, W.L. Dalmijn, "Improvements in separation of non-ferrous scrap metals using an electromagnetic sensor", Phyical Seperation in Science and Engineering, vol 12, No.2, pp. 87-101, 2003

[59] N. Yazdi, A.Mason, K. Najafi, K.D. Wise, "A Low-Power Generic Interface Circuit for Capacitive Sensors", Digest, Solid-State Sensor and Actuator Workshop, pp. 215-218, Jun. 1996

[60] N. Yazdi, A. Mason, K. Najafi, K.D. Wise, "A Smart Sensing Microsystem with a Capacitive Sensor Interface", Digest, IEEE International Symposium on Circuits and Systems, vol. 4, pp. 336-339, May. 1996

[61] A. Mason, N. Yazdi, K. Najafi, K.D. Wise, "A Low-Power wireless micro instrumentation system for environmental monitoring", The 8th International Conference on Solid-State and Actuators, and Eurosensors IX, pp. 107-110, Jun. 1995

Publications

Publications related to Sensors

1. C. Gooneratne and S.C. Mukhopadhyay, "Application of a Novel Planar Sensor to Estimate the Life of Turbine", Proceeding of AUPEC 2004 conference, paper no. 16, Sep. 26- Sep. 29, 2003, Brisbance, Australia, ISBN 1-884-99775-3.

2. C. Gooneratne, S.C. Mukhopadhyay, and G. Sen Gupta, "A Review of Sensing Technologies for Landmine Detection: Unmanned Vehicle Based Approach", Proceedings of Second International Conference on Autonomous Robots and Agents, December 13 – 15, 2004, Palmerston North, New Zealand, pp. 401-407.

3. C. Gooneratne, S.C. Mukhopadhyay and Y. Yamada, "Novel Planar Electromagnetic Sensors – Characterization and Comparative Evaluation", IEEE Intermag Conference, April 4-8, 2005, Nagoya, Japan, paper number EF-07, Conference digests, page number 483.

4. C.P. Gooneratne, S.C. Mukhopadhyay, G. Sen Gupta and K. Thakur, "Characterization and Comparative Evaluation of Novel Planar Electromagnetic Sensors", Proceedings of ISEMA 2005, 6th International Conference on Electromagnetic Wave Interaction with Water and Moist Substances, Weimer, Germany, May 29- June 1, 2005, page number 243-250.

5. S. C. Mukhopadhyay, C. P. Gooneratne, S. Demidenko and G. Sen Gupta, "Low Cost Sensing System for Dairy Products Quality Monitoring", Proceedings of 2005 International Instrumentation and Measurement Technology Conference, May 17-19, 2005, Ottawa, Canada, IEEE Catalog Number 05CH37627C, ISBN 0-7803-8880-1, Page number 244-249.

6. J. Akramy, C. Gooneratne, S.C. Mukhopadhyay and G. Sen Gupta, "A Controlled Frequency Signal Source for Electromagnetic Sensing Applications", Proceedings of 11th Electronics New Zealand Conference (ENZ Con), November 15-16, 2004, Palmerston North, New Zealand, pp. 124 – 129.

7. S.C. Mukhopadhyay, C.P. Gooneratne, G. Sengupta and S. Yamada, "Characterization And Comparative Evaluation Of Novel Planar Electromagnetic Sensors" IEEE Transactions on Magnetics, October 2005, Vol. 41, No. 10, pp. 3658-3660.

8. C. Gooneratne, S.C. Mukhopadhyay, R. Purchas and G. Sen Gupta, "Interaction of Planar Electromagnetic Sensors with Samples From Pork Belly Cuts", Paper accepted for the International Conference on Sensing Technology, November 21-23, 2005, Palmerston North, New Zealand.

Papers on other topics

9. S.C. Mukhopadhyay, C. Gooneratne, M. Staines, I. Vajda, M. Iwahara and S. Yamada, "Feasibility study of developing high temperature superconducting fault current limiter: A New Zealand perspective", Proc. *ISEM 2003*, pp. 100-101, France, May 12-14, 2003.

10. S.C. Mukhopadhyay, C. Gooneratne and M. Staines, "Transition of magnetic current limiter to superconducting fault current limiter", Proceeding of AUPEC conference, paper no. 3, Sep. 28- Oct. 1, 2003, Christchurch, New Zealand.

11. S. C. Mukhopadhyay and C. Gooneratne, "Studies of various configuration of permanent magnets to develop repulsive type magnetic bearing", Proceeding of AUPEC conference, paper no. 4, Sep. 28- Oct. 1, 2003, Christchurch, New Zealand.

12. S.C. Mukhopadhyay, C. Gooneratne and G. Sen Gupta, "Magnetic Bearing: An Integrated Platform for Teaching and Learning", Proceedings of 2nd International Conference on Autonomous Robtos and Agents, December 13 – 15, 2004, Palmerston North, New Zealand, pp. 283-288.

13. D.P. Salvador, C. Gooneratne, S.C. Mukhopadhyay and G. Sen Gupta, "Microcontroller-based Control for Sensorless Active Magnetic Bearing", Proceedings of 11th Electronics New Zealand Conference (ENZ Con) November 15-16, 2004, Palmerston North, New Zealand, pp. 190 – 195.